Analysis of Dynamics and Learning of the Stochastic Spiking Neurons

Ken-ichi Amemori

Graduate School of Information Science
Nara Institute of Science and Technology
8916-5 Takayama, Ikoma, Nara 630-0101, Japan
(Tel) +81-743-72-5256, (Fax) +81-743-72-5259
(E-mail) keniti-a@is.aist-nara.ac.jp

Ph.D. thesis

May 7, 2001

This dessertation is submitted to
Graduate School of Information Science,
Nara Institute of Science and Technology
in partial fulfillment of the requirement for the degree of
DOCTOR of SCIENCE

Thesis committee:

Shin Ishii, Professor
Kunihiro Chihara, Professor
Minoru Ito, Professor
Kenji Sugimoto, Professor

Abstract

This thesis discusses and analyses the dynamics and learning of the spiking neurons where stochastic input spikes are provided. One of the important problems in neural computation is to understand how the neurons process their information. Throughout this thesis, we try to discuss this neural coding problem by assuming two hypotheses. First is the stochastic property of spikes, and second is that the neuronal activities can be modeled by the spiking neuron model. The spiking neuron model is one of the simplified neuron models, but it can directly treat spikes and enables us to analyze theoretically.

In chapter 1, we state our motivation and aim of the stochastic spiking neurons which we have developed. The stochastic property of spikes is a common phenomenon, and the neuronal coding problems are often described by spike generation probability. However, most of the neuron models and their discussions are very simplified, and cannot treat how the spikes are generated. Through the analysis of the stochastic spiking neurons, we try to make more realistic description of neuron models that can deal a temporal aspect of the spike generation probability.

Chapter 2 and 3 are the main contents of this thesis. We develop a new theoretical framework to consider the dynamics of a stochastic spiking neuron model with general membrane response to input spike. We assume that the input spikes obey an inhomogeneous Poisson process. The stochastic process of the membrane potential then becomes a Gaussian process. When a general type of the membrane response is assumed, the stochastic process becomes a Markov-Gaussian process. We present a calculation method for the membrane potential density and the firing probability density. Our new formulation is the extension of the existing formulation based on diffusion approximation. Although the single Markov assumption of the diffusion approximation simplifies the stochastic process analysis, the calculation is inaccurate when the stochastic process involves a multiple Markov property. We find that the variation of the shape of the membrane response, which has often been ignored in existing stochastic process studies, significantly affects the firing probability. Our approach can consider the reset effect, which has been difficult to be dealt with by analysis based on the first passage time density.

In chapter 4, we discuss a theoretical framework of spike-based Hebbian learning. The spike-based Hebbian learning can be decomposed by the dynamics of internal variable which changes its values by the spike arrival and spike emission of neurons. For the application of this theoretical results, we consider the the self-organization and formation of neural circuits based on coincidence detector neurons. Through competitive learning among spikes, the network can preserve a spatio-temporal spike pattern.

In chapter 5, we theoretically examine the stochastic process of a spiking neuron whose spike responses are similar to those of the Hodgkin-Huxley (H-H) model. Our simplified model based on a linear differential equation can successfully reproduce the sub-threshold membrane properties of the H-H model. Analyzing the stochastic pro-

cess of this model, we find that the neuron resonates with Poisson input spikes whose intensity oscillates with a certain frequency. This frequency corresponds to so-called natural frequency of the H-H model. This chapter is one of the evidences of ability of the stochastic spiking neurons to model physiologically plausible phenomena.

We will conclude this thesis in chapter 6 with discussions about what the viewpoint of the stochastic spiking neuron clarifies about the neural coding problems, and what the future of this model will be. There, we will see the relationship between the conventional rate coding and the stochastic spiking neuron model which we have discussed. Our stochastic spiking neuron model has various application, and will bridge the gap between spikes and psychophysical phenomena through population coding scheme.

Contents

List of Figures

Chapter 1

Basic Concept of Stochastic Spiking Neurons

Abstract. In this chapter, we state the motivation and aim of the stochastic spiking neurons which we have developed. One of the important problems in neural computation is to understand how the neurons process their information. Here, we clarified what the problem is and state the viewpoint that we assume. Throughout this thesis, we adopt two assumption. First is the stochastic property of spikes, and second is that the neuronal activities can be modeled by the spiking neuron model. The stochastic property of spikes is a common phenomenon, and the neuronal coding problems are often described by spike generation probability. However, most of the neuron models and their discussions are very simplified, and cannot consider how the spikes are generated. Spiking neuron model that we adopt is an appropriate one that can directly treat spikes, and enables us to analyse by stochastic process method.

1.1 Introduction

Brain is an astonishing organism which can flexibly learn, think and make decision among a large amount of input information. The information processing unit in the brain is a neuron. Every sensory information such as a sight, hearing, smell, taste, touch and so on is expressed and encoded by the action potentials that the neurons emit. Such pulsed information spreads throughout the brain, and each neurons communicates by the pulses. In this thesis, we will focus on this pulsed action potentials which we call “spikes”.

Although the studies of information processing of brain have flourished in these days, the issue how the neurons process their spike information has remained as an unsolved problem. The reason why the role of spikes has still been unknown is because the spikes can only be partially observed. A basic measurement method of spikes is to penetrate the brain with a electrode, and observe the voltage within a very limited area of the brain. What we can observe from the *in vivo* (living-brain) experiment are the spikes that single neurons emit. As a result, it is very difficult to capture the

whole activities of neural coding. Because one cannot specify the connection of the neuronal circuit, the only thing that we can psychologically imagine is to link the spiking events with the stimulus that the experimenter provides or with the behaviors of the subject. This fundamental lack makes the role of spikes an important topic which many researchers discuss. In the next section, we will review and define the problem of neural coding, and state our standpoint to explain the role of the spikes.

1.2 Neural coding problems

How do the spikes convey information?

This is the first problem that we will discuss. A classical research of the neuroscience also includes this neural coding problem. An English neuroscientist Adrian studied about the neural coding of muscle. The Adrian's fundamental observations (Adrian and Zotterman, 1926) was that, in response to a static stimulus such as a continuous load on a stretch receptor, the rate of spiking increases as the stimulus becomes larger. Then, the number of spikes in a fixed time window following the onset of a static stimulus represents the intensity of the stimulus that the sensory receptors detect. In this case, only the temporally summed and averaged number of spikes from the onset of the stimulus has information.

Rate coding hypothesis

Rate coding hypothesis insists that the information among the spikes can be extracted by the temporal averaging of spikes. From the Adrian's experiment, the temporally summed and averaged number of the spikes concerns with the information of the weight of the load that the sensory receptors detect. Mathematically, we can describe the transmitted information such as weight of load as

$$\mathcal{I}_{\mathrm{rate}} = \frac{1}{M\mathcal{T}} \sum_{l=1}^{M} \int_0^{\mathcal{T}} n_l(t) dt, \tag{1.1}$$

where M is the number of trial and $\mathcal{T}$ is the duration time of each trial. The number of spikes of the l-th trial until time t can be described by random variable $n_l(t)$. Based on this hypothesis, the timing of a spike emission does not have information. This rate coding viewpoint simplifies the neuron model very much, and fortunately corresponds to the spin glass system of magnetic matter which has been analytically studied in statistical physics. Many techniques of statistical mechanics can be applied to the analysis. However, these simplification motivated by mathematical tractability does not consider how the spikes and neurons process their information.

Temporal coding hypothesis

On the contrary, detail measurement of coded spikes in other area such as MT (medial temporal) area of the cerebral cortex (Bair and Koch, 1995), the temporal resolution of the conveyed information is found to be important. Moreover, the correlation of the spikes, or the deterministic property of spikes, which make the spiking information richer, is also found (Riehle *et al.*, 1996; Hatsopoulos *et al.*, 1998). Recent discoveries find that temporal timings of spikes is important for information processing and learning. Many researchers has begun to reevaluate the temporal aspect of the spike coding system.

1.2.1 Redefinition of the controversy

Complexity of the spikes in the cerebral cortex

The controversy about neural coding is so diverse that we should redefine and limit what the problems is. Here, we limit the discussion to the spikes in the cerebral cortex. One of the property of the neurons in the cerebral cortex is the large number of the projecting (input) neurons. Many types of input information flood into a single neuron. As a result, the dynamics of neurons become complex. One of the problems about spikes in the cerebral cortex is that the spikes are seemingly stochastic. Even if the same experimental stimulus are provided to the brain, the spike trains are not the same among the trials. What makes this variation over trials? Why the brain adopt such seemingly uncertain coding scheme? There are two extreme point of view, that is, spikes are deterministic or stochastic.

Chaotic viewpoint

One of the explanation for the seemingly stochastic spikes is an deterministic point of view such as “chaos”. From the “chaotic” point of view, every single spike has their meaning. The chaotic spike trains are encoded there. From the viewpoint of information theory, such a precise system may be efficient coding scheme (Softky, 1995; Stevens and Zador, 1996a; Fujii *et al.*, 1996). However, roughly speaking, any arrangements, such as temporal ensemble or population averaging of the spikes, damage the precise coding. Because the spike generation of neuron itself has chaotic property, this view of the spikes may be interesting. However, information that enters the neuronal assembly is not such a delicate one. Spike information needs robustness and should be able to be compensated.

Stochastic viewpoint

From the rough stochastic point of view, the spike variation is considered the results of the “uncorrelated” stochastic fluctuation. There are three uncorrelation factors, which

permit us to average spike events over. In order to extract the information from the spike data, which is the better assumption of the statistical independence?

Temporal averaging In classical neural network theory, the basic view of spike information can be extracted by temporal averaging of their number. It is considered that the number of the spikes which are transfered in a unit of time has information, and the spike timing and their statistical correlations does not have any meaning. This point of view is supported by the experiment of Adrian (1926) , who is the pioneering researcher of neurophysiology. Rough view of the neuronal activities can be discussed from this point of view. However, this viewpoint is extremely simplified, and does not give us how spikes are treated in neuronal information processing.

Trial averaging In the physiological studies, the trial averaging of the spikes are commonly used. This is called "peri-stimulus time histogram" (PSTH). This averaging is based on the concept that spikes are stochastic point process and does not have any correlation among trials. Only the spike generation rate at that timings has its information. This point of view also has very strong simplification. However, because the simultaneous recording of spikes from different areas is technically difficult, many physiological researcher adopt this PSTHs. According to recent experimental research (Arieli *et al.*, 1996), the neuronal responses vary a lot even when they are evoked by the same stimulus. However, by adding the response averaged over trials to the initial neuron states, the actual single response can be well approximated. This implies that the trial averaged spikes or firing probability density may be the expression of information conveyed in the neuronal network.

Population averaging The third way is to average over neuronal activities. This means that a neuron in the summed population does not have any particular information. Only the summation of the emitted spikes in the population has their information. One of the merit of this viewpoint is that it is not necessary to assume the stochastic property of spikes. Ideally, deterministic spike effects can be considered in this formalism, but actually, this point of view needs the homogeneity within the summed neurons. We have experimental evidence that neurons in the same column respond to similar stimulus. For example, neurons in the primary visual cortex are arranged in columns of cells. However, this assumption is very strong and it is hard to divide into population of neurons which have homogeneous property.

Our viewpoint of spikes

The statistical independence of spikes itself is common property of neurons. In the series of papers, Teich, Khanna, and coworkers have measured spike number distributions and the ratio of variance to mean in spike trains from primary auditory neurons

in cats. The results (Teich and Khanna 1985) were in reasonable agreement with predictions from Poisson model. Recently, Sakai *et al.* (2000) have found that an inhomogeneous Poisson process can reproduce spiking statistics of cortical neurons in prefrontal cortex of a monkey. However, some sensory information (de Ruyter van Steveninck and Bialek, 1988) and the responses to stimulus onset (Hatsopoulos *et al.*, 1998) cannot be expressed by uncorrelated spike events. It is not applicable to any cases to assume that the spikes are Poissonian. We will discuss that deterministic spike synchronization causes strong effect to the Hebbian learning in chapter 4.

Our standpoint of the neural coding problem is as follows. First, we hypothesize that the spikes are stochastic point process. The uncertainty of the coded information is converted into an reliable information by the averaging the spikes of the neuronal ensemble every time step. Because the temporal dynamics of spikes whose sampling time window is about 10 [ms] cannot be neglected (Bair and Koch, 1995), we should treat the temporal dynamics of the spike generation rate.

From the requirement of theoretical simplicity, we moreover assume that the spikes have statistical independence with each other. Namely, we assume that spikes obey an inhomogeneous Poisson process throughout this thesis. This independence assumption may be unnatural. It should be noted that the correlation, which we omit, is important. The spiking activity at stimulus onset does not show the statistical independence. However, the complex circuit of the cerebral cortex make the spikes random. Especially, the spontaneous neuronal activity among the cerebral cortex, which is seemingly stochastic, come to lose their correlation (van Vreeswijk and Sompolinsky, 1996, 1998; Kubo *et al.*, 2000).

1.3 Population coding scheme

How does the brain express information?

Based on the hypothesis we adopt, we can further tackle the problem of the information expression among neurons. In this section, we will consider the information representation by stochastic spikes based on the fact that every cortical neuron has its preferred fragment of information. Many modalities of information are expressed in the cerebral cortex. However, when we consider the limited area of the brain such as primary visual, inferior temporal or primary motor cortex, the neuron has its respective psychophysical expression axis. Difference is the modality of the input information, and the encoding and decoding framework may be uniformly discussed.

Orientation Selectivity For instance, we discuss following simple electro-physiological experiment. A monkey whose primary motor cortex neuron is measured is trained to perform the following task. The task consists of two visual stimulus. At the beginning of the experiment, the center button in front of the monkey turns on. When the monkey keeps to press the button, the center button then turns off. Simultaneously, one of the

16 surrounding button randomly selected and turn on a light. The monkey get a reward when he push the surrounding light button.

Schwartz *et al.* (1988) examined how the direction of arms in three dimensional space is expressed among the neurons in primary motor cortex. Then, they found that 475 among 538 (83.6 %) of neurons have their respective preferred direction. Moreover, depending on the difference between its preferred direction and the direction of the arm, the activity of the neuron decreases. Namely, the activity of neuron i, which can be estimated by the number of spikes, can be expressed by the preferred direction Θ_{C_i} and the direction of the arm movement direction Θ_M. The preferred orientation function, which corresponds to the estimated activity of neuron i, forms the cosine tuning curve:

$$d_i(\Theta_M) = b + k \cos \Theta_{MC_i}, \tag{1.2}$$

where $\Theta_{MC_i} = \Theta_M - \Theta_{C_i}$ is the angle between its preferred direction and the direction of the arm movement. This $d_i(\Theta_M)$ is called tuning function of neuron i. They find that the tuning function forms almost same among neurons, and obtain $b = 41.90$ [Hz], $k = 36.55$ [Hz] from the experiment. The function is illustrated in Figure 1.1.

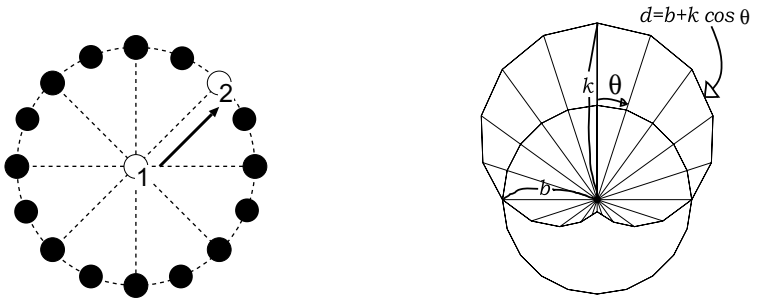

Figure 1.1: The left figure shows how the experiment is carried out. The monley was trained to keep pressing while the center button's light (1) is on, and reach the surrounding button which turns on the light (2). Right figure shows the temporally averaged activities of M1 neurons. The direction of the maximum activity denotes its preferred orientation.

They also find that the preferred directions are equally distributed among neurons. One of the important property of these neuronal activity is that the expressed information in a single neuron is not specified, and generally the neuron responds to all direction of the arm movement. The discovery of this broad tuning imply that one cannot extract the encoded information from single neurons.

Population vector

Based on the orientation selectivity of the neurons in the primary motor cortex, Gergopoulos *et al.* (1986) proposed one decoding scheme of neuronal expression using

"population vector". The "population vector" consists of the ensemble of the probabilistic neuronal activity. Namely, they consider the neurons vote for its preferred direction by the amount of its activity, and the ensemble mean of the activity express the actual command of arm movement. Then, the internal expression becomes

$$\vec{P} = \sum_{i=1}^{N} w_i(\vec{M})\vec{C}_i, \tag{1.3}$$

where $\vec{C}_i$ denotes the preferred direction of neuron i, and has a uniform absolute value. Amplitudes are defined by $w_i(\vec{M})$, which is $w_i(\vec{M}) = d_i(\vec{M}) - b$ which indicates the activity of neuron i under the arm movement $\vec{M}$. N is the number of neurons which have their preferred directions. This internal expression corresponds to the actual arm movement, including its velocity and direction, with certainty of 95 %.

This population vector approach not only imitate the command of the arm movement, but also indicate one psychological interpretation of the neuronal activity. Here, we hypothesize that this population vector is not only the interpretation of the specified experiment, but one of the candidates to explain the way of neural coding in the cerebral cortex. Subsequently, we consider that the information representation of the neuronal ensemble each of which responds to divided character of information is the coding scheme of the cerebral cortex.

1.3.1 Probabilistic model based representation

The voting of neurons for their preferred directions can be interpreted by statistical inference theory. Sanger (1994, 1996) further steps into the interpretation of Georgopoulos' theory. He tries to interpret the population coding by a stochastic model. He assumes that the spikes are generated by Poisson distribution. The spike generation probability of n spikes within time Δt is assumed to be

$$P[n \text{ spikes}|x] = (\sigma(x)\Delta t)^n \frac{e^{-\sigma(x)\Delta t}}{n!}, \tag{1.4}$$

where the Poisson intensity $\sigma(x)$ under the input x can be assumed to correspond to the tuning curve of the neuron. x depends on the psychological axis of the experiment, such as the direction of arm movement or the location of arms. Using the Bayes rule, the coded information of the neuronal activity can be decoded by

$$P[x|n \text{ spikes}] = \sigma(x)^n P[x] e^{-\sigma(x)\Delta t}/\mathrm{N}, \tag{1.5}$$

where N is the normalisation constant, and the prior $P[x]$ depends on the experiment. If the experiment equally select x, the prior becomes constant. Because we assume the neuronal activities are statistically independent, $P[\mathrm{spike}_i, \mathrm{spike}_j|x] = P[\mathrm{spike}_i|x]P[\mathrm{spike}_j|x]$, then, the conditional probability density of x for the neuronal activity becomes

$$P[x|\text{population}] = \frac{1}{N}\left(P[x] \prod_{\text{all cells}} e^{-\sigma_j(x)\Delta t}\right) \prod_{\text{firing cells}} \sigma_i(x)^{n_i}. \tag{1.6}$$

Because the posterior (certainty of x) is the product of the tuning curves of neurons in this equation, the selectivity becomes sharp as the number of neurons increases. Moreover, the standard deviation of the distribution can be interpreted as the uncertainty of the information. In order to extract the best information among the probabilistic distribution, one may use a statistical criterion such as the maximum likelihood condition or minimum squared error condition. Maximum likelihood takes the peak of the distribution, and the minimum squared error takes the mean of the distribution. This statistical interpretation produces better results than simple population vector even if measured preferred directions are not uniformly distributed or a tuning curve does not form cosine function. This statistical inference viewpoint is theoretically interesting and many researchers develop the theoretically efficient encoding and decoding scheme (Anderson and van Essen, 1994; Zemel *et al.*,1998) .

1.4 Discussion about neural coding

The population coding scheme discussed above can be summarized as follows. (1) Spikes, the information unit of the brain, can be approximated by stochastic point events. (2) A neuron has selectivity to some specified input stimulus, such as the fragment of the direction of arm movement. (3) Information in the brain is not encoded in a single spike or single neuron, but expressed by their ensemble. (4) The interaction between neuronal activities may be interpreted by statistical inference theory such as Bayes rule.

1.4.1 Remaining problems

This stochastic spike view point is natural for the interpretation of the coding scheme of the cerebral cortex, but there are many remaining problems to overcome.

One of the problems of this stochastic coding scheme is that one cannot always assume the statistical independence among spikes. deCharms and Merzenich (1996) reported the coordinated spiking activity among neurons in the primary auditory cortex, when a pure tone sound is provided to a monkey. Moreover, based on simultaneous recording of plural neurons, Hatsopoulos *et al.* (1998) reported that synchronous activity is observed on the stimulus onset in the primary motor cortex. Riehle *et al.* (1996) reported such synchronous activity is not estimated by the product of the ensemble rate and call such correlated synchrony “unitary event”. These synchronous activity may be the effect of deterministic spiking activity, which cannot be explained only by the Poisson spike assumption. Effect of the deterministic spikes to the Hebbian learning will be discussed in Chapter 4.

Second is about the temporal and dynamical aspect of the spiking activity. Using simplified conventional neural network models, many research about the dynamics in the cerebral cortex is studied (Amari, 1977; Ben-Yahsai *et al.*, 1995; and many others). However, the coding scheme which has been discussed so far is based on *rate coding*

hypothesis, and does not clearly link to the actual spiking activity of neurons.

This thesis focuses on the temporal aspect of the spike generation rate based on more realistic neuron model than conventional neural networks. The next section will discuss more reliable neuron models which can simulate the spiking activity of neurons. The motivation of this thesis is to bridge the gap between such reliable neuron models and the statistical interpretation of spikes.

1.5 Spike and Neuron models

The relationship about the stochastic neuronal activity and spike generation mechanism has not yet been discussed further. In this section, first, the precise spiking activity of neurons is discussed, and next we will seek a tractable model for stochastic spiking activity.

1.5.1 Conventional neuronal model

At the beginning, a conventional rate coding scheme is discussed. For analytical simplification, we assume that the expression of a neuronal state consists of only two stochastic value, $\sigma = 1$ (active) and $\sigma = 0$ (quiescent). We also assume that the transition probabilities from quiescent to active and from active to quiescent are $g(h)/\tau$ and $(1 - g(h))/\tau$, respectively. Here, τ is the time constant for the state transition, $g(h)$ is the transition function, and h is the internal potential. Through some theoretical discussion (noted in appendix section 1.A.1), the mean dynamics of the system becomes

$$\tau \frac{d}{dt} \langle \sigma_i(t) \rangle = - \langle \sigma_i \rangle + \langle g(h_i) \rangle \, . \tag{1.7}$$

Because $\langle g(h_i) \rangle$ is not easy to calculate, sometimes the mean field approximation is applied and we have

$$\tau \frac{d}{dt} \langle \sigma_i(t) \rangle = - \langle \sigma_i \rangle + g(\langle h_i \rangle). \tag{1.8}$$

The stational solution of equation (1.8) is

$$\nu_i(t) = g(\sum_{j=1}^{N} w_j \nu_j(t)), \tag{1.9}$$

where $\nu_i(t) = \langle \sigma_i(t) \rangle$ is the firing probability. This simplified neuron model has many merits for analytical tractability. The temporal dynamic of neuronal activity may be written by the equation (1.8). However, the parameters, such as τ, are not based on physiological fact. Only the phenomenological explanation can be done with this model. A concept of spike, which will be introduced in the next subsection, is not seen here. One of the motivation of this thesis is to find what this rate coding scheme means from the point of view of physiologically plausible neuron models.

1.5.2 Notation of spikes

Throughout this thesis, we use the mathematical formulation as follows. Formally, the spike train which is emitted by neuron j can be written by

$$S_j(t) = \sum_{f=1}^{n_j(t)} \delta(t - t_j^f), \tag{1.10}$$

where $\delta(\cdot)$ denotes the Dirac's delta function, and t_j^f is the f-th spike timing emitted by neuron j. When the spike train is provided to the post-synaptic neuron i with the delay time Δ_{ij}, the input spike train from neuron j to i can be written as

$$S_{ij}(t) = \sum_{f=1}^{n_j(t)} \delta(t - t_j^f - \Delta_{ij}). \tag{1.11}$$

Every spike causes some effect such as the membrane conductance change or potential change to the post-synaptic neuron. Using the Heaviside (step) function,

$$\mathcal{H}(s) = \begin{cases} 1, & s \geq 0 \\ 0, & s < 0 \end{cases}, \tag{1.12}$$

we can describe the effect of a single spike by causal function, $u(s)\mathcal{H}(s)$. Then, the post-synaptic effect of the spike train, $S_{ij}(s)$, becomes

$$u_{ij}(t) = \int_0^t u(s)\mathcal{H}(s)S_{ij}(s)ds = \sum_{f=1}^{n_j(t)} u(t - t_j^f - \Delta_{ij}). \tag{1.13}$$

Delays, Δ_{ij}, are sometimes omitted for simplicity. If we consider that the spikes are stochastic point process, the spike train can be written as

$$\boldsymbol{S}_j(t) = \sum_{f=1}^{\boldsymbol{n}_j(t)} \delta(t - \boldsymbol{t}_j^f), \tag{1.14}$$

where random variables are written by bold math font.

1.5.3 The Hodgkin-Huxley models

The spikes, which are generated at axon of neurons, are mathematically described by the Hodgkin-Huxley model (1952) . Their model can precisely reproduce the action potential of giant axon of squid. Most of the neurons have similar spiking property. Figure 1.2 is the hardware circuit for the Hodgkin-Huxley model. The membrane potential of axon $v(t)$ is written by

$$C_m \frac{dv(t)}{dt} = \bar{G}_{\mathrm{Na}} m^3(t) h(t) (E_{\mathrm{Na}} - v(t)) + \bar{G}_{\mathrm{K}} n^4(t) (E_K - v(t))$$

$$+G_m(V_{\rm rest} - v(t)) + I_{\rm input}(t), \tag{1.15}$$

where the reversal potentials are $E_{\rm Na} = 115$ [mV], $E_{\rm K} = -12$ [mV] and $V_{\rm rest} = 0$ [mV], and the maximal conductances are $\bar{G}_{\rm Na} = 120$ [mS/cm^2], $\bar{G}_{\rm K} = 36$ [mS/cm^2] and $G_m = 0.3$ [mS/cm^2]. The channel dynamics is voltage dependent. The dynamics of component of the potassium channel is written by

$$\frac{dn(t)}{dt} = \alpha_n(v)(1 - n(t)) - \beta_n(v)n(t), \tag{1.16}$$

where the activating and inactivating probabilities, $\alpha_n(v)$ and $\beta_n(v)$, are denoted by

$$\alpha_n(v) = (0.1 - 0.01v)/(e^{(1-0.1v)} - 1), \quad \beta_n(v) = 0.125e^{-v/80}. \tag{1.17}$$

Membrane potential of the Hodgkin-Huxley model highly affected by sodium and potassium current. The dynamics of components of the sodium channel are written by

$$\begin{aligned} \frac{dm(t)}{dt} &= \alpha_m(v)(1 - m(t)) - \beta_m(v)m(t), \\ \frac{dh(t)}{dt} &= \alpha_h(v)(1 - h(t)) - \beta_h(v)h(t), \end{aligned} \tag{1.18}$$

where the activating and inactivating probabilities are denoted by

$$\begin{aligned} \alpha_m(v) = (2.5 - 0.1v)/(e^{(2.5-0.1v)} - 1), \quad \beta_m(v) = 4e^{-v/18} \\ \alpha_n(v) = 0.07e^{0.05v}, \quad \beta_n(v) = 1/(e^{(3-0.1v)} + 1). \end{aligned} \tag{1.19}$$

Input current is usually written by

$$I_{\rm input}(t) = \sum_{j=1}^{N_E}(v(t) - E_E)\int_0^t g_E(s)S_{ij}^E(s)ds + \sum_{j=1}^{N_I}(v(t) - E_I)\int_0^t g_I(s)S_{ij}^I(s)ds, \tag{1.20}$$

where E_E and E_I are the reversal potentials of excitatory and inhibitory inputs, respectively. We set $E_E = 0$ [mV] and $E_I = 0$ [mV]. $g_E(s)$ and $g_I(s)$ are the synaptic conductances and we define by

$$g_E(s) = -g_I(s) = G_{\rm syn}e^{-\alpha s}\mathcal{H}(s) \tag{1.21}$$

where $G_{\rm syn}$ is conductance gain and α is the decay parameter. Membrane potential of the Hodgkin-Huxley model highly affected by sodium and potassium current.

Figure 1.3 is an example of the dynamics of the Hodgkin-Huxley neuron model. Input spikes are stochastically generated by Poisson process with constant rate. Spikes are almost randomly generated, but we can see sequential firings. Four sequential spikes are seen from 650 [ms] to 700 [ms]. These are called tonic firings. Moreover it is not easy to decide when spikes are generated. The definition of spiking threshold we adopt is increasing of sodium current, $p(t)$. We defined the spiking threshold where

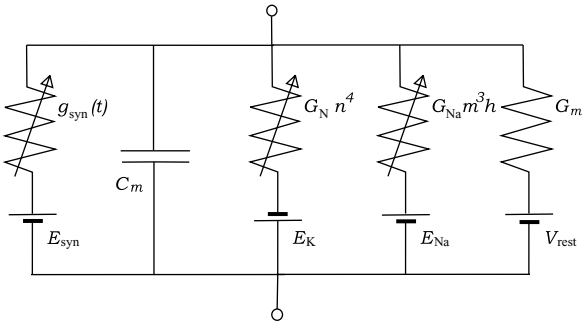

Figure 1.2: Electrical circuit for the H-H model, where a single synaptic input is provided. The membrane property can be described by the conductance change, parametrised by n, m and h.

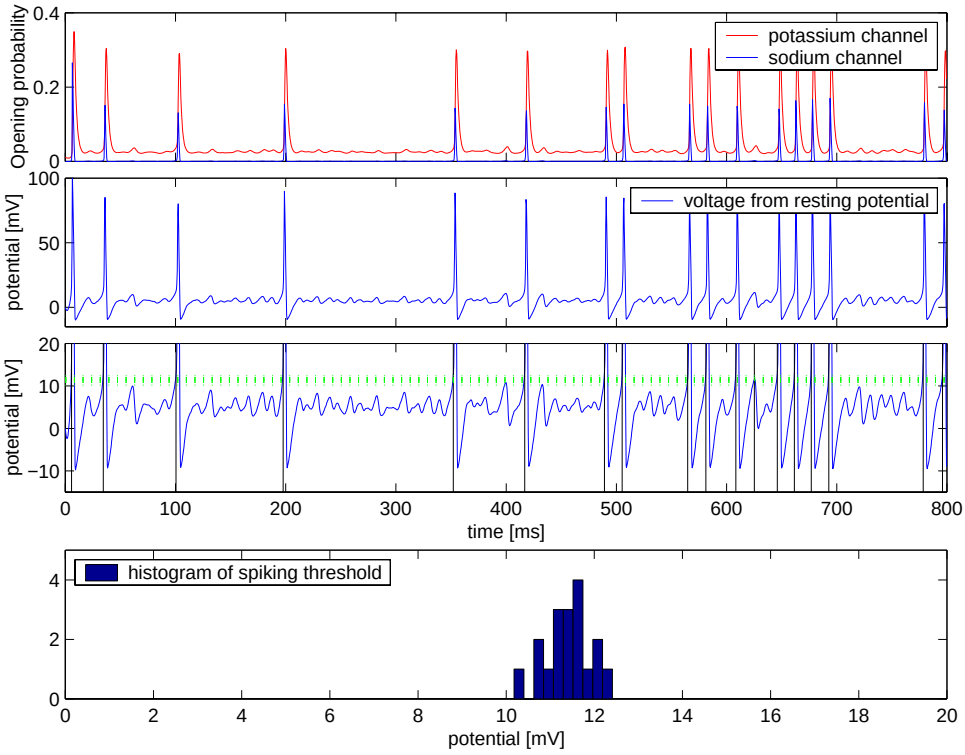

Figure 1.3: Dynamics of the Hodgkin-Huxley neuron model: In the top figure, opening probabilities of potassium and sodium channel is written. Second and third figures denote the membrane potential. In the third figure, the spiking threshold is written in dotted lines. The threshold is defined by the opening probability of sodium channel $p(t)$. We defined the threshold by the membrane potential where $p(t)$ crosses 0.004 and $\dot{p}(t) > 0$. The bottom figure is the histogram of the thresholds.

$p(t) > 0.004$ and $\dot{p}(t) > 0$. Although a spike is not generated at time 630 [ms], this definition regard this as spiking. Spiking thresholds in the bottom figure are variable. These complex phenomena are generated by sodium and potassium current, which is not easy to analyze.

Even this Hodgkin-Huxley model is not a perfect model. This model only consider a very limited area of a neuron. Many researcher devotes to produce more realistic neuron model by introducing more ion channels and considering the shape of dendritic trees.

1.5.4 Spiking neuron models

Spiking neuron model is one of the very simplified model of neurons. Conductance based models such as the Hodgkin-Huxley model have complex channel dynamics. This model assumes that the channel dynamics is expressed by the spiking threshold, and the membrane potential under the threshold is determined by the linear sum of the spike response function. Formally we define the membrane potential by

$$\begin{aligned} v_i(t) &= \sum_{j=1}^{N} \int_0^t u_j(s) S_{ij}(s) ds + \int_0^t \eta(s) S_i(s) ds \\ &= \sum_{j=1}^{N} \sum_{f=1}^{n_j(t)} u_j(t - t_j^f) + \sum_{f=1}^{n_i(t)} \eta(t - t_i^f), \end{aligned} \tag{1.22}$$

where $u(s)$ is the spike response function and $\eta(s)$ is the firing response function. The sub-threshold (under the firing threshold) membrane potential is driven by the sum of the spike response function $u(s)$. If the membrane potential reach the firing threshold θ, a spike is generated, followed by the firing response, $\eta(s)$. Since the first term of equation (1.22) correponds to the (synaptic) inputs, the term is sometimes called the excitatory post synaptic potentials (EPSPs) or inhibitory post synaptic potentials (IPSPs).

The shape of the response functions, $u(s)$ and $\eta(s)$, are free to choose. In order to correspond to integrate-and-fire neuron model, the spike response function is chosen to be exponentially rise and fall function, which will be discussed in chapter 2. Moreover, in order to correspond with the Hodgkin-Huxley model, one can choose more realistic oscillatory response function which will be discussed in chapter 5.

1.5.5 Our standpoint of neuron model

What is the best neuron model to express the brain activity? When we focus on the spike activity of neurons, rate coding model is too coarse. However, precise Hodgkin-Huxley model is too complex to analyse by stochastic process method. In this thesis, we choose the spiking neuron model as an intermediate one. Stochastic spiking neuron model can directly treat spikes, and its sub-threshold potentials are analytically solvable. Analysing the firing probability of this stochastic spiking neuron model is

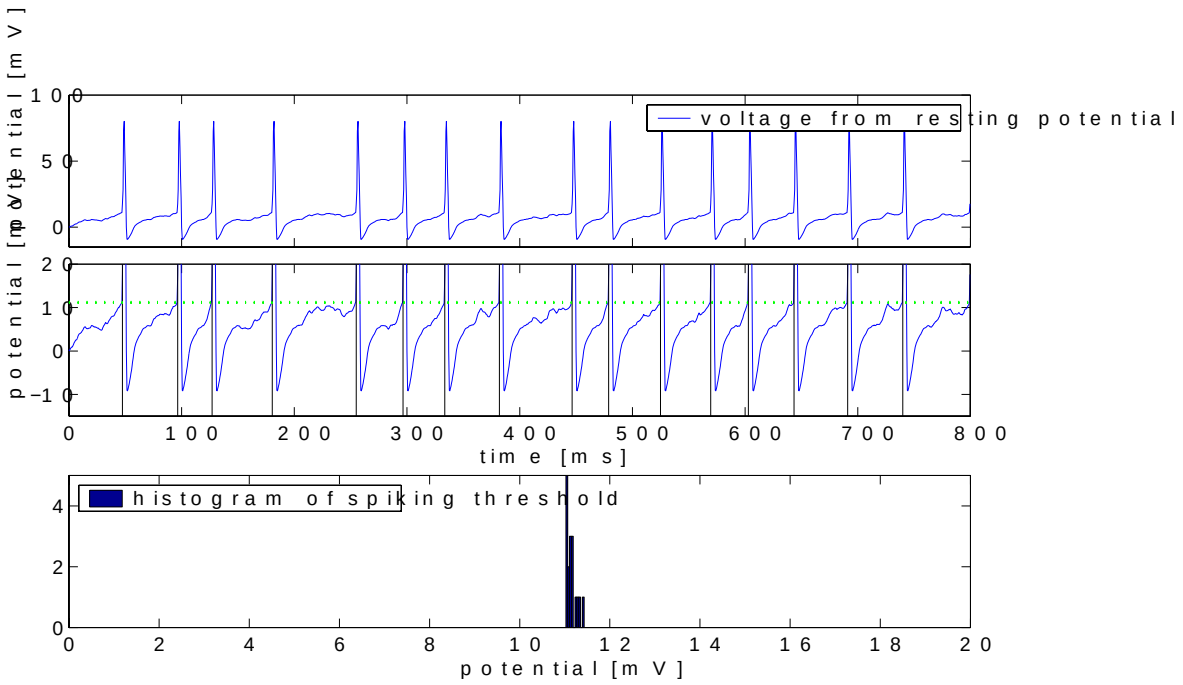

Figure 1.4: Dynamics of the spiking neuron model: The spike response function, $u(s) = q(e^{-\alpha s} - e^{-\beta s})$, is adopted for correspondence with the integrate-and-fire neuron model. $q = \beta/(\beta - \alpha)$, $\beta = 0.3$ [1/ms] and $\alpha = 0.1$ [ms]. The firing response function, $\eta(s)$, mimic the firing of the Hodgkin-Huxley neuron model. 6000 excitatory neuron whose synaptic efficacy w_E =0.15, and 1500 inhibitory inputs whose synaptic efficacy w_I =0.47, are provided. Inputs obey Poisson with intensity $\lambda = 3$ [Hz]. Top two figures denotes the dynamics of the membrane potential and the bottom figure denotes the firing threshold of this model.

very interesting theme for theoretical neuroscientists. However, satisfiable discussion about its stochastic process has not been done yet. Here, we try to present an general framework for this stochastic spiking neuron model whose input spikes obey an inhomogeneous Poisson process.

1.6 Organization of this thesis

The organization of this thesis is as follows. In chapter 2, we discuss a simple calculation method of the ensemble average and variance of the density of the stochastic spiking neuron model. Chapter 3 includes the main theme of this thesis. The dynamics of the density of the stochastic spiking neuron for general spike response function is calculated. In chapter 4, we discuss the spike-based learning, and consider how the spiking neuron can learn a precise temporal sequence. Chapter 5 focuses on the oscillatory property of the membrane potential of the Hodgkin-Huxley model. A simplified stochastic spiking neuron model that mimics the Hodgkin-Huxley model analytically reveals the resonance effect of such oscillatory neuron. We conclude this thesis by the discussion how our methods can be applied to another area of brain science and extended into neural networks in the chapter 6.

1.A Appendix

1.A.1 Rate coding model

Here, the conventional neuron model (Ginzburg and Sompolinsky 1994) is introduced. For the analytical simplification, we assume that the state of neurons consists of only two states, $\sigma = 1$ (active) and $\sigma = 0$ (quiescent). We also assume that the transition probabilities from quiescent to active and from active to quiescent are $g(h)/\tau$ and $(1 - g(h))/\tau$, respectively. Here, τ is the time constant for the state transition, $g(h)$ is the transition function, and h is the internal potential. The transition probability from state σ_i to $(1 - \sigma_i)$ is described by

$$w(\sigma_i \Rightarrow (1 - \sigma_i)) = \frac{1}{2\tau} \left\{1 - (2\sigma_i - 1)[2g(h_i) - 1]\right\}. \tag{1.A1}$$

where i is the neuron index. Generally sigmoidal function is adopted for this function, $g(h)$. The internal potential is often described by the membrane potential of neuron i, and defined by

$$h_i(t) = \sum_{j=1}^{N} w_{ij}\sigma_j(t) - \theta, \tag{1.A2}$$

where θ corresponds to spiking threshold. Here we consider the population dynamics of these spin-like neurons. The states are expressed by $(\sigma_1, \sigma_2, \ldots, \sigma_N)$. From the renewal law (1.A1), we can derive a first-order master equation. The dynamics of the state probability, $(\sigma_1, \sigma_2, \ldots, \sigma_N)$, at time t is described by

$$\begin{aligned}\frac{d}{dt}\mathcal{P}(\sigma_1, \ldots, \sigma_N, t) = &-\sum_{i=1}^{N} w(\sigma_i \Rightarrow (1 - \sigma_i))\mathcal{P}(\sigma_1, \ldots, \sigma_N, t) \\ &+ \sum_{i=1}^{N} w((1 - \sigma_i) \Rightarrow \sigma_i)\mathcal{P}(\sigma_1, \ldots, 1 - \sigma_i, \ldots, \sigma_N, t),\end{aligned} \tag{1.A3}$$

The mean dynamics of the system becomes

$$\frac{d}{dt}\langle\sigma_i(t)\rangle = \frac{d}{dt}\sum_{\{\sigma\}} \sigma_i\mathcal{P}(\{\sigma\}, t) = \sum_{\{\sigma\}} \sigma_i \frac{d}{dt}\mathcal{P}(\{\sigma\}, t), \tag{1.A4}$$

where the summation of the righthand side $\{\sigma\} = (\sigma_1, \ldots, \sigma_N)$. Substituting (1.A3) into (1.A4), we find

$$\begin{aligned}\frac{d}{dt}\langle\sigma_i(t)\rangle = &-\sum_{\{\sigma\}}\sum_{l=1}^{N} \sigma_i w(\sigma_l \Rightarrow (1 - \sigma_l))\mathcal{P}(\sigma_1, \ldots, \sigma_N, t) \\ &+ \sum_{\{\sigma\}}\sum_{l=1}^{N} \sigma_i w((1 - \sigma_l) \Rightarrow \sigma_l)\mathcal{P}(\sigma_1, \ldots, 1 - \sigma_l, \ldots, \sigma_N, t).\end{aligned} \tag{1.A5}$$

We abbreviate the notation by $w(\sigma_l) = w(\sigma_l \Rightarrow (1-\sigma_l))$ and $\{\sigma\}^l = (\sigma_1, \ldots, 1-\sigma_l, \ldots, \sigma_N)$. Considering the counting in the summation, for $\sum_{\{\sigma\}}$, $l \neq i$, we can rewrite $\sigma_i w(1-\sigma_l)\mathcal{P}(\{\sigma\}^l) = \sigma_i w(\sigma_l)\mathcal{P}(\{\sigma\})$, and for $l = i$, we can rewrite $\sigma_i w(1-\sigma_i)\mathcal{P}(\{\sigma\}^i) = (1-\sigma_i)w(\sigma_i)\mathcal{P}(\{\sigma\})$. Then equation (1.A5) becomes

$$\begin{aligned}\frac{d}{dt}\langle\sigma_i(t)\rangle &= \sum_{\{\sigma\}}\left[-\sum_{l=1}^{N}\sigma_i w(\sigma_l) + \sum_{l\neq i}^{N}\sigma_i w(\sigma_l) + (1-\sigma_i)w(\sigma_i)\right]\mathcal{P}(\sigma_1,\ldots,\sigma_N,t) \\ &= \sum_{\{\sigma\}}(1-2\sigma_i)w(\sigma_i)\mathcal{P}(\sigma_1,\ldots,\sigma_N,t) = \langle(1-2\sigma_i)w(\sigma_i)\rangle\,. \qquad \text{(1.A6)}\end{aligned}$$

Substituting (1.A1) into (1.A6) and using $\sigma_i = 0, 1$ and $\sigma_i^2 = \sigma_i$, we can describe as

$$\tau_k\frac{d}{dt}\langle\sigma_i(t)\rangle = -\langle\sigma_i\rangle + \langle\Theta(h_i)\rangle\,. \qquad \text{(1.A7)}$$

Chapter 2

Mean and Variance of Stochastic Spiking Neurons

Abstract. This chapter theoretically shows the ensemble mean and variance of the membrane potential of an integrate-and-fire neuron, when the neuron receives random spikes from the other neurons. In this model, EPSPs rise and fall continuously. Our theoretical result shows good agreement with numerical simulation.

2.1 Introduction

The firing pattern of cortical neurons can be approximated by the random Poisson process. In order to describe this phenomenon, Stein defined the neuron's membrane response function with which excitatory post-synaptic potentials (EPSPs) discontinuously rise and exponentially fall (Stein 1965). The mean and the variance for this neuron model were calculated by Tuckwell (Tuckwell 1977). In this chapter, we calculate the mean and the variance of a more realistic neuron model called integrate-and-fire neuron. EPSPs in this model rise and fall continuously. In this case, we should deal with the correlation between the rising part and falling part of a single EPSP shape.

2.2 Spiking neuron model

2.2.1 Integrate-and-fire neuron model

The membrane potential of an integrate-and-fire neuron can be defined using a hardware circuit illustrated by Figure 2.1. The circuit consists of a register R and a capacitor C. The input current to the circuit is denoted by $I(t)$. The membrane potential of this neuron, $u(t)$, is formulated by

$$I(t) = \frac{u(t)}{R} + C\frac{du(t)}{dt}. \tag{2.1}$$

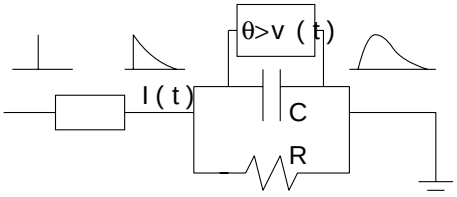

Figure 2.1: Hardware circuit for the integrate-and-fire neuron model.

Defining the membrane time constant by $\tau_m = RC$, equation (2.1) becomes

$$\tau_m \frac{du(t)}{dt} = -u(t) + RI(t). \tag{2.2}$$

An integrate-and-fire neuron emits a spike when the membrane potential exceeds the spiking threshold θ. We here consider a situation where $u(t)$ is less than θ.

The input current is described as

$$I(t) = \sum_{j=1}^{N} c_j \sum_{f=1}^{n_j(t)} \kappa(t - t_j^f), \tag{2.3}$$

where N is the number of synapses projecting to the neuron. $n_j(t)$ is the number of input spikes through synapse j until time t. c_j is the synaptic coefficient from pre-synaptic neuron j. t_j^f is the time at which the f-th pulse enters synapse j, and $\kappa(s)$ is the response function of the spike.

The response function $\kappa(s)$ is often defined by the so-called α-function:

$$\kappa_\alpha(s) = \frac{s}{\tau_s^2} \exp\left(-\frac{s}{\tau_s}\right) \mathcal{H}(s), \tag{2.4}$$

or an exponentially decaying function:

$$\kappa(s) = \frac{1}{\tau_s} \exp\left(-\frac{s}{\tau_s}\right) \mathcal{H}(s), \tag{2.5}$$

where $\mathcal{H}(s)$ is the Heaviside (step) function. τ_s is the synaptic time constant. In this chapter, we adopt the response function (2.5).

2.2.2 Spiking neuron model

From (2.2) and (2.5), the membrane potential is described as a linear ordinary differential equation:

$$\tau_m \frac{du(t)}{dt} = -u(t) + \sum_{j=1}^{N} Rc_j \sum_{f=1}^{n_j(t)} \kappa(t - t_j^f). \tag{2.6}$$

The solution of this equation is

$$u(t) = \sum_{j=1}^{N} w_j \sum_{f=1}^{n_j(t)} \epsilon(t - t_j^f), \tag{2.7}$$

where $w_j = Rc_j/\tau_m$ and

$$\begin{aligned} \epsilon(t) &= \int_0^\infty \exp\left(-\frac{s}{\tau_m}\right) \kappa(t-s) ds = \frac{1}{1-(\tau_s/\tau_m)} \left[e^{-\frac{t}{\tau_m}} - e^{-\frac{t}{\tau_s}}\right] \mathcal{H}(t) \\ &\equiv q\left(e^{-\alpha t} - e^{-\beta t}\right) \mathcal{H}(t). \end{aligned} \tag{2.8}$$

$\alpha \equiv 1/\tau_m$, $\beta \equiv 1/\tau_s$ and $q = \beta/(\beta - \alpha)$. When the membrane potential is described by a linear sum of the response function, the neuron model is called "spike response model" or "spiking neuron model" (Gerstner 1998a).

2.3 The mean and variance of single synaptic response

2.3.1 Interpretation by stochastic differential equation

We assume that the input spikes enter the neuron randomly, namely, according to the Poisson process. Each input timing can be regarded as a random variable. In the followings, random variables are represented using bold fonts. The membrane potential is described as

$$\boldsymbol{u}(t) = \sum_{j=1}^{N} w_j \sum_{f=1}^{n_j(t)} \epsilon(t - \boldsymbol{t}_j^f) \equiv \sum_{j=1}^{N} w_j \boldsymbol{u}_j(t). \tag{2.9}$$

$\boldsymbol{u}_j(t)$ defines the membrane response for the j-th synapse. In this section, we consider the statistics of this single synaptic response function $\boldsymbol{u}_j(t)$.

The number of the input spikes through synapse j until time t, $\boldsymbol{n}_j(t)$, can be described as

$$\mathcal{P}\left\{\boldsymbol{n}_j(t) = k\right\} = e^{-\lambda t} \frac{(\lambda t)^k}{k!}, \tag{2.10}$$

where λ is the frequency of the Poisson inputs. The mean and variance of the random variable $\boldsymbol{n}_j(t)$ are

$$\left\langle \boldsymbol{n}_j(t) \right\rangle = \lambda t, \tag{2.11}$$

$$\left\langle \boldsymbol{n}_j(t)^2 \right\rangle - \left\langle \boldsymbol{n}_j(t) \right\rangle^2 = \lambda t. \tag{2.12}$$

We define $\boldsymbol{r}_j(t)$ by

$$\boldsymbol{r}_j(t) = \frac{d\boldsymbol{n}_j(t)}{dt}. \tag{2.13}$$

This function can be described by the Dirac's delta function as

$$\boldsymbol{r}_j(t) = \sum_{f=1}^{n_j(t)} \delta(t - \boldsymbol{t}_j^f), \tag{2.14}$$

because the integrated value $\boldsymbol{n}_j(t)$ increases by 1 only when the input comes. The membrane potential is described as

$$\boldsymbol{u}_j(t) = \int_0^\infty ds\ \epsilon(t-s)\boldsymbol{r}_j(s). \tag{2.15}$$

Using (2.8), the membrane potential is

$$\begin{aligned} \boldsymbol{u}_j(t) &= \int_0^t ds\ q\ e^{-\alpha(t-s)}\frac{d\boldsymbol{n}_j(s)}{ds} - \int_0^t ds\ q\ e^{-\beta(t-s)}\frac{d\boldsymbol{n}_j(s)}{ds} \\ &\equiv \boldsymbol{a}_j(t) + \boldsymbol{b}_j(t). \end{aligned} \tag{2.16}$$

We set the initial condition:

$$\mathcal{P}\left\{\boldsymbol{u}_j(0) = v_0\right\} = \delta(\boldsymbol{u}_j(0) - v_0). \tag{2.17}$$

2.3.2 Calculation of the mean and variance

Now we calculate the mean and variance of the random variable $\boldsymbol{u}_j(t)$. For simplicity, we set $v_0 = 0$, and drop index j in this subsection.

Means

From the definition:

$$\boldsymbol{a}(t) = \int_0^t ds\ q\ e^{-\alpha(t-s)}\frac{d\boldsymbol{n}(s)}{ds}, \tag{2.18}$$

the stochastic differential equation,

$$\frac{d\boldsymbol{a}(t)}{dt} = -\alpha\boldsymbol{a}(t) + q\frac{d\boldsymbol{n}(t)}{dt} = -\alpha\boldsymbol{a}(t) + q\boldsymbol{r}(t). \tag{2.19}$$

is derived (Gardiner 1985). Similarly, the equation for $\boldsymbol{b}(t)$ is

$$\frac{d\boldsymbol{b}(t)}{dt} = -\beta\boldsymbol{b}(t) - q\frac{d\boldsymbol{n}(t)}{dt} = -\beta\boldsymbol{b}(t) - q\boldsymbol{r}(t). \tag{2.20}$$

Here the random variable $\boldsymbol{r}(t)$ is considered as the fluctuating force which induces the random property. The mean and variance for $\boldsymbol{r}(t)$ take certain values:

$$\begin{aligned} \langle \boldsymbol{r}(t)dt \rangle &= \langle d\boldsymbol{n}(t) \rangle = \lambda dt, \\ \left\langle [d\boldsymbol{n}(t) - \lambda dt]^2 \right\rangle &= \lambda dt. \end{aligned} \tag{2.21}$$

Defining an auxiliary random variable:

$$d\boldsymbol{y}(t) = d\boldsymbol{n}(t) - \lambda dt, \tag{2.22}$$

the stochastic differential equation for $\boldsymbol{a}(t)$ becomes

$$d\boldsymbol{a}(t) = [\lambda q - \alpha \boldsymbol{a}(t)]\, dt + q\, d\boldsymbol{y}(t). \tag{2.23}$$

Then the ensemble mean $\langle \boldsymbol{a}(t) \rangle$ obeys an ordinary differential equation:

$$\frac{d\,\langle \boldsymbol{a}(t) \rangle}{dt} \;=\; \lambda q - \alpha\,\langle \boldsymbol{a}(t) \rangle\,, \tag{2.24}$$

because $\langle d\boldsymbol{y}(t) \rangle = 0$. The solution is

$$\langle \boldsymbol{a}(t) \rangle \;=\; \frac{\lambda q}{\alpha}\left(1 - e^{-\alpha t}\right), \tag{2.25}$$

under the initial condition: $\langle \boldsymbol{a}(0) \rangle = 0$. Similarly the ensemble mean $\langle \boldsymbol{b}(t) \rangle$ obeys

$$\frac{d\,\langle \boldsymbol{b}(t) \rangle}{dt} \;=\; -\lambda q - \beta\,\langle \boldsymbol{b}(t) \rangle\,. \tag{2.26}$$

The solution is

$$\langle \boldsymbol{b}(t) \rangle \;=\; -\frac{\lambda q}{\beta}\left(1 - e^{-\beta t}\right), \tag{2.27}$$

under the initial condition: $\langle \boldsymbol{b}(0) \rangle = 0$.

Variances

The second order statistics, $\langle \boldsymbol{a}(t)^2 \rangle$ and $\langle \boldsymbol{b}(t)^2 \rangle$, are calculated here. The differential of $\langle \boldsymbol{a}(t)^2 \rangle$ is

$$\begin{aligned}
\left\langle d(\boldsymbol{a}(t))^2 \right\rangle &\equiv \left\langle (\boldsymbol{a}(t) + d\boldsymbol{a}(t))^2 - \boldsymbol{a}(t)^2 \right\rangle \\
&= 2\left\langle \boldsymbol{a}(t) d\boldsymbol{a}(t) \right\rangle + \left\langle (d\boldsymbol{a}(t))^2 \right\rangle \\
&= 2\left\langle \boldsymbol{a}(t)\left\{[\lambda q - \alpha \boldsymbol{a}(t)]\, dt + q d\boldsymbol{y}(t)\right\} \right\rangle + \left\langle \left\{[\lambda q - \alpha \boldsymbol{a}(t)]\, dt + q d\boldsymbol{y}(t)\right\}^2 \right\rangle .
\end{aligned} \tag{2.28}$$

Because

$$\left\langle d\boldsymbol{y}(t)^2 \right\rangle = \left\langle [d\boldsymbol{n}(t) - \lambda dt]^2 \right\rangle = \lambda dt, \tag{2.29}$$

the second order term $\langle d\boldsymbol{y}(t)^2 \rangle$ cannot be neglected. By neglecting the terms of order $(dt)^2$ and $dt d\eta(t)$, (2.28) becomes

$$d\langle \boldsymbol{a}(t)^2 \rangle \;=\; 2\left[\lambda q\,\langle \boldsymbol{a}(t) \rangle - \alpha \langle \boldsymbol{a}(t)^2 \rangle + \frac{q^2 \lambda}{2}\right] dt, \tag{2.30}$$

because $\langle \boldsymbol{a}(t) d\boldsymbol{y}(t) \rangle = \langle \boldsymbol{a}(t) \rangle \langle d\boldsymbol{y}(t) \rangle = 0$. Using (2.25),

$$\frac{d \langle \boldsymbol{a}(t)^2 \rangle}{dt} = -2\alpha \langle \boldsymbol{a}(t)^2 \rangle + \lambda q^2 \left[\frac{2\lambda}{\alpha} \left(1 - e^{-\alpha t} \right) + 1 \right]. \tag{2.31}$$

By setting the initial condition $\langle \boldsymbol{a}(0)^2 \rangle = 0$, the solution becomes

$$\langle \boldsymbol{a}(t)^2 \rangle = \frac{\lambda q^2}{\alpha} \left[\frac{\lambda}{\alpha} + \frac{1}{2} - \frac{2\lambda}{\alpha} e^{-\alpha t} + \left(\frac{\lambda}{\alpha} - \frac{1}{2} \right) e^{-2\alpha t} \right]. \tag{2.32}$$

The variance of $\langle \boldsymbol{a}(t) \rangle$ then becomes

$$\langle \boldsymbol{a}(t)^2 \rangle - \langle \boldsymbol{a}(t) \rangle^2 = \frac{\lambda q^2}{2\alpha} \left(1 - e^{-2\alpha t} \right). \tag{2.33}$$

Similarly we get

$$\langle \boldsymbol{b}(t)^2 \rangle - \langle \boldsymbol{b}(t) \rangle^2 = \frac{\lambda q^2}{2\beta} \left(1 - e^{-2\beta t} \right), \tag{2.34}$$

under the condition: $\langle \boldsymbol{b}(0)^2 \rangle = 0$.

The mean and variance for a single synapse

We here calculate the statistics of $\boldsymbol{u}(t) = \boldsymbol{a}(t) + \boldsymbol{b}(t)$.

The mean $\langle \boldsymbol{u}(t) \rangle$ is

$$\begin{aligned} \langle \boldsymbol{u}(t) \rangle &= \langle \boldsymbol{a}(t) + \boldsymbol{b}(t) \rangle = \langle \boldsymbol{a}(t) \rangle + \langle \boldsymbol{b}(t) \rangle \\ &= \lambda q \left[\frac{1}{\alpha} (1 - e^{-\alpha t}) - \frac{1}{\beta} (1 - e^{-\beta t}) \right]. \end{aligned} \tag{2.35}$$

The variance $\langle \boldsymbol{u}(t)^2 \rangle - \langle \boldsymbol{u}(t) \rangle^2$ is

$$\begin{aligned} \langle \boldsymbol{u}(t)^2 \rangle - \langle \boldsymbol{u}(t) \rangle^2 &= \langle \boldsymbol{a}(t)^2 \rangle - \langle \boldsymbol{a}(t) \rangle^2 + 2 \left[\langle \boldsymbol{a}(t) \boldsymbol{b}(t) \rangle - \langle \boldsymbol{a}(t) \rangle \langle \boldsymbol{b}(t) \rangle \right] \\ &+ \langle \boldsymbol{b}(t)^2 \rangle - \langle \boldsymbol{b}(t) \rangle^2. \end{aligned} \tag{2.36}$$

In order to calculate the cross-correlation $\langle \boldsymbol{a}(t) \boldsymbol{b}(t) \rangle$, we prepare the case where the spike sequence for $\boldsymbol{a}(t)$ and $\boldsymbol{b}(t)$ is the same one. In this case,

$$\begin{aligned} \langle \boldsymbol{a}(t) \boldsymbol{b}(t) \rangle &= -\left\langle \int_0^t dx \int_0^t dz \left(q e^{-\alpha(t-x)} \frac{d\boldsymbol{n}(x)}{dx} \right) \left(q e^{-\beta(t-z)} \frac{d\boldsymbol{n}(z)}{dz} \right) \right\rangle \\ &= -\int_0^t dx \int_0^t dz \left[q^2 e^{-\alpha(t-x)-\beta(t-z)} \left\langle \frac{d\boldsymbol{n}(x)}{dx} \frac{d\boldsymbol{n}(z)}{dz} \right\rangle \right] \end{aligned} \tag{2.37}$$

In the calculation of the last bracket term in (2.37), the correlated and non-correlated terms can be separated (Kempter *et al.* 1999):

$$\left\langle \frac{d\boldsymbol{n}(x)}{dx} \frac{d\boldsymbol{n}(z)}{dz} \right\rangle = \left\langle \sum_{f=1}^{n(x)} \delta(t - \boldsymbol{t}^f) \sum_{l=1}^{n(z)} \delta(t - \boldsymbol{t}^l) \right\rangle$$

$$
\begin{aligned}
&= \left\langle \sum_{f=1}^{n(x)} \delta(t-\boldsymbol{t}^f)^2 + \sum_{f=1}^{n(x)} \delta(t-\boldsymbol{t}^f) \sum_{\substack{l=1 \\ t^l \neq t^f}}^{n(z)} \delta(t-\boldsymbol{t}^l) \right\rangle \\
&= \left\langle \sum_{f=1}^{n(x)} \delta(t-\boldsymbol{t}^f)^2 \right\rangle + \left\langle \sum_{f=1}^{n(x)} \delta(t-\boldsymbol{t}^f) \right\rangle \left\langle \sum_{l=1}^{n(z)} \delta(t-\boldsymbol{t}^l) \right\rangle \quad (2.38)
\end{aligned}
$$

Then (2.37) becomes

$$
\begin{aligned}
\langle \boldsymbol{a}(t)\boldsymbol{b}(t) \rangle &= -\int_0^t dx \int_0^t dz \left[q^2 e^{-\alpha(t-x)-\beta(t-z)} \left\langle \frac{d\boldsymbol{n}(x)}{dx} \right\rangle \left\{ \delta(x-z) + \left\langle \frac{d\boldsymbol{n}(z)}{dz} \right\rangle \right\} \right] \\
&= -\int_0^t dx \; q^2 e^{-(\alpha+\beta)(t-x)} \left\langle \frac{d\boldsymbol{n}(x)}{dx} \right\rangle + \langle \boldsymbol{a}(t) \rangle \langle \boldsymbol{b}(t) \rangle . \quad (2.39)
\end{aligned}
$$

We define $\langle \boldsymbol{\Delta}(t) \rangle \equiv \langle \boldsymbol{a}(t)\boldsymbol{b}(t) \rangle - \langle \boldsymbol{a}(t) \rangle \langle \boldsymbol{b}(t) \rangle$, and it is differentiated by t. The result becomes

$$
\frac{d \langle \boldsymbol{\Delta}(t) \rangle}{dt} = -(\alpha+\beta) \langle \boldsymbol{\Delta}(t) \rangle - q^2 \left\langle \frac{d\boldsymbol{n}(t)}{dt} \right\rangle . \quad (2.40)
$$

The solution for this equation is

$$
\langle \boldsymbol{\Delta}(t) \rangle = -\frac{\lambda q^2}{\alpha+\beta}(1 - e^{-(\alpha+\beta)t}), \quad (2.41)
$$

under the initial condition: $\langle \boldsymbol{\Delta}(0) \rangle = 0$.

Accordingly, the variance of $\boldsymbol{u}(t)$ becomes

$$
\begin{aligned}
&\left\langle \boldsymbol{u}(t)^2 \right\rangle - \langle \boldsymbol{u}(t) \rangle^2 \\
&= \lambda q^2 \Big[\frac{1}{2\alpha} \left(1 - e^{-2\alpha t}\right) + \frac{1}{2\beta} \left(1 - e^{-2\beta t}\right) - \frac{2}{\alpha+\beta}(1 - e^{-(\alpha+\beta)t}) \Big]. \quad (2.42)
\end{aligned}
$$

2.4 Comparison with numerical simulation

We compare our theoretical result with a numerical simulation. In this simulation, constant values are set at $\alpha = 0.2$, $\beta = 0.3$, and $\lambda = 0.1$. The ensemble mean and variance of $\boldsymbol{u}_j(t)$ are calculated at every time using 500 samples. They fit very well as seen in Figure 2.2.

2.5 Stochastic spiking neuron model

The total response of the membrane potential of the neuron is given by (2.9). If we assume that $\boldsymbol{u}_j(t)$ is statistically independent of the response through the other synapses, and the synaptic coefficient values do not vary, i.e., $w_j = 1$, it can be estimated

$$
\boldsymbol{u}(t) \cong N \langle \boldsymbol{u}_j(t) \rangle = \frac{N\lambda\tau_m}{\tau_m - \tau_s} \left[\tau_s \left\{ e^{-\frac{t}{\tau_s}} - 1 \right\} - \tau_m \left\{ e^{-\frac{t}{\tau_m}} - 1 \right\} \right] . \quad (2.43)
$$

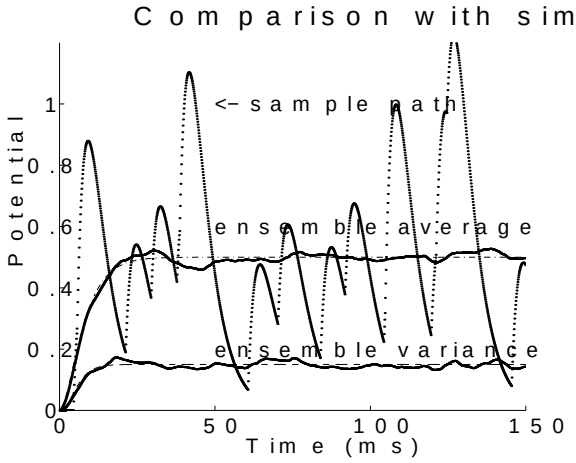

Figure 2.2: Comparison with simulation: A sample path and statistics of $\boldsymbol{u}_j(t)$. The ensemble statistics are obtained from the theoretical result and a numerical simulation in which we calculate from 500 sample paths. The theoretical results of the mean and variance are plotted by a dash-dot line and a dashed line, respectively.

Accordingly, the membrane potential of the integrate-and-fire neuron can be approximated by the following normal distribution

$$\mathcal{P}\left\{\boldsymbol{u}(t)=v\right\} \quad \cong \quad \frac{1}{\sqrt{2\pi n\sigma(t)}}\exp\left(-\frac{(v-n\left\langle \boldsymbol{u}_j(t)\right\rangle)^2}{2n\sigma(t)}\right), \tag{2.44}$$

where $\sigma(t)=\left\langle \boldsymbol{u}_j(t)^2\right\rangle-\left\langle \boldsymbol{u}_j(t)\right\rangle^2$.

2.6 Conclusion

The ensemble mean and the variance of an integrate-and-fire neuron model are calculated by using the stochastic differential equation method. This neuron model employs the response function with which the EPSPs continuously rise and fall. Such a response function has not been treated in the previous study (Tuckwell 1977). Our theoretical result shows good agreement with the numerical simulation.

Chapter 3

Firing Probability and Density of Stochastic Spiking Neurons

Abstract. This chapter presents a new theoretical framework to consider the dynamics of a stochastic spiking neuron model with general membrane response to input spike. We assume that the input spikes obey an inhomogeneous Poisson process. The stochastic process of the membrane potential then becomes a Gaussian process. When a general type of the membrane response is assumed, the stochastic process becomes a Markov-Gaussian process. We present a calculation method for the membrane potential density and the firing probability density. Our new formulation is the extension of the existing formulation based on diffusion approximation. Although the single Markov assumption of the diffusion approximation simplifies the stochastic process analysis, the calculation is inaccurate when the stochastic process involves a multiple Markov property. We find that the variation of the shape of the membrane response, which has often been ignored in existing stochastic process studies, significantly affects the firing probability. Our approach can consider the reset effect, which has been difficult to be dealt with by analysis based on the first passage time density.

3.1 Introduction

Spiking neuron models aim to describe neuronal activities based on spikes that pass through the neuron. The spike response model (Gerstner 1998) is one of the spiking neuron models. In that model, the membrane potential of a neuron is defined by the weighted summation of the post-synaptic potentials, each of which is induced by a single input spike. When the membrane potential becomes larger than a certain firing threshold, the neuron emits a spike to connecting neurons.

Stochastic nature of spikes has been suggested in recent physiological studies. The expression of cerebellum Purkinje cells is based on the ensemble rate coding, and each spike is a temporally variable stochastic event. The ensemble spike rate obtained by averaging over trial is correlated with the motor command (Shidara *et al.* 1993; Gomi *et al.*. 1998). Stochastic spikes are also seen in the cerebral cortex. Spike variability

that seemingly obeys a Poisson process is observed at low spontaneous firing rate, 2-5 Hz, and even at high firing rate up to 100 Hz (Softky and Koch 1993). In spite of this variablity, stimulus-induced spike modulation can be observed in temporal patterns of spikes averaged over trials. Spike histograms over trials are called *post-stimulus time histograms* (PSTHs). MT neurons of a behaving monkey exhibit spike modulation among background spikes of 3-4 Hz, and the modulation is almost invariant over different trials (Bair and Koch 1996). According to Arieli *et al.* (1996), the neuronal responses vary a lot even when they are evoked by the same stimulus. By adding the response averaged over trials to the initial neuron states, however, the actual single response can be well approximated. This implies that the trial averaged spikes or firing probability density may be the expression of information conveyed in the neuronal network. The physiological studies above suggest that spikes are stochastic events while their temporally variable frequency represents the temporal information. Such stochastic nature of spikes can be theoretically modeled by an *inhomogeneous* Poisson process, where the Poisson intensity corresponds to the represented information.

In this chapter, we adopt two assumptions. First, a neuron can be described by the spiking neuron model. Second, spikes input to the neuron are described by an inhomogeneous Poisson process. We consider that these two assumptions are fairly plausible especially in the cortical areas whose spike rates are low. Under these assumptions, the dynamics of the membrane potential can be expressed by a Gaussian process. Moreover, it often involves a Markov property. In this case, the dynamics can be formulated as a Markov-Gaussian process. This chapter presents a new theoretical approach to the Markov-Gaussian process, which can precisely calculate the dynamics of the membrane potential and the firing probability.

There have been many stochastic process studies dealing with integrate-and-fire neuron models. The membrane response to a single input spike is approximated as an exponentially decaying function (Stein 1967; Tuckwell 1988, 1989). The existing studies based on the diffusion approximation have also adopted the same approximation (Tuckwell and Cope 1980; Tuckwell 1989; Ricciardi and Sato 1988; many other Ornstein-Uhlenbeck process studies). This approximation significantly simplifies the stochastic process analysis. When one considers a more general type of the membrane response, however, the above-mentioned studies cannot accurately describe the dynamics of the membrane potential. This chapter discusses that the consideration of the membrane response could be important for neuronal information processing.

On the other hand, there have been studies based on the backward resolution of the Volterra integral equation (Plesser and Tanaka 1997; Burkitt and Clark 1999, 2000). These studies can deal with the general type of the membrane response. Since these studies mainly aim to calculate the first passage time density, however, they are not suitable for considering a situation where the neuron may fire many times, i.e., multiple firings. Because we assume the neuronal information is represented by the temporally variable rate, this is a flaw.

Comparing with the existing studies above, our new approach has several important advantages. First, the calculation is precise. Second, the general type of the membrane

response of the spiking neuron model can be considered. Third, multiple firings can be considered. Our approach is thus a general framework to deal with the spiking neuron model.

This chapter is organized as follows. Section **3.2** introduces the spiking neuron model. In section **3.3**, we show that the probability density of the membrane potential is described as a Markov-Gaussian process. In section **3.4**, numerical simulations are shown. The theoretical results agree very well with those by Monte-Carlo simulations. In sections **3.4.1** and **3.4.2**, we also show that the single Markov assumption, which corresponds to the diffusion approximation, is not accurate for some type of the membrane response. In section **3.4.3**, our method is extended so as to deal with the multiple firings. Section **3.5** is devoted to discussion. Section **3.5.1** suggests the importance of the general type of the membrane response. Section **3.5.2** shows the comparison between our study and the existing stochastic process studies. Section **3.6** summarizes this chapter.

3.2 Spiking neuron model

Integrate-and-fire neuron model The membrane potential of an integrate-and-fire neuron can be defined using a hardware circuit illustrated by Figure 3.1. The circuit consists of a register R and a capacitor C. The input current to the circuit is denoted by $I(t)$. The membrane potential of this neuron, $v(t)$, is formulated by $I(t) = \frac{v(t)}{R} + C\frac{dv(t)}{dt}$. Defining the membrane time constant by $\tau_m = RC$, this equation becomes

$$\tau_m \frac{dv(t)}{dt} = -v(t) + RI(t). \tag{3.1}$$

The input current is described as

$$I(t) = \sum_{j=1}^{N} c_j \sum_{f=1}^{n_j(t)} \varphi(t - t_j^f), \tag{3.2}$$

where N is the number of synapses projecting to the neuron. $n_j(t)$ is the number of spikes input through synapse j until time t. c_j is the synaptic coefficient from presynaptic neuron j. t_j^f is the time at which the f-th spike enters synapse j. The response function $\varphi(s)$ is often defined by an exponentially decaying function:

$$\varphi(s) = \frac{1}{\tau_s} \exp\left(-\frac{s}{\tau_s}\right) \mathcal{H}(s), \tag{3.3}$$

where $\mathcal{H}(s)$ is the Heaviside (step) function defined by

$$\mathcal{H}(s) = \begin{cases} 1 & (s \geq 0) \\ 0 & (s < 0) \end{cases}, \tag{3.4}$$

and τ_s is the synaptic time constant. An integrate-and-fire neuron emits a spike when the membrane potential exceeds a certain spiking threshold θ, and after that the membrane potential is reset to $v_{\rm reset} = 0$. The threshold introduces nonlinearity.

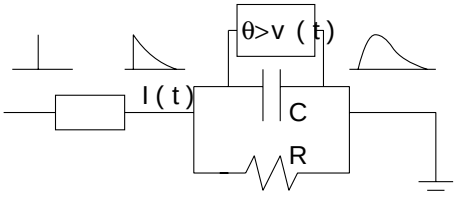

Figure 3.1: Hardware circuit for the integrate-and-fire neuron model.

Spiking neuron model The solution of (3.1), (3.2) and (3.3) becomes

$$v(t) = \sum_{j=1}^{N} w_j \sum_{f=1}^{n_j(t)} u(t - t_j^f), \tag{3.5}$$

where $w_j = Rc_j/\tau_m$ and

$$u(s) = \frac{\tau_m}{\tau_m - \tau_s}\left[\exp\Big(-\frac{s}{\tau_m}\Big) - \exp\Big(-\frac{s}{\tau_s}\Big)\right]\mathcal{H}(s) \equiv q(e^{-\alpha s} - e^{-\beta s})\mathcal{H}(s), \tag{3.6}$$

where $\alpha \equiv 1/\tau_m$ and $\beta \equiv 1/\tau_s$. $q = \beta/(\beta - \alpha)$ is the normalization term so that the integral $\int_{-\infty}^{\infty} u(s)ds$ is set to $1/\alpha = \tau_m$. $u(s)$, which is called the spike response function, defines the membrane response to a single input spike. When the membrane potential is described by a linear sum of the response function, the neuron model is called the spike response model or the spiking neuron model (Gerstner 1998) .

When $\beta \to \alpha$, function (3.6) approaches

$$u(s) = \frac{s}{\tau_m}\exp\Big(-\frac{s}{\tau_m}\Big)\mathcal{H}(s) = qse^{-\alpha s}\mathcal{H}(s), \tag{3.7}$$

which is called the alpha-function. When $\beta \to \infty$, function (3.6) approaches

$$u(s) = \exp\Big(-\frac{s}{\tau_m}\Big)\mathcal{H}(s) = qe^{-\alpha s}\mathcal{H}(s). \tag{3.8}$$

The normalization term is set at $q = 1$ for equation (3.8) and $q = \alpha$ for equation (3.7). The shapes of the response functions are shown in Figure 3.2. Both response functions, (3.7) and (3.6), are the solutions of the second order linear differential equation. In this chapter, we assume that the spike response function has the form (3.8), (3.7) or (3.6).

3.3 Density of the membrane potential for stochastic inputs

In this chapter, we examine stochastic properties of a single neuron defined by the spiking neuron model. We assume that the input spikes, $\{t_j^f | f = 1, \ldots, n_j(t)\}$, are

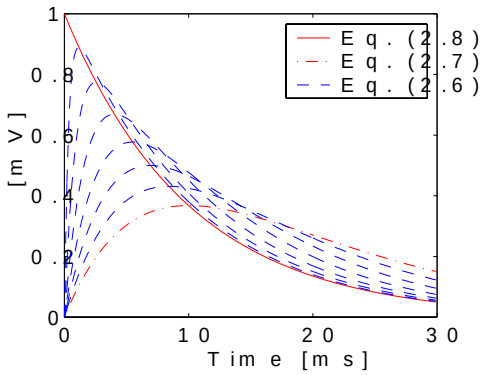

Figure 3.2: Shape of the response function $u(s)$, where $\alpha = 0.1$ [1/ms]. The solid line denotes function (3.8), and dash-dotted line denotes function (3.7). The dash lines denote function (3.6), where $\beta = 3.0, 1.0, 0.5, 0.3, 0.2$ and 0.14 [1/ms] from left to right. All of the functions are normalized so that their integrals are $1/\alpha$.

stochastic events. Subsequently, random variables are denoted by bold-math fonts. Given the spike response function $u(s)$, we examine the property of the membrane potential:

$$\boldsymbol{v}(t) = \sum_{j=1}^{N} w_j \sum_{f=1}^{\boldsymbol{n}_j(t)} u(t - \boldsymbol{t}_j^f) \equiv \sum_{j=1}^{N} w_j \boldsymbol{x}_j(t), \tag{3.1}$$

where $w_j \boldsymbol{x}_j(t)$ is the membrane response (Post-Synaptic Potential; PSP) corresponding to synapse j. This neuron generates a spike when $\boldsymbol{v}(t) > \theta$. When a spike is generated, the membrane potential is reset to $v_{\rm reset} = 0$. Sample paths of this stochastic process are shown in Figure 3.3.

3.3.1 Free membrane potential density

In this subsection, we examine the dynamics of the density of the membrane potential when the threshold is ignored. The effect of the threshold will be discussed in section **3.3.2**. We assume that the input spikes obey an inhomogeneous Poisson process. If the spike frequency, which is indicated by Poisson intensity, is large enough in comparison to the decay of the membrane potential, the density of the membrane potential can be represented by a Gaussian distribution due to the central limit theorem.

For the time being, synapse index j and transmission efficacy w_j are omitted. The probability density of the membrane response for a single synapse, $\boldsymbol{x}(t) = \sum_{f=1}^{\boldsymbol{n}(t)} u(t - \boldsymbol{t}^f)$, is described as

$$g(x^t) \;=\; \langle \delta(x^t - \boldsymbol{x}(t)) \rangle = \int_{-\infty}^{\infty} \frac{d\xi}{2\pi} \exp(\mathrm{i}\xi x^t) \Big\langle \exp\Big(-\mathrm{i}\xi \boldsymbol{x}(t)\Big) \Big\rangle, \tag{3.2}$$

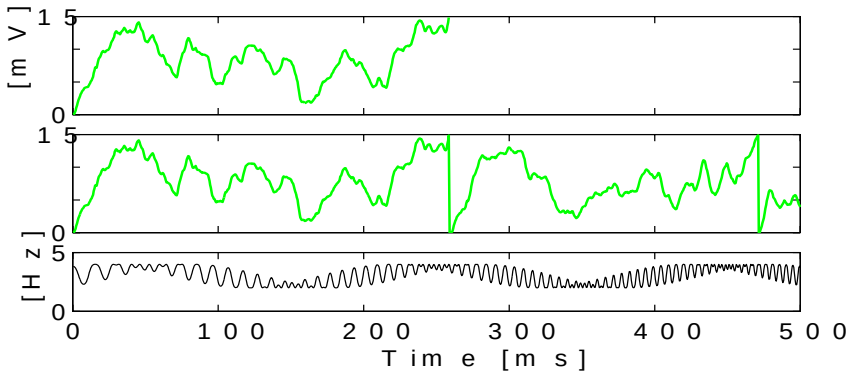

Figure 3.3: Sample paths of the membrane potential. Upper figure denotes the membrane potential when the absorbing threshold is assumed. Middle figure denotes the membrane potential when the reset after firing is considered. The input spikes obey an inhomogeneous Poisson process whose intensity is described in the lower figure. $\theta = 15$ [mV], $\alpha = 0.1$ and $\beta = 0.3$ [1/ms]. Other parameter are defined in section **3.4**.

where $\mathrm{i} = \sqrt{-1}$ and $\langle\cdot\rangle$ denotes an ensemble average over trials. Time $[0, t]$ is partitioned into intervals $[s_l, s_{l+1}]$ ($l = 0, \ldots, T-1$) whose period is Δs; namely, $s_l = l\Delta s$, $s_0 = 0$, and $s_T = T\Delta s = t$. If the time step Δs is small enough, the change of the membrane response at time t, which is caused by the spikes input within $[s_l, s_{l+1}]$, can be approximated as $\Delta \boldsymbol{x}^l(t) \approx u(t - s_l)\Delta \boldsymbol{n}_l$. Here, $\Delta \boldsymbol{n}_l$ denotes the number of spikes input within $[s_l, s_{l+1}]$. Then, the membrane response $\boldsymbol{x}(t)$ can be described by the summation of statistically independent random variables $\{\Delta \boldsymbol{x}^l(t) | l = 0, \ldots, T-1\}$, and the characteristic function of $\boldsymbol{x}(t)$ becomes

$$\Big\langle \exp\Big(-\mathrm{i}\xi \boldsymbol{x}(t)\Big)\Big\rangle \approx \prod_{l=0}^{T-1} \Big\langle \exp\Big(-\mathrm{i}\xi u(t - s_l)\Delta \boldsymbol{n}_l\Big)\Big\rangle = \exp\Big(\sum_{l=0}^{T-1} \ln\Big\langle \exp\Big(-\mathrm{i}\xi u(t - s_l)\Delta \boldsymbol{n}_l\Big)\Big\rangle\Big)$$
$$= \exp\Big(-\mathrm{i}\xi \sum_{l=0}^{T-1} u(t - s_l)\langle \Delta \boldsymbol{n}_l\rangle - \frac{\xi^2}{2} \sum_{l=0}^{T-1} u^2(t - s_l)(\langle \Delta \boldsymbol{n}_l^2\rangle - \langle \Delta \boldsymbol{n}_l\rangle^2) + O(\xi^3)\Big). \tag{3.3}$$

Denoting the Poisson intensity at time s by $\lambda(s)$, we obtain $\langle \Delta \boldsymbol{n}_l\rangle \approx \lambda(s_l)\Delta s$ and $\langle \Delta \boldsymbol{n}_l^2\rangle - \langle \Delta \boldsymbol{n}_l\rangle^2 \approx \lambda(s_l)\Delta s$. The mean and the variance are given by

$$\eta^o(t) = \int_0^t u(t - s)\lambda(s)ds, \quad (\sigma^o)^2(t) = \int_0^t u^2(t - s)\lambda(s)ds. \tag{3.4}$$

The spike response $u(t)$ decays with $\alpha = 1/\tau_m$. When $10^{-3}\lambda(t)\tau_m \gg 1$,[2] a number of spike responses are accumulated within their decay time τ_m. In this case, the density of the membrane potential can be well estimated by a Gaussian distribution due to the

[2]The coefficient 10^{-3} is added because $\lambda(t)$ has unit [Hz] and τ_m has unit [ms].

central limit theorem; namely, the components of $O(\xi^3)$ can be omitted. Then, we obtain the following equation for $\Delta s \to 0$:

$$g(x^t) = \int_{-\infty}^{\infty} \frac{d\xi}{2\pi} \exp\Big(\mathrm{i}\xi x^t - \mathrm{i}\xi\eta^o(t) - \frac{\xi^2}{2}(\sigma^o)^2(t)\Big) = \frac{1}{\sqrt{2\pi(\sigma^o)^2(t)}} \exp\Big[-\frac{(x^t - \eta^o(t))^2}{2(\sigma^o)^2(t)}\Big] \quad (3.5)$$

When the input spikes are statistically independent with respect to the synapse indices j, the density of the integrated membrane potential becomes

$$g(v^t) = \frac{1}{\sqrt{2\pi\sigma^2(t)}} \exp\Big[-\frac{(v^t - \eta(t))^2}{2\sigma^2(t)}\Big], \quad \eta(t) = \sum_{j=1}^{N} w_j \eta_j^o(t), \quad \sigma^2(t) = \sum_{j=1}^{N} (w_j)^2 (\sigma_j^o)^2(t). \quad (3.6)$$

$\eta_j^o(t)$ and $(\sigma_j^o)^2(t)$ are the mean and the variance of the j-th membrane response evoked by the j-th synapse whose input spike intensity is $\lambda_j(t)$. They are given similarly to (3.4).

When the spikes are independent with respect to the synapse index j, the condition of a Gaussian distribution can be written as $10^{-3}\sum_{j=1}^{N} \lambda_j(t)\tau_m \gg 1$. Even if the input intensity $\lambda_j(t)$ is small in comparison to the decay constant $\alpha = 1/\tau_m$, the density becomes a Gaussian distribution for large number of synapses. This corresponds to the well-known Gaussian approximation (Burkitt and Clark 1999).

3.3.2 Membrane potential density with threshold

In this subsection, we examine the density of the membrane potential when the absorbing threshold is assumed; namely, once the membrane potential reaches the threshold, the sample is removed from the density.

It is assumed that the neuron behaviors are observed at every Δt time step, namely, along a discretized time sequence $\{t_0 = 0, t_1 = \Delta t, \ldots, t_m = m\Delta t = t\}$, where Δt is sufficiently small time-interval. Our description approaches that of the continuous-time stochastic process as $\Delta t \to 0$. This will be discussed in appendix section **3.A.4**. We denote the membrane potential at time t as v^t. For expression simplicity, v^{t_m} is abbreviated as v^m, and let the sequence of variables, $\{v^m, \ldots, v^1\}$, be denoted as $\{v\}_1^m$.

Time evolution of the membrane potential before firing

The time evolution of the neuron ensemble can be determined by the joint probability density

$$g(\{v\}_1^m) \equiv \langle \delta(v^m - \boldsymbol{v}(t_m)) \ldots \delta(v^1 - \boldsymbol{v}(t_1)) \rangle \quad (3.7)$$

of the membrane potential. The density is decomposed as

$$g(\{v\}_1^m) = g(v^m | \{v\}_1^{m-1}) g(v^{m-1} | \{v\}_1^{m-2}) \ldots g(v^1), \quad (3.8)$$

where $g(v^m|\{v\}_1^{m-1}) = g(\{v\}_1^m)/g(\{v\}_1^{m-1})$ is the conditional probability density of the membrane potential, which is subsequently called the transition probability density.

Let $g_0(v^m)$ be the density at time t_m, whose neuron samples have not fired until time t_{m-1}. Then, $g_0(v^m)$ becomes

$$g_0(v^m) = \int_{-\infty}^{\theta} dv^{m-1} \dots \int_{-\infty}^{\theta} dv^1 g(v^m|\{v\}_1^{m-1}) g(v^{m-1}|\{v\}_1^{m-2}) \dots g(v^1). \quad (3.9)$$

By using $g_0(v^m)$, the density whose samples have not fired until time t_m is given by

$$g_u(v^m) = \begin{cases} 0 & v^m \geq \theta \\ g_0(v^m) & v^m < \theta \end{cases} . \quad (3.10)$$

The density whose sample have fired until time t_m is given by

$$g_f(v^m) = g(v^m) - g_u(v^m). \quad (3.11)$$

The relation of the densities are illustrated in Figure 3.4. Density $g(v^m)$, which is the free density in the absence of the threshold, always forms a Gaussian distribution. The probability that the neuron sample for the first time fires at time t_m is given by

$$\rho(t_m) = \int_{\theta}^{\infty} g_0(v^m) dv^m. \quad (3.12)$$

$\psi(t) \equiv \rho(t)/\Delta t$ is called the first passage time density. This threshold effect in the continuous time is discussed at **3.A.4**.

Transition probability densities

In order to obtain the density before firing (3.9) or (3.10), we need the transition probability density $g(v^m|\{v\}_1^{m-1})$ in each time step. Here, we develop the method which incrementally calculates the transition probability density.

Joint probability density Since the transition probability density is given by the joint probability density as $g(v^m|\{v\}_1^{m-1}) = g(\{v\}_1^m)/g(\{v\}_1^{m-1})$, we first consider $g(\{v\}_1^m)$. If $\lambda(t)$ and t_m are not small, the joint probability density can be well approximated by a Gaussian distribution:

$$g(\{v\}_1^m) = \frac{1}{\sqrt{(2\pi)^m |\Sigma^m|}} \exp\left(-\frac{1}{2}(\vec{v} - \vec{\eta})'(\Sigma^m)^{-1}(\vec{v} - \vec{\eta})\right), \quad (3.13)$$

where $\vec{v} = (v^1, \dots, v^m)'$ and $\vec{\eta} = (\eta(t_1), \dots, \eta(t_m))'$. Prime ($'$) denotes a transpose. $\eta(t_m)$ is the mean of $\boldsymbol{v}(t_m)$, which is given by (3.6). $\Sigma^m \equiv (\Sigma_{kl}^m)$ is an m-by-m autocorrelation matrix of $\vec{v}$, whose components are $\Sigma_{kl}^m \equiv \langle \boldsymbol{v}(t_k)\boldsymbol{v}(t_l)\rangle - \langle \boldsymbol{v}(t_k)\rangle\langle \boldsymbol{v}(t_l)\rangle$. Equation (3.13) is derived in appendix section **3.A.1**. When the joint probability density is represented by a Gaussian distribution, the stochastic process is called a Gaussian process.

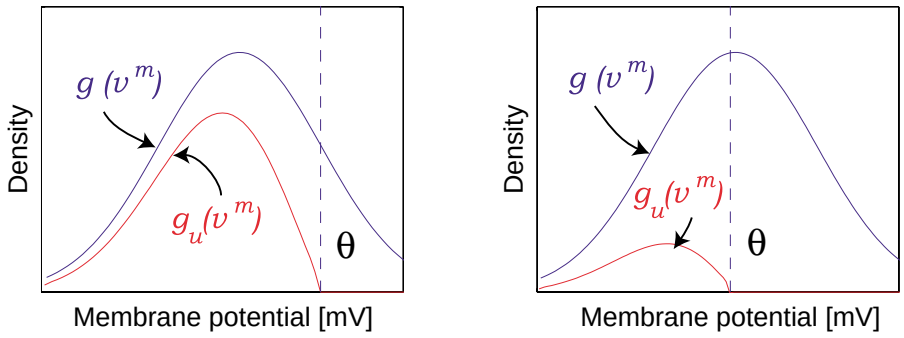

Figure 3.4: Density of the membrane potential at time t_m. $g(v^m)$ is the density of the membrane potential ignoring the threshold, where v^m is the membrane potential at time t_m. $g_u(v^m)$ is the density of the membrane potential with the threshold. $g_f(v^m) = g(v^m) - g_u(v^m)$ is the density of the membrane potential which has already fired. It should be noted that $g_u(v^m)$ is continuously zero at θ when $\Delta t \to 0$. Left: the case in which threshold θ is high in comparison to mean $\eta(t_m)$ of the free density $g(v^m)$. Right: the case in which threshold θ is relatively low.

Time evolution of Gaussian process $(\Sigma^m)^{-1}$ can be incrementally calculated as follows. Because the synaptic inputs are statistically independent of each other, Σ^m_{kl} can be described by the weighted summation of the auto-correlation of single synaptic inputs. Namely,

$$\Sigma^m_{kl} = \sum_{j=1}^{N} w_j^2 \int_0^{\min(t_k,t_l)} u(t_k - s)u(t_l - s)\lambda_j(s)ds. \tag{3.14}$$

For simplicity, we discuss the case where the input intensity is common for all of the synapses. In this case,

$$\Sigma^m_{kl} = w^2 \int_0^{\min(t_k,t_l)} u(t_k - s)u(t_l - s)\lambda(s)ds, \tag{3.15}$$

where $w = \sqrt{\sum_{j=1}^{N} w_j^2}$. In order to see the time evolving characteristics of the auto-correlation matrix Σ^m, its incremental (recursive) definition along the discretized time sequence $\{t_1, \ldots, t_m\}$ is derived here. At time t_m, Σ^m is an m-by-m matrix.

$$\Sigma^m_{kl} = w^2 \sum_{n=1}^{\min(k,l)} u(t_k - t_n)u(t_l - t_n)\lambda(t_n)\Delta t. \tag{3.16}$$

Because Σ^m is symmetric and positive definite, it can be decomposed into $(U^m)'U^m$, where $U^m = (u_{kl})$ is an upper triangular matrix. From equation (3.16), the components of U^m are described as

$$u_{kl} = \begin{cases} w \cdot u(t_l - t_k)\sqrt{\lambda(t_k)\Delta t} & k \le l \\ 0 & k > l. \end{cases} \tag{3.17}$$

Later we will see that these components are important for describing the time evolution of the Gaussian process. By using U^{m-1} and $\boldsymbol{u}^m \equiv (u_{1m}, \ldots, u_{m-1\ m})'$, U^m can be obtained as

$$U^m = \begin{pmatrix} U^{m-1} & \boldsymbol{u}^m \\ \mathbf{0}' & u_{mm} \end{pmatrix}, \tag{3.18}$$

where $\mathbf{0} = (0, \ldots, 0)'$ whose dimension is $m-1$. Let $\Gamma^m \equiv (\Gamma^m_{kl})$ be the inverse of U^m, which is given by

$$\Gamma^m = \begin{pmatrix} \Gamma^{m-1} & -\dfrac{1}{u_{mm}}(\Gamma^{m-1}\boldsymbol{u}^m) \\ \mathbf{0}' & \dfrac{1}{u_{mm}} \end{pmatrix}. \tag{3.19}$$

The m-th column of Γ^m is constructed by the Gram-Schmidt orthogonalization. The inverse of Σ^m is then given by

$$(\Sigma^m)^{-1} = \Gamma^m(\Gamma^m)' = \begin{pmatrix} \Gamma^{m-1}(\Gamma^{m-1})' + \dfrac{(\Gamma^{m-1}\boldsymbol{u}^m)(\Gamma^{m-1}\boldsymbol{u}^m)'}{(u_{mm})^2} & -\dfrac{1}{(u_{mm})^2}(\Gamma^{m-1}\boldsymbol{u}^m) \\ -\dfrac{1}{(u_{mm})^2}(\Gamma^{m-1}\boldsymbol{u}^m)' & \dfrac{1}{(u_{mm})^2} \end{pmatrix}. \tag{3.20}$$

Equation (3.20) introduces an incremental calculation of the inverse of the auto-correlation matrix, $(\Sigma^m)^{-1}$, along the time sequence.

When one of the response functions, (3.8), (3.7), or (3.6), is used, the inverse auto-correlation matrix $(\Sigma^m)^{-1}$ becomes simple. This simplicity also implies that the transition probability density is strictly determined by a multiple Markov process along the discretized time sequence. The order of this Markov process for each response function is discussed in appendix section **3.A.2**.

Transition probability density We obtain the transition probability density of the Gaussian process. From equation (3.13), the transition probability density $g(v^m|\{v\}_1^{m-1}) = g(\{v\}_1^m)/g(\{v\}_1^{m-1})$ becomes

$$\begin{aligned} g(v^m|\{v\}_1^{m-1}) &= \frac{1}{\sqrt{2\pi|\Sigma^m|/|\Sigma^{m-1}|}} \exp\left(-\frac{1}{2}\sum_{i=1}^{m}\sum_{j=1}^{m}\zeta_{ij}^m\omega^i\omega^j - \frac{1}{2}\sum_{i=1}^{m-1}\sum_{j=1}^{m-1}\zeta_{ij}^{m-1}\omega^i\omega^j\right) \\ &= \frac{1}{\sqrt{2\pi\gamma^m}} \exp\left(-\frac{\left(\omega^m - \sum_{i=1}^{m-1}\kappa_i^m\omega^k\right)^2}{2\gamma^m}\right), \end{aligned} \tag{3.21}$$

where $(\zeta_{ij}^m) \equiv (\Sigma^m)^{-1}$ and $\omega^i \equiv v^i - \eta(t_i)$. From (3.19) and (3.20), the conditional variance γ^m and the correlation coefficient κ_i^m are given by

$$\gamma^m = \frac{|\Sigma^m|}{|\Sigma^{m-1}|} = (u_{mm})^2, \quad \kappa_i^m = (u_{mm})^2\zeta_{im}^m. \tag{3.22}$$

In the general case, an incremental calculation along the time sequence is necessary for obtaining ζ_{im}^{m} in (3.22). If we can assume a Markov property, however, the calculation becomes drastically simplified, as will be discussed below.

3.3.3 Markov property

When the spiking neuron model employs the spike response function (3.8), (3.7) or (3.6), the transition probability density of the neuron ensemble has a Markov property. This feature is discussed in appendix section **3.A.2**. If we know that the stochastic process has an n-ple Markov property, the transition probability density is theoretically given as follows.

Time evolution of multiple Markov process

If the conditional probability density has an n-ple Markov property, $g(v^m|\{v\}_1^{m-1}) = g(v^m|\{v\}_{m-n}^{m-1})$. Under this assumption, $g_0(v^m)$ is given by

$$g_0(v^m) = \int_{-\infty}^{\theta} dv^{m-1} \int_{-\infty}^{\theta} dv^{m-2} \ldots \int_{-\infty}^{\theta} dv^1 g(v^m|\{v\}_{m-n}^{m-1}) g(v^{m-1}|\{v\}_{m-n-1}^{m-2}) \\ \ldots g(v^{n+1}|\{v\}_1^n) g(\{v\}_1^n). \tag{3.23}$$

Let $g_0(\{v\}_{m-n}^{m-1})$ be the joint probability density between t_{m-n} and t_{m-1}, whose sample has not reached the threshold until time t_{m-n}. Then,

$$g_0(\{v\}_{m-n}^{m-1}) \equiv \int_{-\infty}^{\theta} dv^{m-n-1} \ldots \int_{-\infty}^{\theta} dv^1 g(\{v\}_1^{m-1}). \tag{3.24}$$

$g_0(\{v\}_{m-n}^{m-1})$ can be incrementally calculated by

$$g_0(\{v\}_{m-n+1}^{m}) = \int_{-\infty}^{\theta} dv^{m-n} g(v^m|\{v\}_{m-n}^{m-1}) g_0(\{v\}_{m-n}^{m-1}). \tag{3.25}$$

From (3.23) and (3.24), $g_0(v^m)$ is given by the n-dimensional integral:

$$g_0(v^m) = \int_{-\infty}^{\theta} dv^{m-1} \ldots \int_{-\infty}^{\theta} dv^{m-n} g(v^m|\{v\}_{m-n}^{m-1}) g_0(\{v\}_{m-n}^{m-1}). \tag{3.26}$$

The firing probability at time t_m is given by

$$\rho(t_m) = \int_{\theta}^{\infty} g_0(v^m) dv^m. \tag{3.27}$$

For examples, two special cases are described below.

Markov process Under the Markov property $g(v^m|\{v\}_1^{m-1}) = g(v^m|v^{m-1})$, density $g_0(v^m)$ is calculated by very simple equations:

$$g_0(v^1) = g(v^1); \quad g_0(v^m) = \int_{-\infty}^{\theta} g(v^m|v^{m-1}) g_0(v^{m-1}) dv^{m-1} \quad (m = 2, 3 \ldots) \tag{3.28}$$

If we can calculate $g(v^m|v^{m-1})$, which will be discussed in section **3.3.3**, we obtain the firing probability density from (3.27) and (3.28).

Double Markov process Under the double Markov property $g(v^m|\{v\}_1^{m-1}) = g(v^m|\{v\}_{m-2}^{m-1})$, density $g_0(v^m)$ is calculated by equations:

$$\begin{aligned} g_0(v^1) = g(v^1),\ g_0(v^2) = \int_{-\infty}^{\theta} g(v^2, v^1)dv^1,\ g_0(v^2, v^1) = g(v^2, v^1); \\ g_0(v^m) = \int_{-\infty}^{\theta}\int_{-\infty}^{\theta} g(v^m|v^{m-1}, v^{m-2})g_0(v^{m-1}, v^{m-2})dv^{m-1}dv^{m-2}, \\ g_0(v^m, v^{m-1}) = \int_{-\infty}^{\theta} g(v^m|v^{m-1}, v^{m-2})g_0(v^{m-1}, v^{m-2})dv^{m-2}, \quad (m = 3, 4\ldots). \end{aligned} \tag{3.29}$$

Firing probability of Markov-Gaussian process

We have seen that the transition probability density of the Gaussian process is given by a Gaussian distribution (3.21). Here, we see how equation (3.21) is simplified under the Markov property. If an n-ple Markov process is assumed, $\kappa_i^m = 0$ ($i = 1, \ldots, m-n$). In this case, the transition probability density is described by $\lambda(t_m)$, u_{mm},..., $u_{m-n\,m}$, and $\eta(t_m)$, ..., $\eta(t_{m-n})$. Namely, the transition probability density is determined by the present intensity and the membrane properties for the previous n steps.

Markov-Gaussian process In the Markov-Gaussian process, the transition probability density $g(v^m|v^{m-1})$ is calculated as

$$g(v^m|v^{m-1}) = \frac{1}{\sqrt{2\pi\gamma^m}}\exp\left(-\frac{\left(\omega^m - \kappa_{m-1}^m\omega^{m-1}\right)^2}{2\gamma^m}\right), \tag{3.30}$$

where $\omega^m = v^m - \eta(t_m)$, and γ^m and κ_{m-1}^m are simply obtained from (3.20) as

$$\gamma^m = (u_{mm})^2,\ \ \kappa_{m-1}^m = \frac{u_{m-1\,m}}{u_{m-1\,m-1}}. \tag{3.31}$$

The definition of u_{kl} is given by (3.17). The firing probability is determined by equations (3.27) and (3.28) as

$$\begin{aligned} \rho(t_m) &= \int_{\theta}^{\infty} dv^m \int_{-\infty}^{\theta} g(v^m|v^{m-1})g_0(v^m)dv^{m-1} \\ &= \int_{-\infty}^{\theta} \frac{1}{2}\mathrm{erfc}\left(\frac{\theta - \eta(t_m) - \kappa_{m-1}^m\omega^{m-1}}{\sqrt{2\gamma^m}}\right)g_0(v^{m-1})dv^{m-1}, \end{aligned} \tag{3.32}$$

where $\mathrm{erfc}(x) = 1 - \frac{2}{\sqrt{\pi}}\int_0^x e^{-y^2}dy$ and $g_0(v^{m-1})$ is incrementally calculated by using equations (3.28) and (3.30). Although we cannot avoid the numerical integration for v^{m-1}, this integration does not cost much computation.

Double Markov-Gaussian process In the double Markov-Gaussian process, the transition probability density $g(v^m|v^{m-1}, v^{m-2})$ is calculated as

$$g(v^m|v^{m-1}, v^{m-2}) = \frac{1}{\sqrt{2\pi\gamma^m}} \exp\left(-\frac{\left(\omega^m - \kappa^m_{m-1}\omega^{m-1} - \kappa^m_{m-2}\omega^{m-2}\right)^2}{2\gamma^m}\right) \quad (3.33)$$

where $\omega^m = v^m - \eta(t_m)$, and κ^m_{m-1} and κ^m_{m-2} are theoretically obtained from equation (3.20) as

$$\kappa^m_{m-1} = \frac{u_{m-1\,m}}{u_{m-1\,m-1}}, \quad \kappa^m_{m-2} = \frac{u_{m-2\,m}}{u_{m-2\,m-2}} - \frac{u_{m-2\,m-1}u_{m-1\,m}}{u_{m-2\,m-2}u_{m-1\,m-1}}, \quad (3.34)$$

and $\gamma^m = (u_{mm})^2$. The firing probability is given by

$$\begin{aligned}\rho(t_m) &= \int_\theta^\infty dv^m \int_{-\infty}^\theta dv^{m-1} \int_{-\infty}^\theta dv^{m-2} g(v^m|v^{m-1}, v^{m-2}) g_0(v^{m-1}, v^{m-2}) \\ &= \int_{-\infty}^\theta \int_{-\infty}^\theta \frac{1}{2}\mathrm{erfc}\left(\frac{\theta - \eta(t_m) - \kappa^m_{m-1}\omega^{m-1} - \kappa^m_{m-2}\omega^{m-2}}{\sqrt{2\gamma^m}}\right) g_0(v^{m-1}, v^{m-2}) dv^{m-1} dv^{m-2},\end{aligned} \quad (3.35)$$

where $g_0(v^{m-1}, v^{m-2})$ is incrementally calculated by equations (3.29) and (3.33). This numerical integration is fairly expensive. The simplification of the integration is discussed in section **3.4.2**

It should be noted that under the Markov assumption there is no need for the incremental calculation of (3.20).

3.4 Examples of stochastic spiking neuron models

As a simplified model of the cerebral cortex, we consider a network of excitatory and inhibitory neurons. The number of excitatory inputs and inhibitory inputs are set at $N_E = 6000$ and $N_I = 1500$, respectively. We also set the synaptic efficacy values to be the same within each of the excitatory and inhibitory input groups, and they are given by $w_E = 0.21$ and $w_I = 0.63$, respectively. These experimental conditions follow Amit and Brunel (1997b). Total weight w, which is defined in section **3.3.2**, is $w^2 = N_E w_E^2 + N_I w_I^2$.

We compare the results obtained by our method with those of the Monte-Carlo simulation. As an example for the inhomogeneous Poisson process, we assume that the Poisson intensity $\lambda(t)$ [Hz] changes with time according to

$$\lambda(t) = \lambda_0 + \lambda \sin\left(2\pi(t+\tau)/\tau + \sin\left((2\pi(t+\tau)/\tau)^2\right)\right), \quad (3.36)$$

where $\lambda_0 = 3.0$ [Hz], $\lambda = 1.0$ [Hz] and $\tau = 0.2$[s]. The numerical calculation is done with the time step $\Delta t = 0.5$ [ms].

3.4.1 Variation of the synaptic time constant and the firing threshold

This subsection shows application results of our method to the spike response functions (3.8), (3.7) and (3.6). Since these response functions imply the Markov or double Markov property, the calculation becomes very simple. γ^m and κ_i^m, whose definitions are given by (3.31) or (3.34), are theoretically given in very simple forms. Moreover, κ_i^m becomes constant. Then, the transition probability density depends only on $\lambda(t)$ and $\eta(t)$.

Case 1: Equation (3.8), i.e., $u(s) = qe^{-\alpha s}\mathcal{H}(s)$. In this case, the Markov assumption can be adopted (see appendix **3.A.2**). From (3.17) and (3.31), the correlation coefficient is $\kappa_{m-1}^m = e^{-\alpha\Delta t}$, and the conditional variance is $\gamma^m = w^2q^2\lambda(t_m)\Delta t$. The result obtained by the calculation of equations (3.28), (3.30) and (3.32), and its comparison to that by the Monte-Carlo simulation are shown in Figure 3.5. Our method exhibits very good agreement with the Monte-Carlo simulation.

Case 2: Equation (3.7), i.e., $u(s) = qse^{-\alpha s}\mathcal{H}(s)$. In this case, the double Markov assumption can be adopted (see appendix section **3.A.2**). From (3.A9) and (3.34), the correlation coefficients are given by $\kappa_{m-1}^m = 2e^{-\alpha\Delta t}$ and $\kappa_{m-2}^m = -e^{-2\alpha\Delta t}$. The conditional variance is $\gamma^m = w^2q^2e^{-2\alpha\Delta t}\lambda(t_m)(\Delta t)^3$.

Case 3: Equation (3.6), i.e., $u(s) = q(e^{-\alpha s} - e^{-\beta s})\mathcal{H}(s)$. In this case, the double Markov assumption can be adopted (see appendix section **3.A.2**). From (3.A9) and (3.34), the correlation coefficients (3.34) are given by

$$\kappa_{m-1}^m = \frac{e^{-2\alpha\Delta t} - e^{-2\beta\Delta t}}{e^{-\alpha\Delta t} - e^{-\beta\Delta t}}, \quad \kappa_{m-2}^m = \frac{e^{-3\alpha\Delta t} - e^{-3\beta\Delta t}}{e^{-\alpha\Delta t} - e^{-\beta\Delta t}} - \left(\frac{e^{-2\alpha\Delta t} - e^{-2\beta\Delta t}}{e^{-\alpha\Delta t} - e^{-\beta\Delta t}}\right)^2 \quad (3.37)$$

The conditional variance is $\gamma^m = w^2q^2(e^{-\alpha\Delta t} - e^{-\beta\Delta t})^2\lambda(t_m)\Delta t$. Calculation of equations (3.29), (3.33) and (3.35) is done for $\beta = 1/\tau_s$ =3.0, 1.0, 0.5, 0.3, 0.2 and 0.14. Results are shown in Figure 3.6.

It should be noted that our method does not introduce any approximation except the Gaussian approximation discussed in section **3.3.1**. Therefore, the results by Monte-Carlo simulation will exactly agree with the theoretical results as the number of Monte-Carlo trials increases as seen in Figure 3.6 and 3.7.

3.4.2 Simplification of the double Markov to single Markov process

Here, we examine whether the double Markov process can be simplified into a single Markov process. The double Markov process is replaced by the single Markov process whose first- and second-order statistics are the same with those of the double Markov

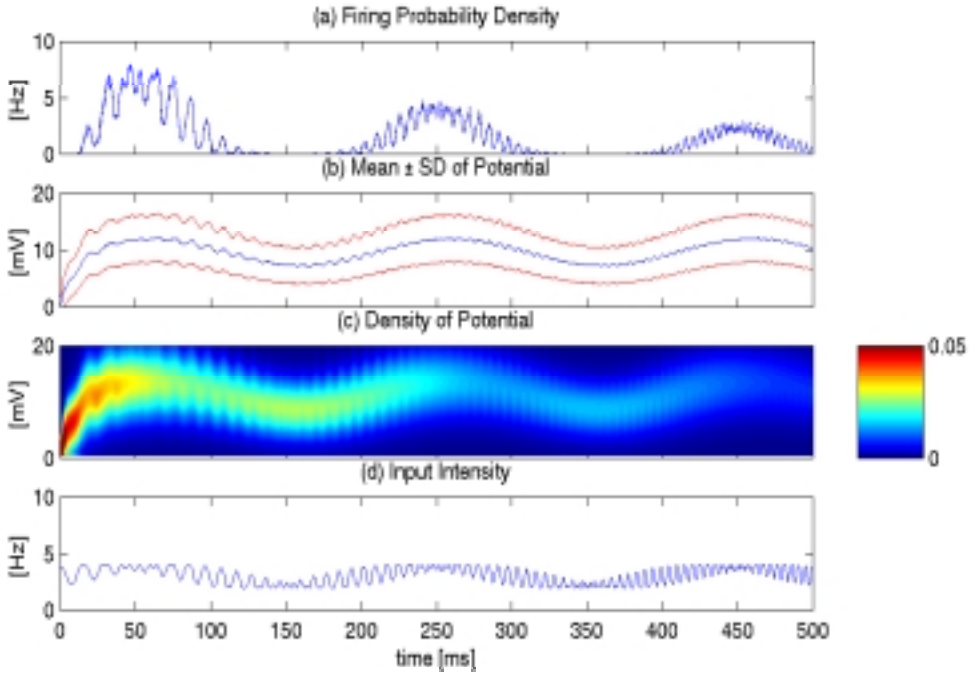

Figure 3.5: Dynamics of the membrane potential for the spike response function (3.8), i.e., $u(s) = qe^{-\alpha s}\mathcal{H}(s)$. (a): Firing probability density. (b): Ensemble mean $\pm$ standard deviation (SD) of $g(v^t)$ when the firing is not considered. Center line denotes the mean, and the upper and the lower lines denote the mean $\pm$ SD. (c): Probability density of samples that have not fired yet, $g_u(v^t)$. When a sample neuron fires, it is removed from the ensemble. (d): Input intensity $\lambda(t)$ given by (3.36). In sub-figures (a) and (b), solid and dashed lines denote theoretical results and Monte-Carlo simulation results obtained from 160000 trials, respectively. The *maximum* difference between the theoretical result and that by the Monte-Carlo simulation, is 0.8 for (a), 0.02 for (b), and these errors are too small to be observed. Then the two kinds of lines are overlapped in each figure.

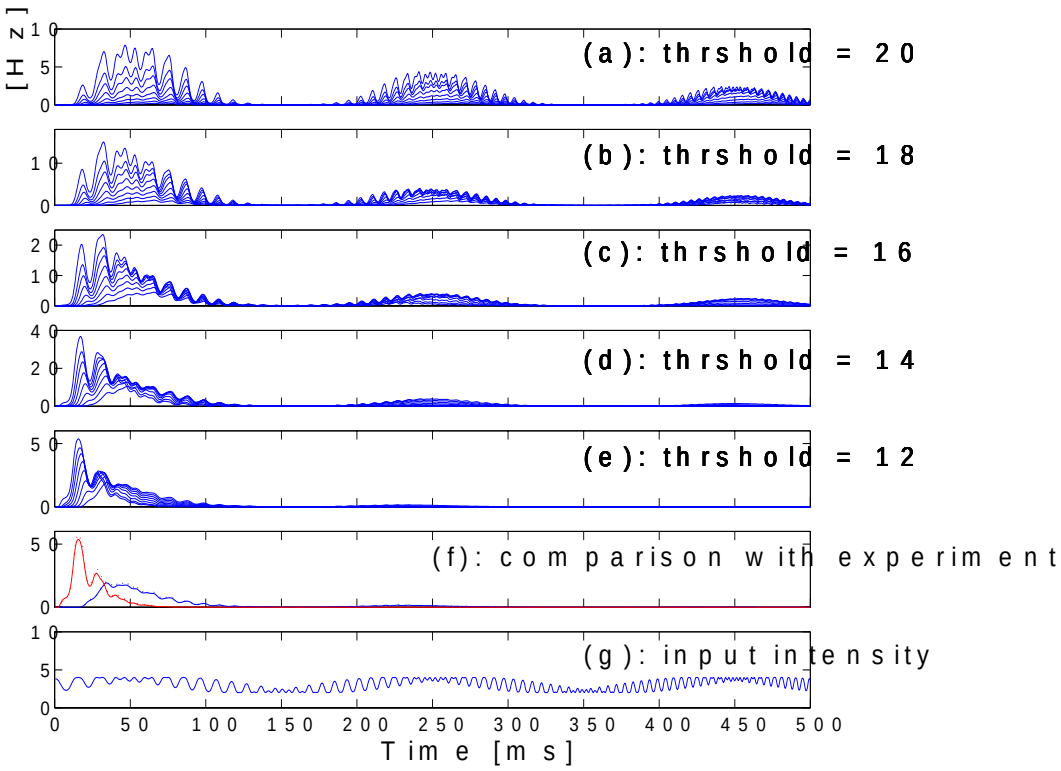

Figure 3.6: Variation of the firing probability density due to variation of the synaptic time constants $\tau_m = 1/\beta$. (a)-(e): Firing probability density when the threshold is 20 for (a), 18 for (b), 16 for (c), 14 for (d), and 12 for (e). In each figure, lines are for $\beta = \infty$ (function (3.8)), 3.0, 1.0, 0.5, 0.3, 0.2, 0.14 and α (function (3.7)) from top to bottom. (f): Comparison with Monte-Carlo simulation results in the case of $\theta = 12$ [mV]. $\beta \to \infty$ and $\beta \to \alpha$ cases are considered. Solid and dotted lines denote theoretical and Monte-Carlo results, respectively. (g): Input intensity $\lambda(t)$ given by (3.36).

process. The reduced Markov process is described in appendix section **3.A.3**. Figure 3.7 shows the results when this approximation is applied to the response function (3.6). As seen in the left figure, this simplification works fairly well when the threshold is low and the firing probability density is high. However, the error induced by the simplification may not be ignored when the threshold is high and the firing probability density is low, as can be seen in the right figure. The error becomes large especially when β is small. Note that the approximation is exact when $\beta \to \infty$, because the case of $\beta \to \infty$ corresponds to the response function (3.8). Accordingly, the simplification to the single Markov process is not valid in the case of a high threshold value and a large $\tau_s = 1/\beta$ value.

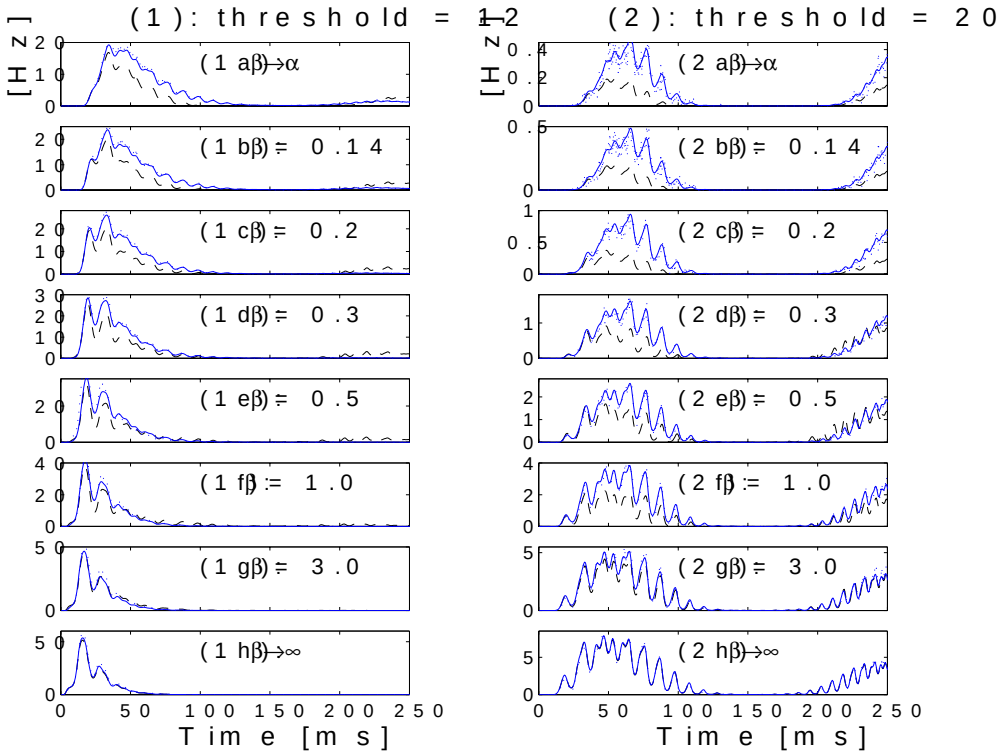

Figure 3.7: Difference between the double (solid line) and single (dashed line) Markov models, both of which have the same ensemble mean and variance. Input conditions are the same as those used in Figure 6. Monte-Carlo simulation results are overwritten by dotted lines. (1a-h): Firing probability density when the threshold is 12. β increases from top to bottom. As β increases, the error of the simplified model becomes small. (2a-h): Firing probability density when the threshold is 20. The error becomes large as β decreases.

3.4.3 Stochastic spiking neurons with resets

The conventional studies (Plesser and Tanaka 1997; Burkitt and Clark 1999, and so on) based on the backward resolution of the Volterra equation have put focus on the first passage time density (FPTD), namely, the event that for the first time the neuron sample reaches the firing threshold. In those studies, when a sample neuron fires, it is removed from the ensemble; this is called the absorbing threshold (see Figure 3.3). When one assumes that neuron samples may fire many times, which corresponds to the introduction of the reset after firing, an extension of the FPTD-based analysis can be used only when the input spikes obey a homogeneous Poisson process. The distribution of neuron samples for the first passage and for the second passage are different when the inputs are inhomogeneous. Since the FPTD-based analysis cannot consider the multiple crossing of the threshold, it is necessary to prepare a lot of distributions whose Poisson intensities are different (Plesser and Geisel 1998). Due to this difficulty, the backward approach is not appropriate for dealing with the reset after firing.

On the other hand, forward calculation methods such as our method and the studies based on the Fokker-Planck equation can consider the reset after firing. In the forward approach, the density whose samples have fired at time t_{m-1} is moved at time t_m to the density whose potential is $v_{\rm reset}(=0)$. Although the transition probability density depends on the inhomogeneous spike rate, the density of the membrane potential does not depend on it.

Under the single Markov assumption, the firing probability $\rho(t_m)$ and the density of the membrane potential $g_0(v^m)$, which have been given by (3.27) and (3.28), are modified into

$$\rho(t_m) = \int_\theta^\infty g_0(v^m)dv^m, \quad g_0(v^m) = \int_{-\infty}^\theta g(v^m|v^{m-1})g_0(v^{m-1})dv^{m-1} + \rho(t_{m-1})\delta(v^m), \tag{3.38}$$

where $\delta(\cdot)$ is the Dirac's delta function. The second term of $g_0(v^m)$ is the distribution whose sample has fired at t_{m-1} and has potential $v^m = 0$ at time t_m. Here, note that the meaning of $g_0(v^m)$ is changed. In sections **3.3.2** and **3.3.3**, it indicates the distribution of samples that have not fired until time t_{m-1}. In this subsection, it indicates the distribution of samples that do not fire between the interval $[t_{m-n-1}, t_{m-1}]$ where n is the Markov order.

Under the double Markov assumption, the firing probability $\rho(t_m)$ and the density $g_0(v^m)$, which have been given by (3.27) and (3.29), are modified into

$$\begin{aligned}\rho(t_m) = \int_\theta^\infty g_0(v^m)dv^m, \quad g_0(v^m) &= \int_{-\infty}^\theta \int_{-\infty}^\theta g(v^m|v^{m-1}, v^{m-2})g_0(v^{m-1}, v^{m-2})dv^{m-1}dv^{m-2} \\ g_0(v^m, v^{m-1}) &= \int_{-\infty}^\theta g(v^m|v^{m-1}, v^{m-2})g_0(v^{m-1}, v^{m-2})dv^{m-2} + \rho(t_{m-1})g(v^m, v^{m-1}).\end{aligned} \tag{3.39}$$

The joint density of reset states, $g(v^m, v^{m-1})$, is given by (3.13).

Figure 3.8 shows the result of these calculations. For the single Markov process, equations (3.30), (3.31) and (3.38) are used. For the double Markov process, equations

(3.33), (3.34) and (3.39) are used. The results are compared with those by the Monte-Carlo simulations. The response function is given by (3.6), (3.7) or (3.8). This figure shows that our method can precisely calculate the membrane potential density and the firing probability density even in the multiple firing situation.

3.5 Discussion

3.5.1 Dependency on the synaptic time constant

Figures 3.6 and 3.8 show that the firing probability density significantly depends on the synaptic time constant τ_s. This dependency is prominent especially when threshold θ is large, and hence the firing probability density is low. The change of the firing probability density is mainly due to the change of the potential variance $\sigma^2(t)$. Mean $\eta(t)$ does not change very much because the integral of the response function is fixed, while variance $\sigma^2(t)$ decreases as τ_s increases. Conventionally, it has been considered that the change of the synaptic efficacy w_j is important for neuronal information processing, like in the Hebb's prescription. On the other hand, our theoretical result implies another possibility for the neuronal information processing, namely, the modulation of the firing probability density by changing the synaptic time constant.

When the threshold is relatively low in comparison to the intensity of the input spikes, the firing probability density is mainly determined by the input intensity. In this case, the change of the synaptic time constant is not very important. When the threshold is relatively high, on the other hand, the above-mentioned modulation is possible. In the cortical areas at which the firing rate is low and coincidental spikes often occur, neurons might process their information by temporally changing the shapes of PSPs. Physiologically, the decrease of parameter $\beta = 1/\tau_s$ may correspond to effect of the dopaminergic (DA) modulation (Durstewiz *et al.* 2000). Vitro experiments find that DA reduces the EPSP amplitude while prolongs its duration (Cepeda *et al.* 1992; Kita *et al.* 1999)

3.5.2 Comparison with other methods

Here, we compare our method with existing stochastic process methods. Many stochastic process studies are based on the first-order Fokker-Planck equation. Section **3.5.2** discusses the relation between our method and the existing studies based on the Fokker-Planck equation (Ricciardi and Sato 1988; Brunel and Hakim 1999; Brunel 2000; and many others). In these studies, the stochastic spiking neuron is assumed to employ the response function (3.8). On the other hand, a useful backward resolution method of the Volterra integral equation has been developed by Plesser and Tanaka (1997; see also Burkitt and Clark 1999). Section **3.5.2** discusses the relation between our approach and the backward approach.

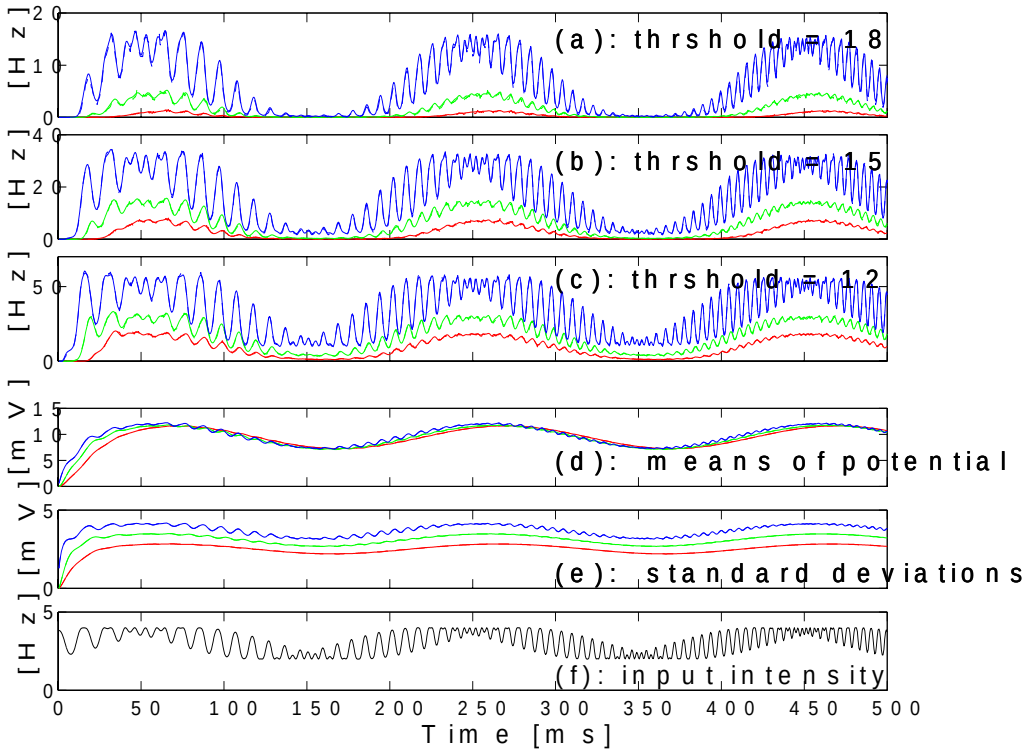

Figure 3.8: Variation of the firing probability density due to variation of the synaptic time constant $\tau_s \equiv 1/\beta$. (a)-(c): Firing probability density when the iterative firings and reset are considered. The threshold is 18 for (a), 15 for (b), and 12 for (c). In each figure, solid lines are for $\beta = \infty$ (function (3.8)), 3.0 (function (3.6)), and α (function (3.7)) from top to bottom. (d): Means of the membrane potential when the firing is not considered. τ_s is not very important for the mean. (e): Standard deviations (SDs) of the membrane potential when the firing is not considered. SDs decreases as τ_s increases. (a-e): The results of Monte-Carlo simulations over 160000 trials are overwritten by dashed lines in all of the sub-figures. Difference between the theoretical results (solid) and the Monte-Carlo results (dashed) is too small to observe in each sub-figure. The *maximum* difference is about 2.0 for the firing probability density, and 0.02 for the mean and SD, which will decrease as the Monte-Carlo trials increase. (f): Input intensity $\lambda(t)$ given by (3.36).

Continuous description and diffusion approximation

The stochastic spiking neuron, whose response function is defined by (3.8), i.e., $u(s) = qe^{-\alpha s}\mathcal{H}(s)$, is called the Stein's model (Stein 1967). By using the diffusion approximation, the Stein's model which includes discontinuous jumps in the spike response can be expressed by the Ornstein-Uhlenbeck (OU) process. The OU process is primarily a continuous stochastic process that assumes infinitesimal jump in the spike response. Appendix section **3.A.4** is devoted to the formulation of the continuous case whose response function is defined by (3.8). We find that our single Markov-Gaussian process formulation whose response function is (3.8) is equivalent to the diffusion approximation of the Stein's model, i.e., the OU process approach. However, the OU process approach cannot deal with the response function (3.6) nor (3.7), which involves a multiple Markov process. In order to consider such higher order response functions, higher order time derivatives such as $\partial_t^2 g(v^t)$ will be necessary. In this point, our formulation is a more general framework than the OU process formulation. In appendix section **3.A.4**, we also find the definition of the firing probability (3.32) is equivalent to that of the Fokker-Planck equation with the boundary condition $g_u(\theta) = 0$ for the consinuous-time limit ($\Delta t \to 0$).

Our method is more accurate than the methods based on the Fokker-Planck equation, even in the single Markov case. In order to calculate density $g_u(v^t)$, instead of equation (3.28), other numerical integration methods for the Fokker-Planck equation can be used. Equation (3.32) can also be replaced by equation (3.A39). According to our simulations, however, the error produced by the numerical calculation of equation (3.A39) is larger than that of equation (3.32)[1]. Under the same experimental condition as that in Figure 5, the maximum error produced by equation (3.32) is about 0.8 [Hz], while the maximum error by equation (3.A39) is about 3 [Hz]. Although both of the error values decrease as Δt becomes small, the error by (3.32) is smaller than that by (3.A39) even with a smaller integration time-interval, e.g., $\Delta t = 0.05$ [ms]. Therefore, our method is more accurate in obtaining the membrane density and the firing probability than the Fokker-Planck equation method. Moreover, according to our simulation, our method using equations (3.28) and (3.32) exhibits good calculation even if Δt is as large as $\Delta t = 0.5$ [ms]; namely, our method is fairly insensitive to the integration time-interval.

Comparison with backward approach

In order to compare our approach with the backward approach (Plesser and Tanaka 1997), we assume that the density whose samples fire at time t_n can be described by $\delta(v^n - \theta)\rho(t_n)$. This means that the membrane potential for every firing is exactly equal to θ. This assumption is valid when $\Delta t \to 0$. The density after firing $g_f(v^m)$,

[1] In both cases, equation (3.28) is used.

which is defined by (3.11), is given by

$$g_f(v^m) = \sum_{n=0}^{m} \int_{-\infty}^{\infty} dv^n \dots \int_{-\infty}^{\infty} dv^m g(v^m|\{v\}_n^{m-1}) \dots g(v^m|\{v\}_n^{m-2}) \dots g(v^{n+1}|v^n)\delta(v^n - \theta)\rho(t_n)$$
$$= \sum_{n=0}^{m} g(v^m|v^n = \theta)\psi(t_n)\Delta t, \tag{3.40}$$

where $\psi(t) \equiv \rho(t)/\Delta t$. In $\Delta t \to 0$, we find

$$g_f(v^t) = \int_0^t g(v^t|v^{t'} = \theta)\psi(t')dt'. \tag{3.41}$$

Because $g_f(v^t) = g(v^t)$ for $v^t \geq \theta$, and $g(v^t)$ and $g(v^t|v^{t'} = \theta)$ are known in the Gaussian process, $\psi(t)$ can be obtained by resolving the Volterra integral equation (3.41) from time t to 0 in a backward fashion over the discretized time sequence. See Burkitt and Clark (2000) and Press *et al.* (1988) for details. Namely, the results obtained by our forward-type calculation method become identical to those by the backward approach, when $\Delta t \to 0$.

Both of the forward and backward approaches can deal with the spike response functions involving multiple Markov property (e.g. in the cases of function (3.6) or (3.7)). However, our method is advantageous when we consider the reset effect after firing, as discussed in section **3.4.3**.

Here, the computational complexity is compared. The calculation of $\psi(t)$ from (3.41) needs to discretize the time-interval $[0, t]$. Let K be the number of the discretization and $t = K\Delta t_v$. The computational complexity of the backward approach is $O(K^2)$. According to our numerical calculation, the permissible value for Δt_v is 0.05 [ms]. On the other hand, the computational complexity of our forward approach is $O(mM^2)$, where m is the number of discretized time sequence, i.e., $t = m\Delta t$. M is the number of the numerical integration for dv^{m-1} in equation (3.28). The permissible value for Δt is 0.5 [ms], and an appropriate value for M is 1000. Therefore, if we need the calculation for more than 5 [s], our forward approach is more efficient. In the double Markov case, however, our forward approach needs the complexity of mM^3. The backward approach is more efficient in this case, if the reset effects are ignored.

3.5.3 Plausibility of the stochastic input

In section **3.1**, we have introduced physiological studies that suggest the information provided to a neuron is expressed by the input spike rates and the spikes are stochastic events. However, the assumption that the spikes are inhomogeneous Poisson events, namely, they are mutually independent, is stronger than what the physiological studies suggest. In this subsection, the plausibility of the Poisson assumption is discussed.

In the cerebral cortex, one of the important characteristics of the spikes is their irregularity. According to the existing studies (Gerstein and Mandelbrot 1964; Shadlen and Newsome 1994, 1998; Tsodyks and Sejnowski 1995), the irregularity is considered to be a result of a balanced state. Namely, even when excitatory inputs are large,

inhibitory inputs increase proportionally to them so that the mean of the membrane potential is suppressed. By assuming the balanced state, the spike irregularity at high firing rate up to 100-200 Hz (Softky and Koch 1993) can be explained (Shadlen and Newsome 1994, 1998). From a physiological data analysis based on a stochastic process method, a random spontaneous firing state is plausible and structurally stable (Amit and Brunel 1997a).

Deterministic mechanism such as the complexity of connections in neuronal circuits can also produces the irregularity similarly to the balanced states. For example, a mean-field approximation theoretically reveals that the asynchronous McCulloch-Pitts model having random and sparse connections and inhibitory reccurents produces Poisson-like spike sequences (Vreeswijk and Sompolinsky 1996, 1998). A large-scale computer simulation for an integrate-and-fire neuron model shows that random and sparse connections produce Poisson-like spikes even if the inputs to the neuron are deterministic and stational (Kubo *et al.* unpublished). These studies suggest that a large-scale network like the cerebral cortex is in a balanced states and hence the spikes are likely to lose their correlation.

The response of neurons in such a random but structurally stable balanced state (Tsodyks and Sejnowski 1995) is very fast in comparison to the response determined by the membrane integration time constant. Such rapid responses are considered to be physiologically important (Thorpe *et al.* 1996).

The Poisson assumption is not valid when a neuron bursts. Burst spikes are correlated with each other even in a large-scale network. Thus, we consider that our Poisson assumption is valid when the neurons tonically fire and their firing rate is as large as the spontaneous firing rate.

3.5.4 Extension of the stochastic spiking neuron model

Here, we briefly discuss an extension of our approach to the analysis of the network of neurons. The spike intensity input from a pre-synaptic neuron i to a post-synaptic neuron j can be represented by the firing rate of neuron i, $\psi_i(t) \equiv \rho(t)/\Delta t$. In the network, $\psi_i(t)$ may vary with time; namely, the firing rate is inhomogeneous. Moreover, in order to observe temporal behaviors of the network, the assumption that the element neurons may fire many times is important. Therefore, we consider that our approach is suitable for analyzing the interesting behaviors of network dynamics, including stability of the balanced state (Amit and Brunel 1997a), synaptic plasticity (Kempter *et al.* 1999, Tsodyks and Markram 1997), syn-fire chain (Diesmann *et al.* 1999), and so on.

Two important issues have not been considered enough in this chapter. First is the reduction of a higher order Markov process into a single one. As discussed in section **3.5.2**, our approach for a higher order response function is expensive than the existing backward approach. A simple reduction scheme discussed in appendix section **3.A.3** is inaccurate especially when the firing probability is low and $\beta = 1/\tau_s$ is small.

Second is the extension of the model itself. Based on the assumption of the spike response model (Gerstner 1998), we have considered the neuron model employing the

response function (3.6), (3.7) or (3.8). However, our spike response model may not be sufficient for modeling the neurons in the brain. Recent studies have suggested that the consideration of reversal potential for excitatory and inhibitory inputs and the partial reset effect after firing will change the stability of the balanced state (Troyer and Miller 1995). Our future work will include the introduction of such effects to our approach.

3.6 Conclusion

In this chapter, we theoretically examined the responses of spiking neurons to spike sequences which obeyed an inhomogeneous Poisson process. When inhomogeneous Poisson inputs are provided to the neuron, the stochastic process of the membrane potential becomes a Gaussian process. Assuming a Markov property, we derived a calculation method which could precisely obtain the dynamics of the membrane potential and the firing probability density. With frequently used response functions, a single or double Markov property can be assumed. Since we did not introduce any approximation, the theoretical results exhibited good agreement with the results by Monte-Carlo simulations. We also found that the firing probability was significantly dependent on the synaptic time constant.

3.A Appendix

3.A.1 The joint probability density

The joint probability density (3.7) is defined by

$$\begin{aligned} g(\{v\}_1^m) &\equiv \langle \delta(v^m - \boldsymbol{v}(t_m)) \dots \delta(v^1 - \boldsymbol{v}(t_1)) \rangle \\ &= \int \frac{d\xi_1}{2\pi} \dots \int \frac{d\xi_m}{2\pi} \exp\Big\{ \sum_{k=1}^m \mathrm{i}\xi_k v^k \Big\} \Big\langle \exp\Big(-\sum_{k=1}^m \mathrm{i}\xi_k \boldsymbol{v}(t_k) \Big) \Big\rangle. \end{aligned} \tag{3.A1}$$

Let the logarithm of the joint characteristic function

$$F(\xi_1, \dots, \xi_m; t_1, \dots, t_m) \equiv \Big\langle \exp(\sum_{k=1}^m \mathrm{i}\xi_k \boldsymbol{v}(t_k)) \Big\rangle \tag{3.A2}$$

be expanded by the second order of ξ_k. Then, we obtain

$$\begin{aligned} \ln F(\xi_1, \dots, \xi_m; t_1, \dots, t_m) &= \ln \Big\langle 1 - \sum_{k=1}^m \mathrm{i}\xi_k \boldsymbol{v}(t_k) - \frac{1}{2} \sum_{k=1}^m \sum_{l=1}^m \xi_k \xi_l \boldsymbol{v}(t_k) \boldsymbol{v}(t_l) + O(\xi_k^3) \Big\rangle \\ &= -\sum_{k=1}^m \mathrm{i}\xi_k \eta(t_k) - \frac{1}{2} \sum_{k=1}^m \sum_{l=1}^m \xi_k \xi_l \Sigma_{kl} + O(\xi_k^3), \end{aligned} \tag{3.A3}$$

where

$$\Sigma_{kl} \equiv \langle \boldsymbol{v}(t_k) \boldsymbol{v}(t_l) \rangle - \langle \boldsymbol{v}(t_k) \rangle \langle \boldsymbol{v}(t_l) \rangle. \tag{3.A4}$$

When $\lambda(t)$ and t_m are not small, the third order term $O(\xi_k^3)$ can be omitted due to the central limit theorem. Then, the joint probability density is approximated as

$$\begin{aligned} g(\{v\}_1^m) &\approx \int_{-\infty}^{\infty} \frac{d\xi_1}{2\pi} \dots \int_{-\infty}^{\infty} \frac{d\xi_m}{2\pi} \exp\Big\{ \sum_{k=1}^m \mathrm{i}\xi_k (v^k - \eta(t_k)) - \frac{1}{2} \sum_{k=1}^m \sum_{l=1}^m \xi_k \xi_l \Sigma_{kl} \Big\} \\ &= \int_{-\infty}^{\infty} \frac{d\xi_1}{2\pi} \dots \int_{-\infty}^{\infty} \frac{d\xi_m}{2\pi} \exp\Big(\mathrm{i}\vec{\xi}'(\vec{v} - \vec{\eta}) - \frac{1}{2} \vec{\xi}' \Sigma \vec{\xi} \Big), \end{aligned} \tag{3.A5}$$

where $\vec{v} = (v^{t_1}, \dots, v^{t_m})'$, $\vec{\eta} = (\eta(t_1), \dots, \eta(t_m))'$, $\vec{\xi} = (\xi_1, \dots, \xi_m)'$, and Σ is an m-by-m auto-correlation matrix of $\vec{v}$. Prime ($'$) denotes a transpose. By defining $\vec{\xi} = \vec{x} + \mathrm{i}\vec{y}$, we obtain

$$g(\{v\}_1^m) = \int_{-\infty}^{\infty} \frac{d\vec{\xi}}{(2\pi)^m} \exp\Big(-\frac{1}{2} \vec{x}' \Sigma \vec{x} - (\vec{v} - \vec{\eta})' \vec{y} + \frac{1}{2} \vec{y}' \Sigma \vec{y} + \mathrm{i}\vec{x}' (\vec{v} - \vec{\eta} - \Sigma \vec{y}) \Big), \tag{3.A6}$$

because Σ is positive definite. When $\vec{y} = \Sigma^{-1}(\vec{v} - \vec{\eta})$, the integral is done only for the real part $\vec{x}$. Then,

$$\begin{aligned} g(\{v\}_1^m) &= \exp\Big(-\frac{1}{2} (\vec{v} - \vec{\eta})' \Sigma^{-1} (\vec{v} - \vec{\eta}) \Big) \int_{-\infty}^{\infty} \frac{d\vec{x}}{(2\pi)^m} \exp\Big(-\frac{1}{2} \vec{x}' \Sigma \vec{x} \Big) \\ &= \frac{1}{\sqrt{(2\pi)^m |\Sigma|}} \exp\Big(-\frac{1}{2} (\vec{v} - \vec{\eta})' \Sigma^{-1} (\vec{v} - \vec{\eta}) \Big), \end{aligned} \tag{3.A7}$$

where $|\Sigma|$ is the determinant of Σ.

3.A.2 Examples of multiple Markov transition probability density

In this appendix section, the Markov order of the transition probability density for the response functions (3.6), (3.7) and (3.8) is obtained through the calculation of $(\Sigma^m)^{-1}$. From (3.22), the correlation coefficients are $\kappa_i^m = (u_{mm})^2 \zeta_{im}^m$, where $(\zeta_{ij}^m) \equiv (\Sigma^m)^{-1}$.

Case 1: Equation (3.8), i.e., $u(s) = qe^{-\alpha s}\mathcal{H}(s)$. From the incremental calculation of (3.19), the j-th column vector of matrix Γ^m is calculated as

$$\boldsymbol{\Gamma}_j^m = \frac{1}{qw\sqrt{\lambda(t_j)\Delta t}}\Big(0,\ldots,0,\ \overset{j}{1},\ \overset{j+1}{-e^{-\alpha\Delta t}},0,\ldots,0\Big)' \tag{3.A8}$$

The component-wise vector notation expresses that the j-th and $(j+1)$-th components are 1 and $-e^{-\alpha\Delta t}$, respectively, and the others are 0. From (3.A8), we see that $\Sigma^{-1} = \Gamma\Gamma'$ is a tridiagonal matrix. Therefore, $\kappa_i^m = 0$ for $i < m-1$. This means that the Gaussian process defined by Σ becomes a Markov process.

Case 2: Equation (3.7), i.e., $u(s) = qse^{-\alpha s}\mathcal{H}(s)$. Since the diagonal elements of U^m, u_{ii} in equation (3.17), are zeros, Σ^m becomes singular. In order to avoid the singularity, we redefine the components of U^m as

$$u_{ij} = \begin{cases} w \cdot u(t_{j+1} - t_i)\sqrt{\lambda(t_i)\Delta t}, & i \le j \\ 0, & i > j. \end{cases} \tag{3.A9}$$

From the incremental calculation of (3.19), the j-th column vector of the inverse of matrix U^m is strictly calculated as

$$\boldsymbol{\Gamma}_j^m = \frac{1}{qw\sqrt{\lambda(t_{j-1})\Delta t}}\Big(0,\ldots,0,\overset{j}{e^{\alpha\Delta t}},\ \overset{j+1}{-2},\ \overset{j+2}{e^{-\alpha\Delta t}},0,\ldots,0\Big)'. \tag{3.A10}$$

From (3.A10), we see that $(\Sigma^m)^{-1}$ becomes a band diagonal matrix whose bandwidth is five. Then, the transition probability density of this Gaussian process is determined by two past components, namely, the process becomes a double Markov process.

Case 3: Equation (3.6), i.e., $u(s) = q(e^{-\alpha s} - e^{-\beta s})\mathcal{H}(s)$. Similarly to the previous case, the diagonal elements of U^m are zeros, and we use definition (3.A9). From the incremental calculation of (3.19), the j-th vector column of the inverse of matrix U^m is strictly calculated as

$$\overset{j}{\qquad}\qquad\overset{j+1}{\qquad}\qquad\overset{j+2}{\qquad}$$

$$\boldsymbol{\Gamma}_j^m = \frac{1}{qw\sqrt{\lambda(t_{j-1})\Delta t}}\left(0,\ldots,0,\frac{1}{e^{-\alpha\Delta t}-e^{-\beta\Delta t}},-\frac{e^{-\alpha\Delta t}+e^{-\beta\Delta t}}{e^{-\alpha\Delta t}-e^{-\beta\Delta t}},\frac{e^{-\alpha\Delta t}e^{-\beta\Delta t}}{e^{-\alpha\Delta t}-e^{-\beta\Delta t}},0,\ldots,0\right)'. \tag{3.A11}$$

$(\Sigma^m)^{-1}$ becomes a band diagonal matrix whose band-width is five, and the stochastic process becomes a double Markov process.

3.A.3 Simplification method from multiple to single Markov process

In this appendix section, the simplification of the membrane dynamics from a multiple Markov process to a single Markov process is considered. By assuming the single Markov property, the membrane dynamics is given by

$$g_0(v^1) = g(v^1); \quad g_0(v^m) = \int_{-\infty}^{\theta} g(v^m|v^{m-1})g_0(v^{m-1})dv^{m-1} \quad (m = 2,3\ldots), \tag{3.A12}$$

where

$$g(v^m|v^{m-1}) = \frac{1}{\sqrt{2\pi\hat{\gamma}^m}}\exp\left(-\frac{(v^m-\eta(t_m)-\hat{\kappa}_{m-1}^m(v^{m-1}-\eta(t_{m-1})))^2}{2\hat{\gamma}^m}\right). \tag{3.A13}$$

Here, $\hat{\kappa}_{m-1}^m$ and $\hat{\gamma}^m$ are defined as

$$\hat{\kappa}_{m-1}^m = \frac{\Sigma_{m\ m-1}}{\Sigma_{m-1\ m-1}}, \quad \hat{\gamma}_m = \frac{\Sigma_{m\ m}\Sigma_{m-1\ m-1}-(\Sigma_{m\ m-1})^2}{\Sigma_{m-1\ m-1}}, \tag{3.A14}$$

where Σ is the auto-correlation matrix of the membrane potential, whose definition is given by (3.A4).

In order to simplify a multiple Markov process to a single Markov-process, therfore, the mean $\eta(t)$ and auto-correlation Σ should be estimated. Here, an estimation method only for the response function (3.6) is shown, but the cases for (3.7) and (3.8) can be similarly considered. For the response function $u(s) = q(e^{-\alpha s}-e^{-\beta s})\mathcal{H}(s)$, the mean of the membrane potential is incrementally calculated as

$$\eta(t_m) = e^{-\alpha\Delta t}A(t_{m-1}) - e^{-\beta\Delta t}B(t_{m-1}). \tag{3.A15}$$

where

$$A(t_m) = w_0 q\int_0^{t_m} e^{-\alpha(t_m-s)}\lambda(s)ds, \quad B(t_m) = w_0 q\int_0^{t_m} e^{-\beta(t_m-s)}\lambda(s)ds \tag{3.A16}$$

Here, $w_0 = \sum_{j=1}^N w_j$. $A(t_m)$ can be incrementally calculated as

$$A(t_m) = e^{-\alpha\Delta t}A(t_{m-1}) + w_0 q\lambda(t_m)\Delta t, \tag{3.A17}$$

and $B(t_m)$ can be similarly calculated. The auto-correlation matrix Σ is calculated by the decomposition:

$$\Sigma_{m\ m-1} = e^{-\alpha\Delta t}D(t_{m-1}) - (e^{-\alpha\Delta t} + e^{-\beta\Delta t})E(t_{m-1}) + e^{-\beta\Delta t}G(t_{m-1}), \tag{3.A18}$$

where

$$D(t_m) = w^2q^2\int_0^{t_m} e^{-2\alpha(t_m-s)}\lambda(s)ds,\ \ G(t_m) = w^2q^2\int_0^{t_m} e^{-2\beta(t_m-s)}\lambda(s)ds,$$
$$E(t_m) = w^2q^2\int_0^{t_m} e^{-(\alpha+\beta)(t_m-s)}\lambda(s)ds. \tag{3.A19}$$

Here, $w^2 = \sum_{j=1}^N w_j^2$. $D(t)$, $E(t)$ and $G(t)$ can be incrementally calculated in a similar manner to (3.A17).

3.A.4 Continuous formulation in first-order case

In this appendix section, we consider the continuous formulation in the first-order case; namely, the response function $u(s) = qe^{-\alpha s}\mathcal{H}(s)$ is employed. In this case, our formulation approaches that based on the Ornstein-Uhlenbeck process as the time step Δt approaches zero. Here, we confirm the equivalence and compare with the standard Fokker-Planck equation approach. Introducing a higher order time derivative $\partial_t^n g(v^t)$, time evolution of the probability density of the higher order case can also be derived.

Density dynamics The time derivative of the expectation of any function $f(v^t)$ with respect to density $g(v^t)$ can be defined by

$$\begin{aligned}\partial_t\int dv^t f(v^t)g(v^t) &\equiv \lim_{\Delta t\to 0}\frac{1}{\Delta t}\left\{\int_{-\infty}^{\infty} dv^{t+\Delta t}f(v^{t+\Delta t})g(v^{t+\Delta t}) - \int_{-\infty}^{\infty} dv^t f(v^t)g(v^t)\right\}\\ &= \lim_{\Delta t\to 0}\frac{1}{\Delta t}\left\{\int_{-\infty}^{\infty} dv^t g(v^t)\Big[\int_{-\infty}^{\infty} dv^{t+\Delta t}f(v^{t+\Delta t})g(v^{t+\Delta t}|v^t) - f(v^t)\Big]\right\}.\end{aligned} \tag{3.A20}$$

In order to clarify the time dependence, we rewrite v^t as v_0, $v^{t+\Delta t}$ as v_1, $g(v^t)$ as $g(v_0,t)$, and $g(v^{t+\Delta t})$ as $g(v_1,t+\Delta t)$. For the calculation of

$$\int_{-\infty}^{\infty} dv^{t+\Delta t}f(v^{t+\Delta t})g(v^{t+\Delta t}|v^t) \equiv \int_{-\infty}^{\infty} dv_1 f(v_1)g(v_1,t+\Delta t|v_0,t) \equiv \mathcal{I}(v_0,t), \tag{3.A21}$$

we use a moment expansion

$$f(x) = \sum_{n=0}^{\infty}\frac{1}{n!}(x-\eta)^n\partial_x^n f(\eta),\ \int_{-\infty}^{\infty} g(x|z)f(x)dx = \sum_{n=0}^{\infty}\frac{1}{n!}\partial_x^n f(\eta)\int_{-\infty}^{\infty}(x-\eta)^n g(x|z)dx, \tag{3.A22}$$

where $0! = 1$ by definition and η is the mean of $g(x|z)$ with respect to x.

If $g(x|z)$ is a Gaussian distribution with mean η and variance σ^2, $g(x|z)$ is a symmetric function on the both sides of η. In this case, the odd terms in (3.A22) vanish, and we obtain

$$\int_{-\infty}^{\infty} g(x|z)f(x)dx = f(\eta) + \frac{\sigma^2}{2}\partial_x^2 f(\eta) + \mathcal{O}(\sigma^4). \tag{3.A23}$$

When we use the response function $u(s) = qe^{-\alpha s}\mathcal{H}(s)$, the transition probability density (3.30) becomes

$$g(v_1, t+\Delta t|v_0, t) = \frac{1}{\sqrt{2\pi B(t)\Delta t}} \exp\left[-\frac{(v_1 - v_0 - A(t, v_0)\Delta t)^2}{2B(t)\Delta t}\right], \tag{3.A24}$$

where $A(t, v_0) = \partial_t \eta(t) - \alpha(v_0 - \eta(t))$ and $B(t) = w^2 q^2 \lambda(t)$. Then, integral (3.A21) is given by

$$\mathcal{I}(v_0, t) = \int_{-\infty}^{\infty} dv_1 g(v_1, t+\Delta t|v_0, t)f(v_1) = f(v_0 + A(t, v_0)\Delta t) + \frac{B(t)\Delta t}{2}\partial_{v_0}^2 f(v_0) + \mathcal{O}((\Delta t)^2). \tag{3.A25}$$

By using (3.A25), equation (3.A20) becomes

$$\partial_t \int dv_0 f(v_0)g(v_0, t) = \int_{-\infty}^{\infty} dv_0 g(v_0, t)\left[A(v_0, t)\partial_{v_0} f(v_0) + \frac{B(t)}{2}\partial_{v_0}^2 f(v_0)]\right], \tag{3.A26}$$

and by integrating by parts,

$$\int_{-\infty}^{\infty} dv_0 f(v_0)\partial_t g(v_0, t) = \int_{-\infty}^{\infty} dv_0 f(v_0)\left[-\partial_{v_0}[A(v_0, t)g(v_0, t)] + \frac{B(t)}{2}\partial_{v_0}^2 g(v_0, t)\right] + \text{Constant}. \tag{3.A27}$$

Finally, the time evolution of the probability density follows

$$\partial_t g(v, t) = -\partial_v[A(v, t)g(v, t)] + \frac{B(t)}{2}\partial_v^2 g(v, t). \tag{3.A28}$$

Because $\partial_t \eta(t) \propto e^{-\alpha t}$, this term can be ignored when $t \sim 1/\alpha = \tau_m$ [ms]. Then, equation (3.A28) becomes

$$\partial_t g(v^t) = \alpha\partial_{v^t}\left[(v^t - \eta(t))g(v^t)\right] + \frac{1}{2}w^2 q^2 \lambda(t)\partial_{v^t}^2 g(v^t). \tag{3.A29}$$

This equation corresponds to the first-order Fokker-Planck equation for the OU process. Corresponding stochastic differential equation can be written as

$$dv^t = -\alpha(v^t - \eta(t))dt + wq\sqrt{\lambda(t)}dW(t), \tag{3.A30}$$

where $W(t)$ is the Wiener process.

The straightforward stochastic differential equation of the Stein's model is

$$dv^t = -\alpha(v^t - \eta(t))dt + wqd\boldsymbol{n}(t), \tag{3.A31}$$

where $\boldsymbol{n}(t)$ is the Poisson process whose intensity is $\lambda(t)$. The replacement from equation (3.A31) into (3.A30) is called the diffusion approximation. If the Gaussian approximation discussed in section **3.3.1** is valid, equation (3.A30) has the same statistics as equation (3.A31), even though they produce different sample paths.

Firing probability Standard firing probability estimation from the Fokker-Planck equation

$$\partial_t g_u(v^t) = \alpha\partial_{v^t}\left[(v^t - \eta(t))g_u(v^t)\right] + \frac{1}{2}w^2q^2\lambda(t)\partial^2_{v^t}g_u(v^t), \tag{3.A32}$$

is obtained by the absorbing boundary condition $g_u(\theta) = 0$ (Abbott and van Vreeswijk 1993; Brunel and Hakim 1999). The Fokker-Planck equation can be interpreted by the continuity equation (Brunel 2000)

$$\partial_t g_u(v,t) = -\partial_v S(v,t), \tag{3.A33}$$

where $S(v,t)$ is the probability current through v at time t and forms

$$S(v,t) = -\frac{B(t)}{2}\partial_v g_u(v,t) + A(v,t)g_u(v,t). \tag{3.A34}$$

Because the probability current $S(\theta,t)$ can be considered as the firing probability density $\psi(t) \equiv \rho(t)/\Delta t$, the firing probability can be calculated from the boundary condition $g_u(\theta) = 0$ as

$$\rho(t) = -\frac{B(t)\Delta t}{2}\partial_v g_u(v,t)\Big|_{v=\theta}. \tag{3.A35}$$

Here, it is shown that the firing probability $\rho(t)$ obtained by our method is equivalent to (3.A35) when $\Delta t \to 0$. The firing probability we define is written as

$$\rho(t;\Delta t) \equiv \int_\theta^\infty dv_1 \int_{-\infty}^\theta g(v_1, t+\Delta t|v_0, t)g_u(v_0)dv_0. \tag{3.A36}$$

Using the moment expansion with respect to v_0,

$$\mathcal{I}(v_1,\Delta t) \equiv \int_{-\infty}^\theta g(v_1|v_0;\Delta t)g_u(v_0)dv_0 = e^{\alpha\Delta t}\Big[g_u(\eta_0) + \frac{(\sigma_0)^2}{2}\partial_v^2 g_u(\eta_0) + \mathcal{O}((\sigma_0)^4)\Big], \tag{3.A37}$$

where $(\sigma_0)^2 = e^{2\alpha\Delta t}B(t)\Delta t$, $\eta_0 = v_1 + \alpha\Delta t(v_1 - \eta)$. In $\Delta t \to 0$, we find

$$\mathcal{I}(v_1, \Delta t) = (1 + \alpha\Delta t)g_u(v_1) + \alpha\Delta t(v_1 - \eta(t))\partial_{v_1}g_u(v_1) + \frac{B(t)\Delta t}{2}\partial_{v_1}^2 g_u(v_1) + \mathcal{O}((\Delta t)^2). \tag{3.A38}$$

Considering $g_u(v_1) = 0$ for $v_1 \geq \theta$, the direct integral with respect to v_1 becomes

$$\rho(t) = \int_\theta^\infty \mathcal{I}(v_1, \Delta t)dv_1 = -\frac{B(t)\Delta t}{2}[\partial_{v_1}g_u(v_1)]_{v_1=\theta}, \tag{3.A39}$$

which is equivalent to (3.A35) based on the Fokker-Planck equation.

Chapter 4

Spike-based Hebbian Learning of Stochastic Spiking Neurons

Abstract. In this chapter, we discuss the self-organization and formation of neural circuits based on the temporal coding hypothesis. We employ an integrate-and-fire neuron model. The same spatio-temporal pattern is provided to all of the neurons in a network, and the network learns the pattern based on spike-based Hebbian learning. The network should select appropriate connections in order to distributedly preserve the input pattern. Since the same input is provided to all of the neurons, competitive learning should proceed. The competitive learning is induced by background random inputs (noise). After the learning, the network works as a spatio-temporal filter for the input patterns. The effect of noise in our model is also discussed theoretically.

4.1 Introduction

Conventionally, it has been assumed that neuronal information is represented by the neuron's firing rate. This is called the rate coding hypothesis. As an experimental example, the firing rate of a Purkinje cell, which is an output unit of the cerebellum, is highly correlated with the activities of its projecting muscle (Shidara et al., 1993). On the other hand, the activities of the prefrontal cortical neurons of a behaving monkey are contradictory (Vaadia et al., 1995). Although the activity rate does not change very much, the spatio-temporal correlation between neurons changes quite a bit. Moreover, in the monkey's primary auditory cortex, neurons process their information by modifying the spike timing without changing their spike rate (deCharms & Merzenich, 1996).

It is thus possible for neurons to process information not only by their spike rate but also by their spike timing. Especially when the firing rate is low, it is efficient for neurons to use their spike timing. Therefore, the temporal structures of neuronal activities may play an important role in defining the functions of the activities. This is called the temporal coding hypothesis.

The temporal coding hypothesis assumes that a single neuron has the capability to precisely resolve spikes input to the neuron. This is a reasonable assumption in an auditory system that deals with fine temporal information (Reyes et al., 1994; 1996). The cortical neurons may have such a precise decoding ability with the help of inhibitory inputs or nonlinear dendritic activities (Softky & Koch, 1993; Softky, 1995; Fujii et al., 1996).

Unsupervised Hebbian learning may play an important role in the primary development of nervous systems. Namely, a nervous system is formed not only by genetic programs but also by inputs provided to the system. For instance, periodical activities of the retina induce synaptic segregation in the lateral geniculate nucleus (Meister et al., 1991). A similar activity induces segregation and development of columnar structures in the visual cortex (Toyama et al., 1996).

Hebbian learning originally defined synaptic plasticity based on the correlation between pre-synaptic and post-synaptic activities. According to recent physiological studies, synaptic change, i.e., long-term potentiation (LTP) or long-term depression (LTD), is dependent on the timing of spikes input from the pre-synaptic neurons and the firing timing of the post-synaptic neuron (Stanton & Sejnowski, 1989; Markram et al., 1997, Zhang et al., 1998). Gerstner and van Hemmen (1993) devised a spike-based Hebbian learning rule to account for synaptic plasticity. Using the learning rule, a network of neurons can store a spatio-temporal pattern. When a new spatio-temporal pattern that is similar to the stored pattern is presented as the initial state, the trained network can retrieve the stored pattern. Namely, the network serves as a spatio-temporal associative memory. Gerstner et al. (1996) also showed that spike-based Hebbian learning can be used for extracting fine temporal information from noisy input spikes.

In this chapter, we propose another spatio-temporal learning model that employs spike-based Hebbian learning. If the input pattern is spatially decomposed and each neuron receives a part of the decomposed pattern, the neuron recognizes its spatial role and the learning proceeds in a manner similar to the above-mentioned associative memory method. On the other hand, this chapter considers a situation where the same spatio-temporal pattern is provided to all of the neurons. In this network architecture, the neurons have no way to recognize their spatial role at the beginning of the learning. They need to obtain their role in a self-organization fashion. This method is called competitive learning.

This chapter also discusses how background noise affects the learning. We first consider the problem of how a neuron extracts a signal represented by coincidental input spikes, when the signal is distributed by dominant random spikes (noise). Such extraction is done by potentiating the synapses from the pre-synaptic neurons providing the signal and by depressing the synapses providing the noise. We next consider the problem of how a neural network extracts a spatio-temporal signal when the signal is disturbed by dominant noise. We will see that background noise induces self-organization, i.e., competitive learning in the network.

After the learning, the network preserves a distributed representation of the input

spatio-temporal pattern, and the network is able to serve as a spatio-temporal filter to discriminate the learned pattern. Since this filtering process is temporally fine, it can be regarded as one of the temporal coding mechanisms. However, how the network deals with temporal information whose precision is higher than the dynamics of the membrane potential (Gerstner et al., 1996) is not in the scope of this chapter.

4.2 Neuron model and learning

4.2.1 Neuron model

We employ an integrate-and-fire neuron model. The membrane potential of the j-th neuron at time t, $v_j(t)$, is given by $v_j(t) = h_j(t) + u_j(t)$. $h_j(t)$ is the refractoriness function. $u_j(t)$ is the integrated synaptic inputs and is defined by

$$\tau_m \frac{du_j(t)}{dt} = -u_j(t) + \sum_i w_{ij} \sum_{f=1}^{n_i(t)} \frac{1}{\tau_{syn}} \exp\left[-\frac{t - t_i^f}{\tau_{syn}}\right] \mathcal{H}(t - t_i^f), \tag{4.1}$$

where i is the index of pre-synaptic neurons, $n_i(t)$ is the number of spikes input from pre-synaptic neuron i before time t, and t_i^f ($f = 1, \ldots, n_i(t)$) is the f-th spike input time from neuron i. $\mathcal{H}(t)$ is the Heaviside function. τ_m and τ_{syn} are the membrane time constant and the synaptic time constant, respectively. w_{ij} is the efficacy value of the synapse projecting from neuron i to j.

The refractoriness function, $h_j(t)$, is defined by

$$h_j(t) = \begin{cases} -\infty & (t_j^n < t < t_j^n + \delta_{ARP}) \\ h_{\mathrm{ref}}(t) & (\mathrm{otherwise}), \end{cases} \tag{4.2}$$

where t_j^n ($n = 1, 2, \ldots n_j(t)$) is the n-th firing time of neuron j. The upper and lower definitions in (4.2) correspond to the absolute refractoriness and the relative refractoriness, respectively. The constant δ_{ARP} denotes the absolute refractory period. The function for the relative refractoriness, $h_{\mathrm{ref}}(t)$, is defined later.

When membrane potential $v_j(t)$ exceeds threshold value θ, neuron j fires. It is assumed that the firing of the i-th neuron induces an EPSP (excitatory post-synaptic potential) on post-synaptic neuron j after fixed delay time Δ_{ij}. Here, Δ_{ij} includes both axonal delay and synaptic delay.

4.2.2 Spike-based Hebbian learning

Recent physiological studies have revealed that synaptic plasticity depends not only on the firing rates of pre- and post-synaptic neurons, but also on the spike input time from a pre-synaptic neuron and the arrival time of the backpropagated current from a post-synaptic neuron's firing (Markram et al., 1997; Zhang et al., 1998). Here, we focus on the plasticity due to the latter effect.

When pre-synaptic neuron i fires at time t_i^f, the corresponding spike input time is $t_i^f + \Delta_{ij}$. When post-synaptic neuron j fires at time t_j^f, the arrival time of the corresponding backpropagated current is t_j^f, where $\Delta_{ij}^{\rm dend}$ is the delay time for the backpropagated current reaching the synapse. The variation of the dendritic delay time, $\Delta_{ij}^{\rm dend}$, can contribute to the learning of a temporal pattern (Pelaez, 1997). In this study, however, we ignore the dendritic delay time ($\Delta_{ij}^{\rm dend} = 0$).[1]

It is assumed that each synaptic efficacy change can be described by dynamics that are temporally and spatially local. In order to describe such dynamics, we introduce synaptic internal variables, $\alpha_{ij}^k(t)$ and $\beta_{ij}^k(t)$ ($k = 1, 2$), between pre-synaptic neuron i and post-synaptic neuron j. $\alpha_{ij}^k(t)$ ($k = 1, 2$) integrates spike effects from pre-synaptic neuron i, and $\beta_{ij}^k(t)$ ($k = 1, 2$) integrates firing effects of post-synaptic neuron j. The dynamics of the internal variables are described as follows:

$$\begin{cases} \dfrac{d\alpha_{ij}^k(t)}{dt} = -\dfrac{1}{\tau_{\alpha^k}}\alpha_{ij}^k(t) + A_{\alpha^k}\displaystyle\sum_{f=1}^{n_i(t)}\delta(t - t_i^f - \Delta_{ij}) & k = 1, 2 \\ \dfrac{d\beta_{ij}^k(t)}{dt} = -\dfrac{1}{\tau_{\beta^k}}\beta_{ij}^k(t) + A_{\beta^k}\displaystyle\sum_{f=1}^{n_j(t)}\delta(t - t_j^f) & k = 1, 2 \end{cases}, \tag{4.3}$$

where τ_{α^k}, τ_{β^k}, A_{α^k} and A_{β^k} are constants. $\delta(\cdot)$ is Dirac's delta function. The internal variables analogically correspond to ions or gating parameters of the synapse. Using the internal variables, the synaptic efficacy $w_{ij}(t)$ is assumed to be described as follows:

$$\frac{dw_{ij}(t)}{dt} = \epsilon\left(\beta_{ij}^2(t) - \beta_{ij}^1(t) + \gamma\right)\sum_{f=1}^{n_i(t)}\delta(t - t_i^f - \Delta_{ij}) + \epsilon\left(\alpha_{ij}^2(t) - \alpha_{ij}^1(t)\right)\sum_{f=1}^{n_j(t)}\delta(t - t_j^i), \tag{4.4}$$

where ϵ is a small constant. γ is a constant parameter. The solution of (4.3) and (4.4) is given by

$$\begin{aligned} w_{ij}(t) \;=\; & w_{ij}(0) + \epsilon\sum_{f=1}^{n_i(t)}\left[\gamma + A_{\beta^1}\sum_{f'=1}^{n_j(t)}\exp\left[\frac{t_j^{f'} - t_i^f - \Delta_{ij}}{\tau_{\beta^1}}\right] - A_{\beta^2}\sum_{f'=1}^{n_j(t)}\exp\left[\frac{t_j^{f'} - t_i^f - \Delta_{ij}}{\tau_{\beta^2}}\right]\right] \\ & + \epsilon\sum_{f=1}^{n_j(t)}\left[A_{\alpha^1}\sum_{f'=1}^{n_i(t)}\exp\left[\frac{t_i^{f'} + \Delta_{ij} - t_j^f}{\tau_{\alpha^1}}\right] - A_{\alpha^2}\sum_{f'=1}^{n_i(t)}\exp\left[\frac{t_i^{f'} + \Delta_{ij} - t_j^f}{\tau_{\alpha^2}}\right]\right] \end{aligned} \tag{4.5}$$

.

The dynamics of the efficacy and the internal variables are illustrated in Figure 4.1. When pre-synaptic neuron i fires, the internal variable α_{ij}^k increases by A_{α^k} and the synaptic efficacy w_{ij} is changed by $\epsilon(\beta_{ij}^2(t) - \beta_{ij}^1(t) + \gamma)$. When post-synaptic neuron j fires, the internal variable β_{ij}^k is changed by A_{β^k}, and w_{ij} increases by $\epsilon(\alpha_{ij}^2(t) - \alpha_{ij}^1(t))$.

[1] If $\Delta_{ij}^{\rm dend}$ is a constant, our model can consider its effect by shifting the learning window given by equation (4.6)

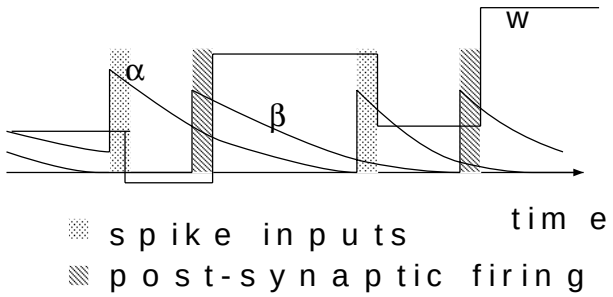

Figure 4.1: Dynamics of synaptic efficacy and internal variables. When a pre-synaptic neuron fires, internal variable α increases and synaptic efficacy changes. When a post-synaptic neuron fires, internal variable β increases and synaptic efficacy changes.

4.2.3 Representation by the learning window

The above dynamics of synaptic efficacy can also be defined by the difference between the pre- and post-firing times. Following an existing study (Gerstner et al., 1996), we introduce a learning window:

$$W(s) = \begin{cases} A_{\beta^1} \exp\left[\dfrac{s}{\tau_{\beta^1}}\right] - A_{\beta^2} \exp\left[\dfrac{s}{\tau_{\beta^2}}\right] & (\text{for } s \leq 0) \\ A_{\alpha^1} \exp\left[-\dfrac{s}{\tau_{\alpha^1}}\right] - A_{\alpha^2} \exp\left[-\dfrac{s}{\tau_{\alpha^2}}\right] & (\text{for } s > 0). \end{cases} \tag{4.6}$$

Then, equation (4.5) simply becomes:

$$w_{ij}(t) \;=\; w_{ij}(0) + \epsilon \sum_{f=1}^{n_i(t)} \left[\gamma + \sum_{f'=1}^{n_j(t)} W(t_j^{f'} - t_i^f - \Delta_{ij}) \right]. \tag{4.7}$$

Since the window function (4.6) requires smoothness at $s = 0$, the following constraints exist:

$$W'(0) = \frac{A_{\beta^1}}{\tau_{\beta^1}} - \frac{A_{\beta^2}}{\tau_{\beta^2}} = -\frac{A_{\alpha^1}}{\tau_{\alpha^1}} + \frac{A_{\alpha^2}}{\tau_{\alpha^2}}, \quad W(0) = A_{\beta^1} - A_{\beta^2} = A_{\alpha^1} - A_{\alpha^2}. \tag{4.8}$$

Figure 4.2 shows the shape of a learning window that satisfies the above constraints. When the learning window has a shape as shown in Figure 4.1, a synapse through which the post-neuron fires just after the pre-input spike is potentiated, and it is depressed otherwise.

In this chapter, we consider the synaptic learning defined by (4.5), which is called spike-based Hebbian learning. This learning can also be defined by (4.6) and (4.7).

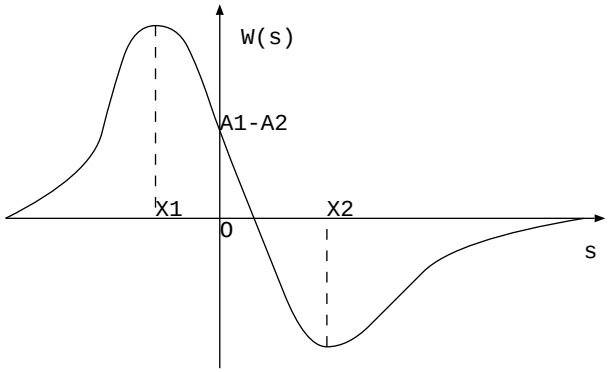

Figure 4.2: A typical function shape of learning window $W(s)$, which is defined by equation (6).

4.3 Hebbian Learning in stochastic inputs

We first consider how spike-based Hebbian learning proceeds when weak coincidental inputs and strong random inputs are simultaneously provided to a single neuron.

4.3.1 Stochastic resonance

Assume that two types of inputs, i.e., deterministic inputs (signal) and stochastic inputs (noise), are simultaneously provided to a single neuron. From equation (4.1), the membrane potential is written by the summation of an EPSP induced via each synapse. Then, the potential is decomposed into the effects of the deterministic inputs and the stochastic inputs:

$$\boldsymbol{u}(t) = \sum_{d=1}^{N_D} w_d \sum_{f=1}^{n_d(t)} u(t - t_d^f) + \sum_{s=1}^{N_S} w_s \sum_{f=1}^{n_s(t)} u(t - \boldsymbol{t}_s^f) \equiv u_d(t) + \boldsymbol{u}_s(t). \tag{4.9}$$

N_D (N_S) is the number of pre-synaptic neurons, called input units, that provide deterministic (stochastic) inputs. w_d (w_s) and $n_d(t)$ ($n_s(t)$) are the synaptic efficacy and the number of input spikes, respectively, from the d-th deterministic (s-th stochastic) input unit. The response kernel $u(\cdot)$ is the shape of an EPSP. The bold font represents a probabilistic variable.

For the stochastic inputs, independent Poisson random inputs are prepared (Softky and Koch, 1993). The ensemble mean and the ensemble variance of the membrane potential evoked by Poisson inputs exponentially converge to a certain value (Tuckwell, 1977). The ensemble mean and the ensemble variance of the potential are given by

$$\begin{aligned} \langle \boldsymbol{u}(t) \rangle &= u_d(t) + \langle \boldsymbol{u}_s(t) \rangle \equiv u_d(t) + u_s(t) \\ \langle \boldsymbol{u}(t)^2 \rangle - \langle \boldsymbol{u}(t) \rangle^2 &= \langle \boldsymbol{u}_s(t)^2 \rangle - \langle \boldsymbol{u}_s(t) \rangle^2 \equiv \sigma^2(t). \end{aligned} \tag{4.10}$$

Here, we see how the deterministic input $u_d(t)$ affects the firing property of a neuron, when the firing threshold is sufficiently high in comparison to the converged value.

When the ensemble distribution of the membrane potential is approximated by a Gaussian function with mean $u_d(t) + u_s(t)$ and variance $\sigma^2(t)$, the firing probability with a given $u_d(t)$ is approximated by the error function:

$$\mathcal{P}(\boldsymbol{u}(t) \geq \theta | u_d(t)) \approx H\left(\frac{\theta - u_d(t) - u_s(t)}{\sqrt{2\sigma^2(t)}}\right), \tag{4.11}$$

where $H(x) = \frac{1}{2} - \frac{1}{\sqrt{\pi}} \int_0^x e^{-t^2} dt$. After the ensemble mean and the ensemble variance of $u_s(t)$ converge like $u_s(t) \to u_s$ and $\sigma^2(t) \to \sigma^2$, the firing probability is given by $H((\theta - u_s - u_d(t))/\sqrt{2\sigma^2})$.

The time derivative of the firing probability is then given by

$$\frac{d\mathcal{P}(\boldsymbol{u} \geq \theta | u_d(t))}{dt} = \frac{\partial \mathcal{P}(\boldsymbol{u} \geq \theta | u_d(t))}{\partial u_d(t)} \frac{du_d(t)}{dt} \approx \mathcal{N}(\theta - u_s - u_d(t), \sigma^2) \frac{du_d(t)}{dt} \tag{4.12}$$

where $\mathcal{N}(x, y)$ denotes the normal distribution whose mean and variance are x and y, respectively. Since $\theta - u_s - u_d(t) \geq 0$, the larger $u_d(t)$ is, the larger $\mathcal{N}(\theta - u_s - u_d(t), \sigma^2)$ becomes. When the deterministic inputs $u_d(t)$ change, the change in the firing probability depends not only on the change in the deterministic inputs, $du_d(t)/dt$, but also on the amplitude of the deterministic inputs, $\mathcal{N}(\theta - u_s - u_d(t), \sigma^2)$. Namely, when the amount of deterministic inputs is large, the firing probability responds sharply to the change in the deterministic inputs.

In order to make deterministic inputs large, coincidental inputs are effective. To discuss this property, we show here a simple experiment. Two kinds of inputs, stochastic inputs and deterministic inputs are prepared:

- Forty random inputs which obey the Poisson process with the frequency 0.6[ms^{-1}].
- Two deterministic periodic inputs that synchronously occur. The period is 5[ms].

The system is described by the left illustration in Figure 4.3. Note that the rate and the number of random inputs are larger than those of deterministic inputs.

The firing probability of a neuron evaluated from the last reset time defines the first passage time density of the membrane potential. Here, the reset time denotes the time at which the membrane potential becomes the zero level.

In the lower right graph of Figure 4.3, the dashed line denotes the ensemble mean of the membrane potential when only the random inputs are provided. The upper solid line denotes the ensemble mean when the deterministic inputs are also provided. The lower solid line denotes the ensemble variance. They are theoretically obtained (Amemori and Ishii, 2000). The upper right graph shows the first passage time density when the deterministic inputs are provided, which is experimentally obtained. Although the deterministic inputs have a small effect on the ensemble behavior, the deterministic inputs significantly increase the firing probability of the neuron.

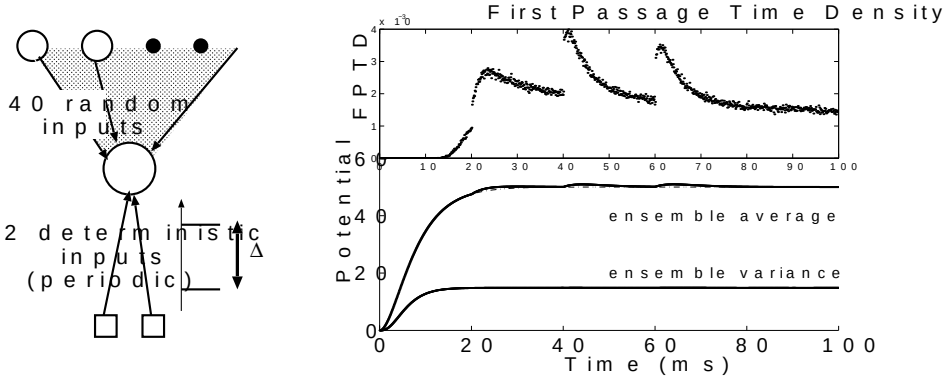

Figure 4.3: Effect of synchronized inputs. (left) The system we consider. A neuron receives spikes from forty random input units and two deterministic input units. (upper right) The first passage time density, i.e., the firing probability of the neuron, which is provided by the deterministic inputs, is shown. The results are experimentally obtained. (lower right) The dashed line denotes the ensemble mean of the membrane potential when only the random inputs are provided to the neuron. The upper solid line denotes the ensemble mean when the deterministic inputs are also provided. The lower solid line denotes the ensemble variance for both cases. These lines are theoretically obtained.

Accordingly, a weak synchronous signal is extracted by the neuron even under dominant random noise. On the other hand, the neuron can hardly fire without the random noise, especially when the firing threshold is high. In this sense, the extraction of the weak synchronous signal is encouraged by the random noise. This reminds us of "stochastic resonance" (Wiesenfeld and Jaramillo, 1998).

4.3.2 Extraction of weak synchronized inputs

Even under dominant random noise, synchronized inputs are helpful to the firing of a post-synaptic neuron. According to spike-based Hebbian learning, a synapse is potentiated when the inputs contribute to the firing of the neuron. Then, the learning is expected to extract the synchronized inputs by potentiating the corresponding synapses. Namely, as the learning proceeds, the neuron responds more to the synchronized inputs.

We consider here the learning of the model shown in Figure 4.3 (left). The simulation is done by equations (4.1), (4.2), (4.3) and (4.5). The simulation conditions are described in appendix section 4.A.1.

Figure 4.4 shows the time-series of membrane potential v at four stages of the learning process. Figure 4.5(a) shows the neuron's firing timing values in the same learning process. The ordinate denotes the phase of each firing in the input period 5[ms]. The neuron randomly fires at the early learning stage, but gradually comes

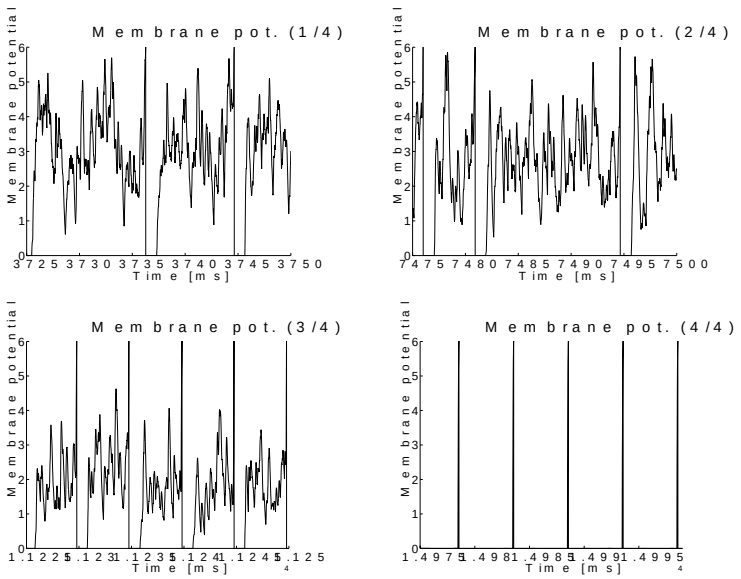

Figure 4.4: The time-series of membrane potential v at four stages of the learning process. The abscissa denotes the learning time, and the ordinate denotes the membrane potential. We can see that random behaviors of the potential, which are due to random inputs, are gradually removed as the learning proceeds.

to fire precisely in a certain phase. Figure 4.5(b) shows the efficacy change of the synapses from the deterministic and random input units during this learning process. The synapses from the deterministic input units are strengthened, while the synapses from the random input units are suppressed to zero.

Accordingly, the potentiation of the synapse is subject to the input coincidence, and consequently the neuron comes to detect the timing of the deterministic input units.

4.4 Competition among delay lines

When the learning mechanism is subject to spike coincidence rather than input rate, how is temporal information dealt with in a network of neurons? In this chapter, we assume that precise temporal information is encoded on the transmission delay between each neuronal pair (Konishi, 1986; Gerstner et al., 1996; Fujii et al., 1996).

In the following sections, we consider the learning of spatio-temporal input patterns, which are repeatedly provided to a network. A single neuron learns its coincidental input synapses (or, lines), and a network of such neurons is able to learn a distributed representation of a spatio-temporal input pattern in a self-organization fashion. We prepare a certain number of synapses whose delays are varied, and let each neuron select synapses appropriate for recording the distributed representation of the input pattern. We assume that the input pattern is common to all neurons, and random

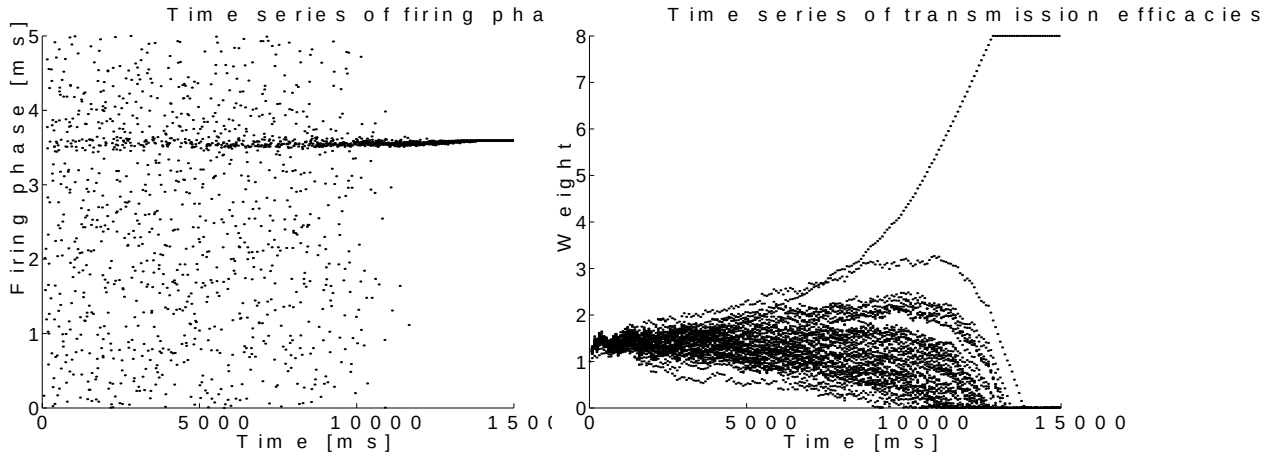

Figure 4.5: The time-series of spikes and weights. (a) The time-series of the firing phase of a neuron. The abscissa denotes the learning time, and the ordinate denotes the phase in the period 5[ms]. Each dot corresponds to a firing timing in the period. (b) The time-series of synaptic efficacies. The abscissa denotes the learning time, and the ordinate denotes the synaptic efficacy. The synapses projected from the regular input units are strengthened, while the synapses from the random input units are depressed to be segregated. There are two lines corresponding to the two deterministic input units, but they are overwritten in this figure.

inputs are independently provided to each neuron (see Figure 4.6(a)).

One of the existing studies on spatio-temporal pattern learning was based on an associative memory method (Gerstner and van Hemmen, 1993), which assumed the network topology shown in Figure 4.6(b). The model we consider here is different from that method. Our network topology (Figure 4.6(a)) includes all-to-all couplings among the input units and neurons, and the same input spike sequences are provided to all of the neurons. Since there is no difference between the neurons, stochastic fluctuations are essential to break the network symmetry.

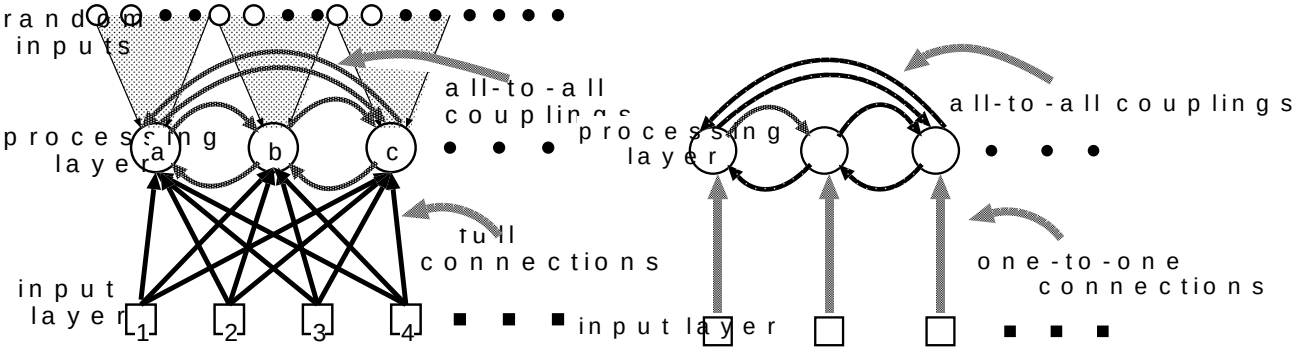

Figure 4.6: Two network learning scheme. (a) The network topology we consider. Since the same input is provided to all of the neurons, this topology is based on a competitive learning scheme. Random inputs are independently provided to the neurons. (b) The network topology in an associative memory learning scheme. The input pattern is spatially decomposed and each portion is provided independently to each neuron. There is no need for the neurons to spatially discriminate the input pattern.

If a neuron has a certain number of synapses whose delay times distribute relatively widely in comparison to the width of the EPSPs, the neuron is able to select the appropriate synapses. It is known that in regions dealing with fine temporal information like an auditory system, the mean and the variance of delay lines are much larger than EPSPs (Konishi 1986; Reyes et al., 1994; Reyes et al., 1996; Gerstner et al. 1996). In particular, in a neuronal system detecting sound sources, the decay of the EPSPs is so fast that there is no need to take a temporal summation of the inputs. Such a neuron can correctly detect the input coincidence (Young, 1998).

We assume here that the mean and the variance of synapses (i.e., delay lines) are larger than the width of the EPSPs. In order to set the mean of the delay lines at a physiologically appropriate value, we assume that the EPSP decay is so fast that the membrane constants are $\tau_m = 0.1$[ms] and $\tau_{syn} = 0.1$[ms].

We consider a situation where there are two groups of input units. The two groups periodically fire in a certain phase, and the phase difference between the groups is fixed. In this situation, the phases can be recognized and represented by two processing

neurons, provided that the two neurons each come to fire in each phase. We assume that the transmission delay between the two neurons is close to the phase difference.

The initial structure of the network is shown in Figure 4.7. Two neurons *a* and *b* are projected from two groups of regular input units, *A* and *B*, that periodically produce spikes. The input units in each group simultaneously produce spikes once in period 5[ms], while the firing timing of the two groups is different. There should be at least two units in each group, because the coincidence of their spikes is important for learning. The units in *A* and *B* fire in the phase of 1.0[ms] and the phase of 3.5[ms], respectively, in period 5[ms]. Neurons *a* and *b* are also projected from groups of random input units, C and D, respectively. The firing rate of a random input unit is $0.8[\mathrm{ms}^{-1}]$ and the spikes obey a Poisson process. There are also connections between the two processing neurons.

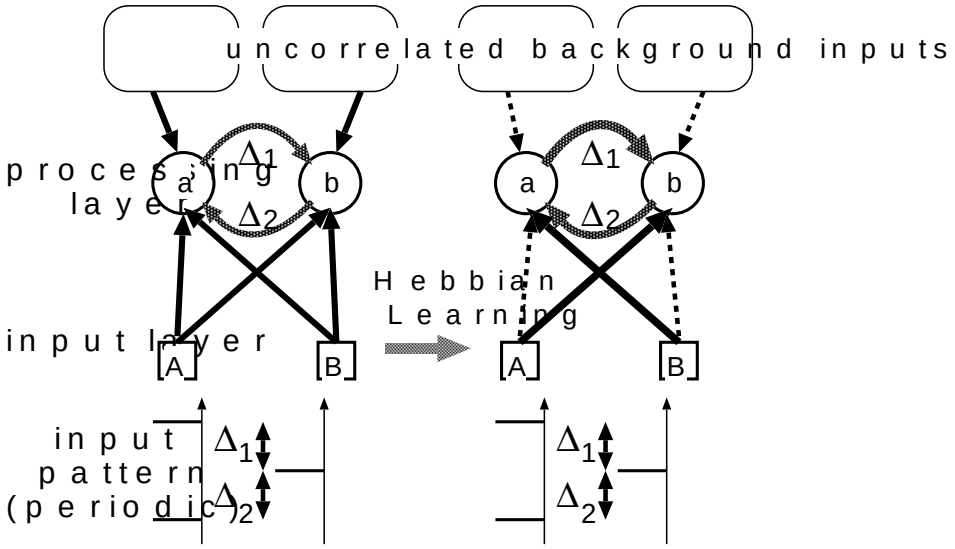

Figure 4.7: The network topology we consider. Two neurons a and b are projected from two groups of input units, A and B. The two neurons are also projected from random input units.

In this simulation, we define the relative refractoriness as

$$h_{ref}(t) = -\sum_{n=1}^{N} A_{AHP} \cdot \exp\left[-\frac{t - t_b^n - \delta_{ARP}}{\tau_{AHP}}\right] \cdot \mathcal{H}(t - t_b^n - \delta_{ARP}), \qquad (4.13)$$

where A_{AHP} and τ_{AHP} are constant values. The suffix AHP denotes "after hyperpolarization."

The number of synapses projected from neuron *a* to *b* is set at $m = 3$, and the delays of the synapses are defined by

$$\Delta_{ab}^{q} = \mathcal{D}_0 + \mathcal{D} \cdot \frac{q}{m} \qquad (q = 1, \ldots, m), \qquad (4.14)$$

where q is the index of the synapses from neuron *a* to *b*, and $\mathcal{D} = 0.3$[ms]. $\mathcal{D}_0 = 2.2$[ms]. The synapses from neuron *b* to *a* are similarly defined. Then, the transmission delays are distributed as slightly smaller values than the phase difference of the two regular input groups. Further simulation conditions are described in appendix section 4.A.2.

Figures 4.8(a) and 4.8(b) show the time-series of firing phases of neurons *a* and *b*, respectively, in a learning process. At the early learning stage until about 3[s], the two neurons respond to the spikes from both regular input groups. After that, the two neurons come to respond to the inputs from only one of the two regular input groups.

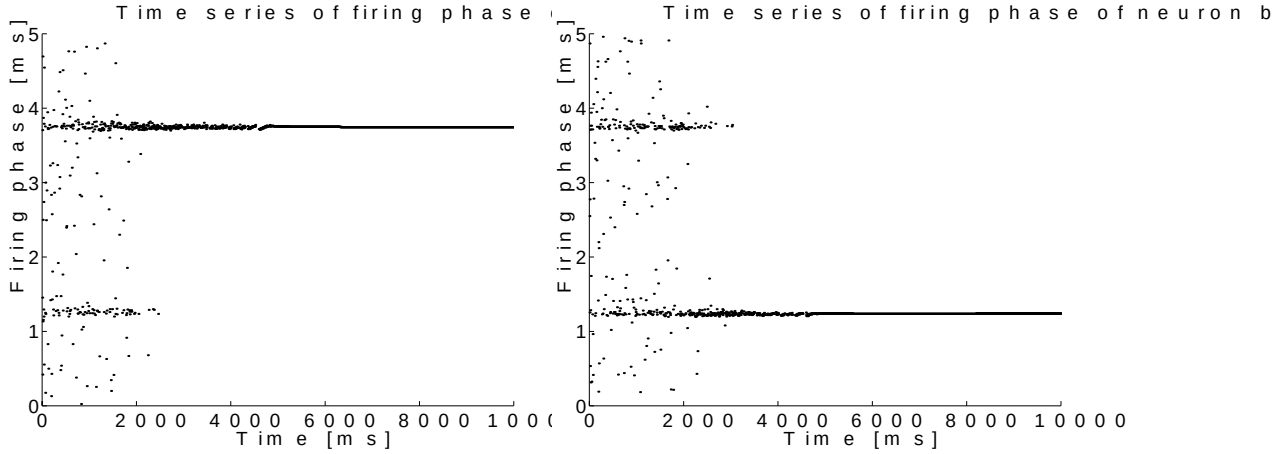

Figure 4.8: The time-series of the firing phase of neurons a (a) and b (b). The abscissa and ordinate are the same as in Figure 4.5(a). We can see that neuron a responds to one of the two regular input groups. Neuron b responds to the other regular input group.

In this model, the firing of neuron *b* (*a*) induces the firing of neuron *a* (*b*) after a fixed transmission delay time. If a spike from an input unit enters neuron *a* at a very close timing to a spike from neuron *b*, the probability for strengthening the connection from the input unit increases due to the coincidence of the two inputs. When there is a connection whose delay time is close to the phase difference of the two input groups, the connection will help the neurons fire in synchronization with the input phase.

Thus, an oscillator whose two firing timing values correspond to the two input phases is formed. Although the same input patterns are provided to the neurons, this formation is induced by the random inputs independently provided to each neuron. It should be noted that the relative refractoriness is important here. Because the relative refractoriness decreases the probability for firing immediately after the previous firing, it encourages the neurons to fire in different phases.

4.5 Learning of a spatio-temporal pattern

In order to deal with general input patterns, we prepare a network of neurons, each of which has a certain number of synapses whose delay times vary. We assume there are several input timing values in an input pattern. Therefore, there are several phase differences in the set of input timing values. If there are a certain number of synapses between each neuron pair, the firing of a neuron induces the projected neurons to fire in various phases. Then, the projected neurons are able to select an appropriate connection among them, whose delay time corresponds to one of the phase differences of the inputs. We also assume that the network of neurons is exposed to a lot of random spikes. The network is expected to respond to the input pattern in a similar self-organized fashion to the experiment described in the previous section.

4.5.1 Input pattern

Figure 4.9 shows the deterministic input units used in our simulation, where four input groups, *A*, *B*, *C*, and *D*, are prepared. Each of them has four input units. Every input unit has the same firing period T, and the units in a group fire simultaneously. The firing phase of each group differs from the others. In addition to these, random input units are prepared, whose spikes obey a Poisson process. The random input spikes provided to a processing neuron are independent of those provided to the other processing neurons.

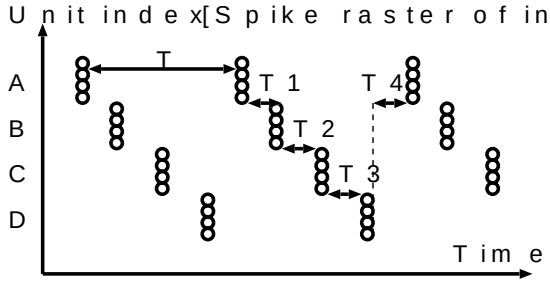

Figure 4.9: The input pattern produced by the regular input units. Four input groups, A, B, C, and D, are prepared, each of which has four input units that fire simultaneously. The firing period T is the same for all of the units, but the firing phase of each group differs from those of the other groups. T_1, T_2, T_3, and T_4 are the differences of the phases between A and B, B and C, C and D, and D and A, respectively.

$T = 7.5$[ms], and the phase differences between groups are $T1 = 2.25$[ms], $T2 = 1.75$[ms], $T3 = 2.0$[ms], and $T4 = 1.5$[ms]. The spikes from the 16 input units reach all of the neurons after a fixed delay time $\mathcal{D}_0$, and they generate EPSPs. Note that every neuron receives the same spikes from the deterministic input units, although the spikes from the random input units are different.

In this experiment, the temporal pattern can be set arbitrarily if the time differences in the pattern are smaller than the width of the variation of the delay times, which is described as $\mathcal{D}$ in the next subsection. On the other hand, the spatial pattern has some limitations. As the number of input timings increases, the network needs more neurons to learn the pattern. In addition, at least two units should produce spikes simultaneously at each input timing.

4.5.2 Learning by network

We prepare 16 neurons, all of which connect with each other. Let m be the number of synapses between each neuronal pair, and $n(=15)$ be the number of projecting neurons. The delay time of the q-th synapse $(q = 1, \ldots, m)$ between neurons i and j is described as

$$\Delta_{ij}^{q} = \mathcal{D}_0 + \rho, \quad \rho \in \left\{ \frac{\mathcal{D}}{n \cdot m} k \middle| k = 1, \ldots, (n \cdot m) \right\},$$

where ρ is randomly chosen under the condition that every synapse projecting to a single neuron has a different value. Due to a computational limitation, we cannot prepare a lot of synapses between each neuronal pair. We instead make the synaptic delay vary. This delay time is initially set and does not change.

We set $m = 4$. Forty random input units are prepared for each neuron. The random units fire at the rate of 0.7[ms^{-1}]. The number of synapses from each random or regular input unit is 1. In this system, the effect of the random units on the membrane potential is initially superior to that of the regular input units. The former is 2.5 times larger than the latter in number, and 5.25 times larger in the firing rate of a single unit. Further simulation conditions are described in appendix section 4.A.3.

After 400[s] of learning, the synaptic efficacies for almost all of the synapses become the lower limit or the upper limit.[2] Figure 4.10 shows the spike raster produced by the network after the learning. In this case, the input pattern is also provided to the network. The ordinate -1 denotes the spike arrival times from the regular input units. Each neuron responds to one of the four regular input groups.

Figure 4.11 shows the spike transmission diagram after learning. Each line connects a pair consisting of the firing time and the index of a pre-synaptic neuron, with a pair consisting of the spike arrival time and the index of a post-synaptic neuron. Before learning, every spike produced by a neuron is transmitted to all of the other neurons. After learning, the spike transmissions are restricted to those shown in Figure 4.11, and this self-organized spatio-temporal structure enables the network to produce regular output spikes.

Figure 4.12 shows the connections among the neurons before learning (a) and after learning (b). It can be seen that the connections are selected from among the initial full connections.

[2]Only four synapses among 1856 did not reach the upper or lower limit at 400[s].

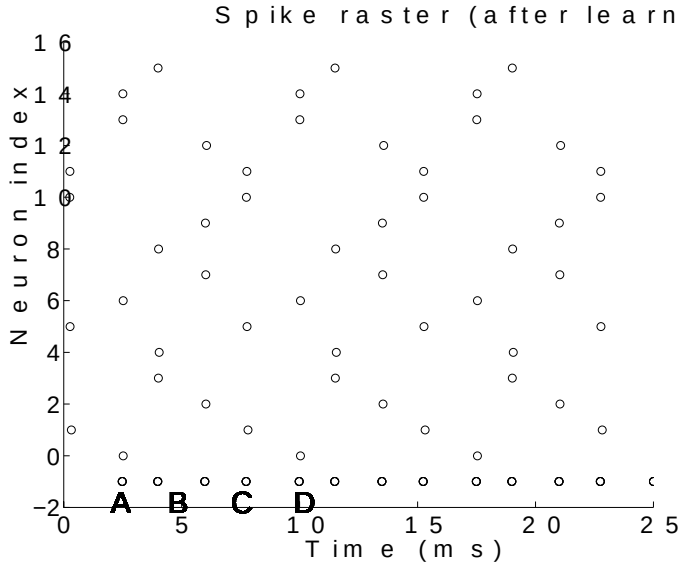

Figure 4.10: The spike raster produced by the network after 400[s] of learning. The abscissa denotes the time, and the ordinate denotes the neuron index. The 'o' mark denotes a firing. Neuron index -1 indicates spikes received from regular input units.

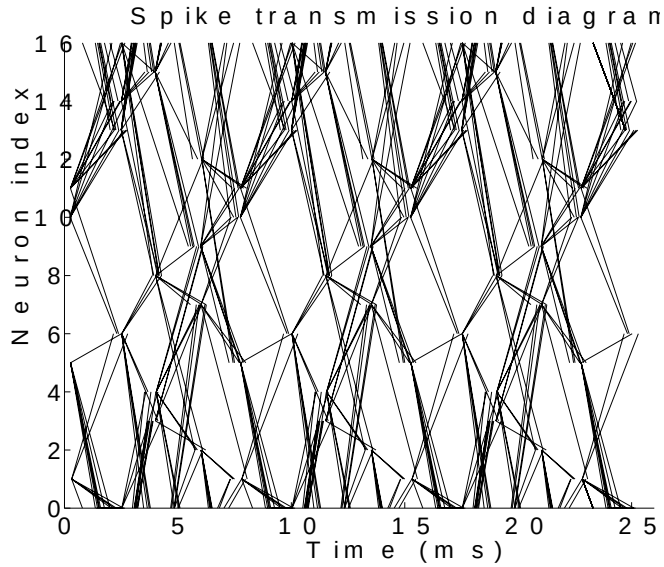

Figure 4.11: A spike transmission diagram of the network after 400[s] of learning. Each line connects a pair consisting of 'firing time' and 'firing neuron index' with a pair consisting of 'receiving time' and 'receiving neuron index'.

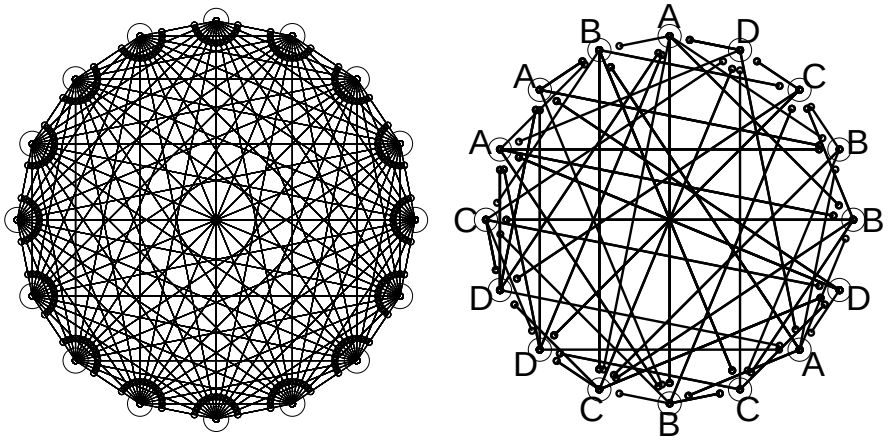

Figure 4.12: The remaining synapses before learning (a) and after learning (b). Each synapse projects from the center of a circle (pre-neuron) to a black point (post-neuron). The line width corresponds to the magnitude of the synaptic efficacy. Synapses whose efficacy value is smaller than 0.5 are not drawn. (a) Initially, the network has all-to-all couplings. (b) After 400[s] of learning, some of the synapses are enhanced to their maximum efficacy value, while the others are depressed to be segregated. The attached indices correspond to the order of the input groups projecting to the neurons.

After 400[s] of learning, every neuron removes the connections from the random input units, and comes to fire periodically by the inputs from the regular input units and the other processing neurons.

4.6 Retrieval of spatio-temporal pattern

4.6.1 Correlation between training sequence and test sequence

The temporal information of the input sequence is expected to be preserved among the network connections achieved through learning. In this section, the precision of the encoded information is examined. We prepare test input sequences that are different from the training sequence and examine the network responses to the test sequences. Each test sequence has the same period T as the training sequence, and each input unit fires once in period T.

Subsequently, the input sequence (Fig. 8) provided during the learning stage is called the training sequence, and is described as $\boldsymbol{a}(t)$, where $a_i(t) = \sum_f \delta(t - t_i^f)$. i is the index of an input unit, and t_i^f is its f-th firing time. The network after learning is called the trained network. The test input sequence is described as $\boldsymbol{b}(t)$. The response sequence (Fig. 10) of the trained network for the training sequence is called the learned sequence, and is described as $\boldsymbol{x}(t)$. The response sequence for the test sequence is

called the output sequence, and is described as $\boldsymbol{y}(t)$.

To consider the phase differences between $\boldsymbol{a}(t)$ and $\boldsymbol{b}(t)$, we define their correlation values by

$$C(\boldsymbol{a}(t), \boldsymbol{b}(t)) = \max_{\tau} E\left\{\boldsymbol{a}(t) \cdot \boldsymbol{b}(t-\tau)\right\},$$

where the dot $(\cdot)$ denotes the internal product of two vectors. $E\{\cdot\}$ gives the expectation value over the trials. C is an integer between 1 and n, where n is the number of input units.[3]

By providing test sequences to the trained network, we examine the output sequences. We can classify the output sequences into two categories. One is the case where each neuron hardly fires, and the other is the case where a spatio-temporal spike pattern is continuously generated. The output sequence $\boldsymbol{y}(t)$ in the latter case is highly correlated with the learned sequence $\boldsymbol{x}(t)$, and the firing periods of the neurons are almost equal to T. Therefore, it is assumed that all of the firing timing values have period T, for the time being. However, we will check this assumption later.

In order to examine the response of the trained network, we also prepare two quantities that are defined for two sequences, $\boldsymbol{\eta}(t)$ and $\boldsymbol{\xi}(t)$. $C'(\boldsymbol{\eta}(t), \boldsymbol{\xi}(t))$ $(0 \leq C' \leq n)$ indicates the number of spikes that match between $\boldsymbol{\eta}(t)$ and $\boldsymbol{\xi}(t)$ in period T. The matching considers some small temporal variation ϑ in the sequences. In order to estimate the temporal difference between $\boldsymbol{\eta}(t)$ and $\boldsymbol{\xi}(t)$, we define $d(\boldsymbol{\eta}(\mathrm{t}),\boldsymbol{\xi}(\mathrm{t}))$, which is the criterion of the firing timing values between the sequences. Their detailed definitions are described in appendix section 4.A.4.

Based on these quantities, the properties of the trained network are examined. We generate test sequences $\boldsymbol{b}(t)$ which have various correlation values with the training sequence $\boldsymbol{a}(t)$, $C(\boldsymbol{a}(t), \boldsymbol{b}(t))$ and provide them to the trained network during 10[s]. At the first period T in each trial, all of the synaptic efficacies from the input units are strengthened by 1.5 times so as to encourage the neurons to start firing. Since the threshold is set to be relatively large in this model, the trained network often shows no response without the spikes from the network itself. Then, we temporally magnify the synaptic efficacies from the input units so that the processing neurons start firing without the help of the other processing neurons. For each correlation value of $C(\boldsymbol{a}(t), \boldsymbol{b}(t))$ between 1 and 16, we prepare 200 test sequences, and examine the responses.

If the total number of firings in the network during the 10[s] is smaller than N_{th}, we classify the trial into category 1. If the total number exceeds N_{th} and at least one neuron does not fire at all, we classify the trial into category 2. If the total number exceeds N_{th} and every neuron fires at least once, we classify the trial into category 3.

If the output sequence $\boldsymbol{y}(t)$ belongs to category 3, we calculate the following three criteria.

[3] A test sequence $\boldsymbol{b}(t)$, whose correlation value is c $(1 \leq c \leq n)$, is generated as follows. First, c timing values in $\boldsymbol{a}(t)$ are randomly chosen and c timing values in $\boldsymbol{b}(t)$ are set to be those. The remaining $n - c$ timing values in $\boldsymbol{b}(t)$ are set randomly under the condition that they differ with those in $\boldsymbol{a}(t)$.

1. output pattern difference (correlation) between $\boldsymbol{x}(t)$ and $\boldsymbol{y}(t)$, $C'(\boldsymbol{x}(t), \boldsymbol{y}(t))$.
2. spike timing difference between $\boldsymbol{x}(t)$ and $\boldsymbol{y}(t)$, $d(\boldsymbol{x}(t), \boldsymbol{y}(t))$.
3. the criterion that $\boldsymbol{y}(t)$ is periodic, $d(\boldsymbol{y}(t), \boldsymbol{y}(t))$.

If criterion 3 is small enough, all of the firing timing values in $\boldsymbol{y}(t)$ have almost the same phase in period T. Experimentally, $d(\boldsymbol{y}(t), \boldsymbol{y}(t))$ is very close to 0 in almost every case, implying that the assumption described earlier in this section is valid.

4.6.2 Response of trained network

We set N_{th} =100. Figure 4.13 shows the ratio of firings against the input correlation value $C(\boldsymbol{a}, \boldsymbol{b})$. The larger the input correlation value is, the better the network responds.

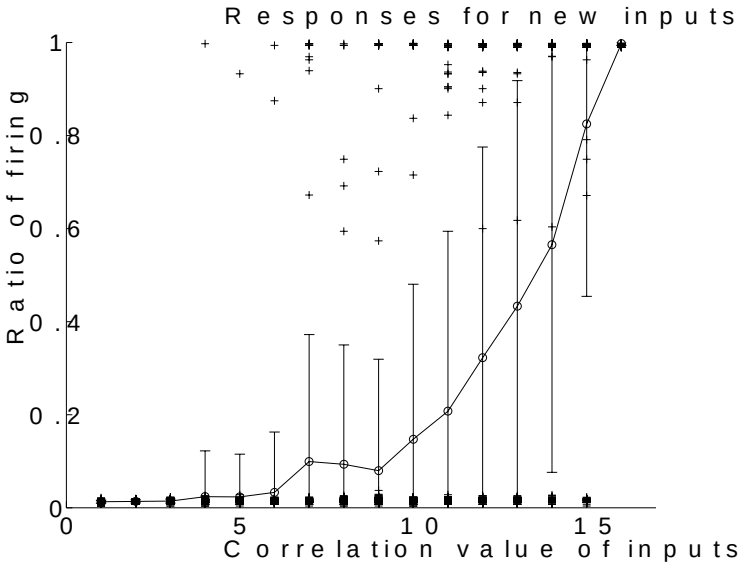

Figure 4.13: Network responses to newly provided inputs. The abscissa denotes the correlation value between training sequence $\boldsymbol{a}(t)$ and test sequence $\boldsymbol{b}(t)$, i.e., $C(\boldsymbol{a}(t), \boldsymbol{b}(t))$. The ordinate denotes the ratio of the spikes produced when test sequence $\boldsymbol{b}(t)$ is provided to the network. The firing ratio is 1 when every neuron fires once in period T continuously through a trial. The '+' mark corresponds to a single trial. The 'o' mark and the error-bar denote the mean of the firing ratio for each correlation value and its standard deviation, respectively.

Figure 4.14 shows the ratio of each category against the input correlation $C(\boldsymbol{a}, \boldsymbol{b})$. In the 200 trials for each correlation value, the black, gray, and white bars denote the ratio of category 1, category 2, and category 3, respectively. A typical case of category

1 is that every neuron ceases to respond at all after several initial firings. Namely, when the test sequence $\boldsymbol{b}(t)$ is apart from the training sequence $\boldsymbol{a}(t)$, the network does not respond. This implies that the firing of each neuron needs not only the spikes from the input units, but also the coincident spikes produced by the other neurons. The larger the input correlation is, the more frequently category 3 appears.

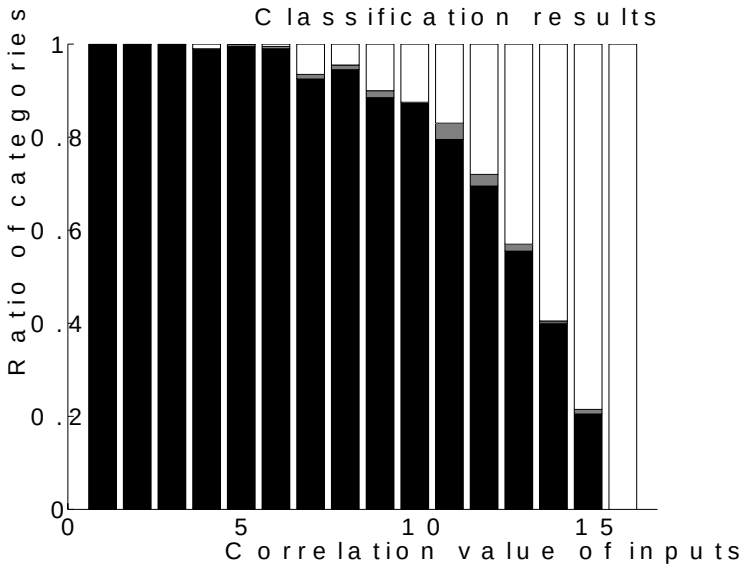

Figure 4.14: Classification results. The abscissa denotes the correlation value between training sequence $\boldsymbol{a}(t)$ and test sequence $\boldsymbol{b}(t)$, i.e., $C(\boldsymbol{a}(t), \boldsymbol{b}(t))$. The ordinate denotes the ratio of three categories among 200 trials. The black, gray, and white bars denote the ratio of categories 1, 2, and 3, respectively.

Figure 4.15 shows the ratio of trials against pairs of the input correlation $C(\boldsymbol{a}, \boldsymbol{b})$ and the output correlation $C'(\boldsymbol{x}, \boldsymbol{y})$. Here, trials belonging to category 3 are shown. Even when $C(\boldsymbol{a}, \boldsymbol{b})$ is smaller than 16, $C'(\boldsymbol{x}, \boldsymbol{y})$ becomes 16. Namely, when the test sequence $\boldsymbol{b}(t)$ is similar to the training sequence $\boldsymbol{a}(t)$, the network often responds well and its output sequence $\boldsymbol{y}(t)$ becomes almost equal to the learned sequence $\boldsymbol{x}(t)$.

Figure 4.16 shows $d(\boldsymbol{x}, \boldsymbol{y})$ against the input correlation $C(\boldsymbol{a}, \boldsymbol{b})$, for the trials belonging to category 3. When $C(\boldsymbol{a}, \boldsymbol{b})$ is more than 6, the $d(\boldsymbol{x}, \boldsymbol{y})$ values are very close to 0[ms], and their standard deviations are as small as 0.005$\sim$0.05[ms]. Therefore, when the network successfully recalls a sequence, the sequence is equal to the learned sequence $\boldsymbol{x}(t)$ with high temporal precision, that is, smaller than 0.05[ms].

Consequently, the trained network responds well when the test sequence is fairly well correlated with the learned sequence. If the trained network successfully responds, its output sequence is almost equal to the output sequence for the training sequence.

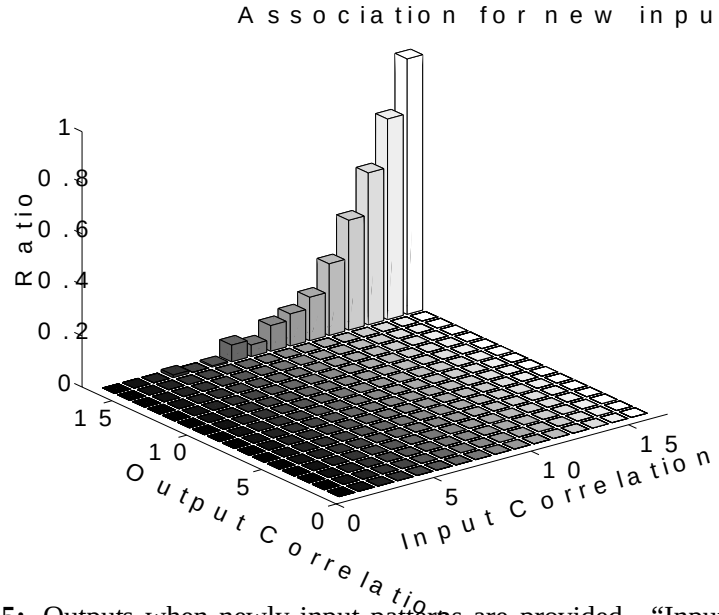

Figure 4.15: Outputs when newly input patterns are provided. "Input Correlation" denotes the correlation value between training sequence $\boldsymbol{a}(t)$ and test sequence $\boldsymbol{b}(t)$, i.e., $C(\boldsymbol{a}(t), \boldsymbol{b}(t))$. "Output Correlation" denotes the correlation quantity between learned sequence $\boldsymbol{x}(t)$ and output sequence $\boldsymbol{y}(t)$, i.e., $C'(\boldsymbol{x}(t), \boldsymbol{y}(t))$. "Ratio" denotes the ratio of appearing for the case, among 200 trials for each input-output correlation pair. A trial is counted only when the output sequence is classified into category 3.

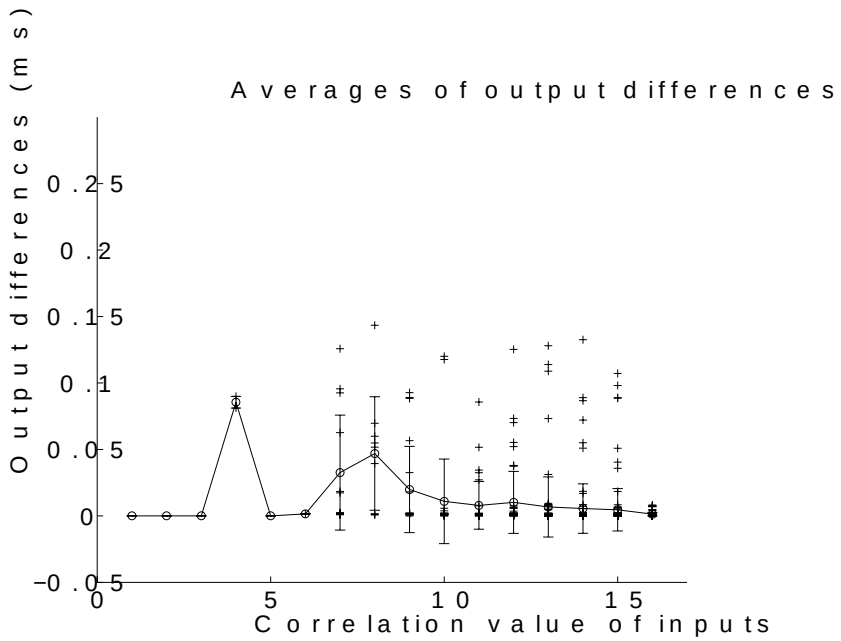

Figure 4.16: Averages of output differences. The abscissa denotes the correlation value between training sequence $\boldsymbol{a}(t)$ and test sequence $\boldsymbol{b}(t)$, i.e., $C(\boldsymbol{a}(t), \boldsymbol{b}(t))$. The ordinate denotes the criterion of time difference between learned sequences $\boldsymbol{x}(t)$ and output sequence $\boldsymbol{y}(t)$, i.e., $d(\boldsymbol{x}, \boldsymbol{y})$. Each '+' denotes a $d(\boldsymbol{x}, \boldsymbol{y})$ value. The 'o' mark and the error-bar are the mean and its standard deviation, respectively. A trial is counted only when the sequence is classified into category 3.

4.7 Discussion

Let us discuss the results shown in this chapter. In the first simulation, we found that the spike-based learning rule can extract coincidence inputs that are contaminated by dominant random inputs.

In the second simulation, we considered the situation where a couple of neurons are input from two regular input groups that fire in opposite phases in the same period. Here, we found that the neurons are able to form an oscillator whose firing phases correspond to the two timing values of the regular inputs, although they are contaminated by dominant random inputs and the same regular inputs enter the two neurons. This is achieved because the transmission delay between the two neurons corresponds to the difference of the phases, and it works to break the symmetry of the initial connections.

In the last simulation, we prepared a certain number of connections in the network of neurons, and made the neurons select appropriate connections (or, lines) among them. Then, the network was able to learn a spatio-temporal input sequence in a self-organizing manner. The learning and retrieval of spatio-temporal sequences based on an associative memory learning scheme have been discussed in (Gerstner and van Hemmen, 1993). However, our learning is based on a competitive learning scheme. If the variation of the delay lines is wider than the spike precision, the competitive learning among delay lines is able to preserve the spike pattern. It should be noted that the trained network needs the training sequence to retrieve the learned pattern. This is also the difference with the associative learning scheme, in which the training sequence is only provided at the beginning of the retrieval phase. According to our learning, therefore, the network achieves "resonance" or "synchronization" between the network structure and the training spatio-temporal pattern provided to the network.

An important problem of the last simulation involves the membrane time constant, which is smaller than physiological data. In this chapter, we intend to limit the information processing by a network of neurons to the aspect of temporal coding. The small membrane time constant is a reasonable assumption for an auditory system which deals with fine temporal information (Reyes et al., 1994; 1996). The cortical neurons may use such a precise coding framework with the help of inhibitory inputs (Softky & Koch, 1993; Softky, 1995; Fujii et al., 1996). Without strong leaks, however, it is still unclear how the precise temporal coding is achieved.

In our model, the number of projections to a single neuron is much smaller than that in the real nervous system. This is due to the limitation of the computational power needed to conduct a simulation. This limitation is due to the large number of connections among neurons and the temporal precision necessary in the simulation. In our network topology, the learning proceeds based on competitive selection among neuronal connections. The number of connections required in this topology is $m \cdot N(N-1) + NN'$, where N is the number of neurons, N' is the number of input units, and m is the number of synapses between neurons. Since the number of connections increases quadratically to N, it is difficult to prepare a lot of neurons. Moreover, since we also consider precise temporal processing, the time step is set to be fine in

comparison to the existing study based on a temporal associative memory topology (Gerstner and van Hemmen, 1993). Actually, the simulation required about ten hours on a fairly powerful workstation (Origin2000, CPU: R10000).

We also assume that the same input sequence is repeatedly provided to the learning network. The need for spontaneous periodic inputs, i.e., "reverberation", for self-organization has been pointed out (Hebb, 1949). Actually, there are spontaneously generated rhythmic activities in the retina, and they induce synaptic segregation in the lateral geniculate nucleus (Shatz 1990; Meister et al., 1991). Similar wavy activities are considered to be related to the construction of columnar structures in the visual cortex (Toyama et al., 1996). Periodic activities are also found in the entorhinal cortex, which holds the input sequence for a certain period of time and provides information to the hippocampus (Iijima et al., 1996).

Our remaining problems include examining the possibility of the learning of multiple patterns in a network, although this is fairly difficult for the present model itself due to its capacity.

4.8 Conclusion

In this chapter, we showed that a neuron is able to select connections that have appropriate transmission delay times from other neurons. A network of such neurons is able to learn a temporal sequence by self-organizing the connections in the network. When a test sequence different from the training sequence is provided to the trained network, the network does not respond at all, or regularly produces an output sequence. In the latter case, the output sequence is almost equivalent to the response for the training sequence with high temporal precision. The rate of the latter case increases as the correlation value between the training sequence and the test sequence becomes large. Hence, the trained network filters a temporal sequence with high temporal precision. This self-organization is achieved by segregation of the connections, which is induced by repeatedly provided inputs, i.e., reverberation, to the network.

4.A Appendix

4.A.1 Experimental conditions for the simulation in section 3.2

The integration is done using the Runge-Kutta method with the time step 0.005[ms]. The absolute refractory period is $\delta_{ARP} = 1$[ms]. The relative refractoriness is not considered here for simplicity. The learning parameters are $\epsilon = 0.04$, $\gamma = 0.15$, $w_0 = 1$, $A_{\beta^1} = 0.5$, $A_{\beta^2} = 0.3$, $A_{\alpha^1} = 0.5$, $A_{\alpha^2} = 0.3$, $\tau_{\beta^1} = 0.5$[ms], $\tau_{\beta^2} = 5.0$[ms] and $\tau_{\alpha^1} = 0.2$[ms]. τ_{α^2} is determined by the smoothness condition (4.8). The upper bound of the synaptic efficacy is limited to 8.0.

4.A.2 Experimental conditions for the simulation in section 4

The simulation is done with the integration time step of 0.005[ms] until 10[s]. The threshold value $\theta = 5$, and the time constants for the refractoriness are $\delta_{ARP} = 1.0$[ms], $\tau_{AHP} = 0.5$[ms], and $A_{AHP} = 4.0$[ms]. The learning coefficients are $\epsilon = 0.04$, $\gamma = 0.15$, $A_{\beta^1} = A_{\alpha^1} = 0.5$, $A_{\beta^2} = A_{\alpha^2} = 0.3$, $\tau_{\beta^1} = 0.5$[ms], $\tau_{\beta^2} = 5.0$[ms], and $\tau_{\alpha^1} = 0.2$[ms], and τ_{α^2} is defined by the smoothness condition (4.8). The upper bound of the synaptic efficacy is 3.0. The initial value w_0 is set at 1.0 for the synapses from the input units (random and regular) and 0.5 between the two neurons.

4.A.3 Experimental conditions for the simulation in section 5

The simulation is done with the time step of 0.005[ms] until 400[s]. We set $\mathcal{D} = 2.0$[ms], $\mathcal{D}_0 = 1.0$[ms], $\theta = 5$, $\tau_{ARP} = 0.8$[ms], $A_{AHP} = 15.0$, $\delta_{ARP} = 1.0$[ms], $\epsilon = 0.006$, $\gamma = 0.15$, $A_{\beta^1} = A_{\alpha^1} = 0.9$, $A_{\beta^2} = A_{\alpha^2} = 0.5$, $\tau_{\beta^1} = 0.5$[ms], $\tau_{\beta^2} = 5$[ms], and $\tau_{\alpha^1} = 0.2$[ms], and τ_{α^2} is determined by the smoothness condition (4.8). The synaptic efficacy w_{ab} is restricted so as not to exceed 3 for a synapse from an input unit, and 2 for a synapse between neurons. The initial synaptic efficacy w_0 is set at 1 for a synapse from an input unit, and 0.5 for a synapse between neurons. With the threshold value $\theta = 5$, a neuron does not fire due only to the regular input units even when all of the synapses from the regular inputs are strengthened to their upper limit.

4.A.4 Detailed definitions of the correlation values

The correlation between two output patterns, $\boldsymbol{x}(t)$ and $\boldsymbol{y}(t)$, can be simplified due to their periodicity. Since $\boldsymbol{x}(t)$ and $\boldsymbol{y}(t)$ are not identical in time, the correlation between $\boldsymbol{x}(t)$ and $\boldsymbol{y}(t)$ should allow for some small temporal variation. In order to estimate its average firing phase, we first define the following operation. For a sequence $\xi_i(t) = \sum_j \delta(t - t_i^j)$ having a period T, we define:

$$\bar{\xi}_i(t) = \delta(t - \bar{t}_i), \quad \check{\xi}_i(t) = \delta(t - \bar{t}_i) + \delta(t - \bar{t}_i - T),$$

where $\bar{t_i}$ is given by

$$\bar{t_i} = \frac{1}{N}\sum_{j=0}^{N}(t_i^j - \left\lfloor \frac{t_i^j}{T} \right\rfloor \cdot T).$$

N is the number of firings. $\lfloor x \rfloor$ is the maximum integer that does not exceed x. In order to allow for some small variation in the output sequences, we next define the following operation. For a sequence $\xi_i(t)$, we define:

$$\tilde{\xi}_i(t) = \sum_j \int_{-\vartheta}^{\vartheta} \delta(t - t_i^j - \tilde{t}) d\tilde{t},$$

where $\vartheta \ll T$. Using these operations, we describe the correlation value between $\boldsymbol{x}(t)$ and $\boldsymbol{y}(t)$ as

$$C'(\boldsymbol{x}(t), \boldsymbol{y}(t)) = \max_{\tau} E\left\{\tilde{\bar{\boldsymbol{x}}}(t) \cdot \bar{\boldsymbol{y}}(t-\tau)\right\}.$$

To examine the difference of the firing timing values between two sequences, $\xi_i(t) = \sum_j \delta(t - t_i^j)$ and $\eta_i(t) = \sum_j \delta(t - s_i^j)$, we define:

$$d(\boldsymbol{\eta}(t), \boldsymbol{\xi}(t)) = \frac{1}{n}\sum_{i=1}^{n}\left\{\frac{1}{N}\sum_{j=0}^{N}\min_m (t_i^j - \bar{s_i} - m \cdot T + \tau)^2\right\}^{\frac{1}{2}},$$

where m is a positive integer number. n is the number of neurons, and τ is given by

$$\tau = \arg\max_{\tau}\left\{\sum_{i=1}^{n}\min\left[\begin{array}{l}(\bar{t_i} - \bar{s_i} - T - \tau)^2 \\ (\bar{t_i} - \bar{s_i} - \tau)^2\end{array}\right]\right\}.$$

In the evaluations shown in section 6, we set $\vartheta = 0.25$[ms].

Chapter 5

Stochastic Spiking Neurons that Mimic the Hodgkin-Huxley Equation

Abstract. This chapter theoretically examines the stochastic process of a spiking neuron whose spike response is similar to that of the Hodgkin-Huxley (H-H) model. Our simplified model based on a linear differential equation can successfully reproduce the sub-threshold membrane properties of the H-H model. Analyzing the stochastic process of this model, we find that the neuron resonates with Poisson input spikes whose intensity oscillates with a certain frequency. This frequency corresponds to the natural frequency of the H-H model.

5.1 Introduction

Nonlinear dynamics can often be approximated by linear differential equations when weak stimuli are added to the system. Although firing activities of a neuron are highly nonlinear, sub-threshold potentials caused by weak inputs to the neuron can be reproduced by linearization (Mauro *et al.*, 1970; Koch, 1984; Koch, 1999). Moreover, the Hodgkin-Huxley model can be reduced into a spiking neuron model (Kistler, *et al.*, 1997). Spiking neuron models assume that neuronal activities are described based on spikes, and the membrane potential of a neuron is given by the weighted summation of post-synaptic potentials, each of which is induced by a single input spike (Kistler *et al.*, 1997; Gerstner, 1999). In this chapter, we discuss the stochastic process of a spiking neuron model whose response function imitates the spike response of the Hodgkin-Huxley model.

Stochastic spiking neuron model

We first describe a stochastic spiking neuron model. When stochastic spikes are provided, the membrane potential of the i-th stochastic spiking neuron is given by

$$\boldsymbol{v}_i(t) = \sum_{j=1}^{N} w_{ij} \sum_{f=1}^{\boldsymbol{n}_j(t)} u(t - \boldsymbol{t}_j^f) + \sum_{f=1}^{\boldsymbol{n}_i(t)} \eta(t - \boldsymbol{t}_i^f),$$

where random variables are described by bold math fonts. Here, N is the number of synapses projecting to neuron i, w_{ij} is the transmission efficacy of synapse j, $\boldsymbol{n}_j(t)$ is the number of spikes that enter through synapse j until time t, and $\boldsymbol{t}_j^f$ is the time at which the f-th spike enters through synapse j. $\boldsymbol{n}_i(t)$ is the number of spikes emitted by neuron i until time t, and $\boldsymbol{t}_i^f$ is the f-th emission time of neuron i. In this chapter, we assume that $\eta(t)$, which represents the potential reduction caused by spike emission, takes a constant value η for simplicity. $u(s)$ is called the spike response function, and we assume that this function has the following function form:

$$u(s) \quad = \quad qe^{-\alpha s} \sin(\beta s) \mathcal{H}(s), \tag{5.1}$$

where $\mathcal{H}(s)$ is a Heaviside (step) function. α, β and q are constant parameters.

The Hodgkin-Huxley neuron model

According to the Hodgkin-Huxley (H-H) neuron model (Hodgkin and Huxley, 1952), the membrane potential of an axon, $v(t)$, is given by

$$C_m \frac{dv}{dt} \quad = \quad \bar{G}_{\mathrm{Na}} m^3 h (E_{\mathrm{Na}} - v) + \bar{G}_{\mathrm{K}} n^4 (E_K - v) + G_m (V_{\mathrm{rest}} - v) + I_{\mathrm{input}},$$

where the reversal potentials are $E_{\mathrm{Na}} = 115$ [mV], $E_{\mathrm{K}} = -12$ [mV] and $V_{\mathrm{rest}} = 10.6$ [mV], and the maximal conductances are $\bar{G}_{\mathrm{Na}} = 120$ [mS/cm^2], $\bar{G}_{\mathrm{K}} = 36$ [mS/cm^2] and $G_m = 0.3$ [mS/cm^2]. The channel dynamics are voltage dependent. The dynamics of components corresponding to the potassium and sodium channels are given by

$$\frac{dx}{dt} = \alpha_x(v)(1 - x) - \beta_x(v)x,$$

where x is n, m or h. The activating and inactivating probabilities, $\alpha_x(v)$ and $\beta_x(v)$, are given by

$$\begin{array}{ll} \alpha_n(v) = (0.1 - 0.01v)/(e^{(1-0.1v)} - 1), & \beta_n(v) = 0.125e^{-v/80}. \\ \alpha_m(v) = (2.5 - 0.1v)/(e^{(2.5-0.1v)} - 1), & \beta_m(v) = 4e^{-v/18} \\ \alpha_n(v) = 0.07e^{0.05v}, & \beta_n(v) = 1/(e^{(3-0.1v)} + 1). \end{array}$$

The input current is written by $I_{\mathrm{input}}(t) = \sum_{j=1}^{N} \sum_{f=1}^{n_j(t)} g_E(t - t_j^f)(v(t) - E_E)$, where $E_E = 65$ [mV] is the reversal potential for excitatory inputs. N is the number of

inputs. $g_E(s)$ is the synaptic conductance defined by $g_E(s) = G_{\rm syn} e^{-\gamma s} \mathcal{H}(s)$, where $G_{\rm syn} = 1.0$ [mS] is the conductance gain and $\gamma = 0.5$ [1/ms] is the decay parameter.

Simple neuron models like the leaky integrate-and-fire model intend to describe the membrane behaviors based on the input current $I_{\rm input}(t)$. On the other hand, the membrane potential of the H-H model is significantly dependent on the sodium and potassium currents. In order to mimic the H-H model, a spiking neuron then model needs to employ a spike response function that includes those ionic effects.

Mimicking the Hodgkin-Huxley model

Here, we present a spiking neuron model which imitates the dynamics of the sub-threshold potential of the H-H model. When the input currents do not produce an output spike, the membrane potential is said to keep sub-threshold potential. In the sub-threshold potential, membrane responses to a single input spike are almost the same. This single spike response can be mimicked by function (5.1), whose parameters are $\alpha = 0.1$ [ms], $\beta = 0.5818$ [rad/ms], $q = 0.055$ [mV] and $\eta = -1.8$ [mV]. Figure 5.1 shows that the spike response function successfully mimics the sub-threshold potential of the H-H model. Because the dynamics of the sub-threshold potential are composed of responses to weak stimuli, a linear differential equation can well approximate the dynamics. The spike response function (5.1) is one of the solutions of linear differential equations.

Linearization procedure of the H-H model is discussed in appendix section 5.A.1. Although equation (5.1) is not exactly the same as the spike response of the linearized H-H model, both functions are known to have similar shapes (Koch, 1984).

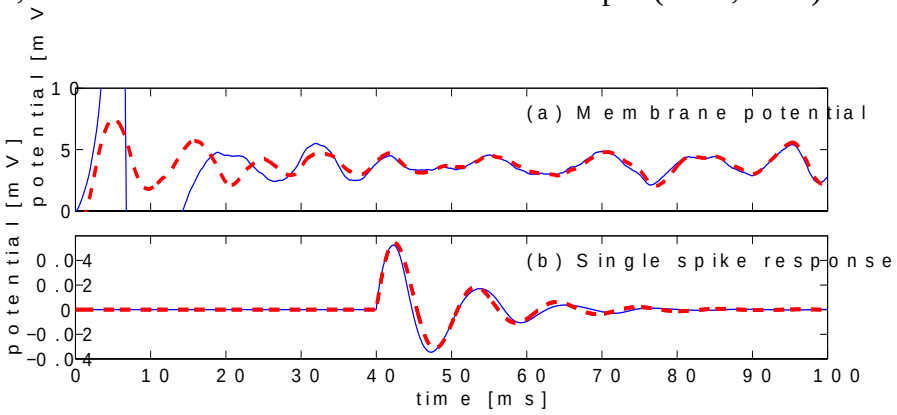

Figure 5.1: (a) Dynamics of the membrane potential of the H-H model (solid line) and the spiking neuron model (dash line). The same inputs, generated by Poisson process with fixed intensity, are provided to the both models. (b) Single spike response of the H-H model in the middle of its dynamics (solid line) and the response function (5.1) we adopted (dash line).

5.2 Analysis of sub-threshold potential

We theoretically examine the stochastic process of the membrane potential of the stochastic spiking neuron model, $\boldsymbol{v}(t) = \sum_{j=1}^{N} w_{ij} \sum_{f=1}^{\boldsymbol{n}(t)} u(t - \boldsymbol{t}_j^f) \equiv \sum_{j=1}^{N} w_{ij} \boldsymbol{x}_j(t)$, where input spikes obey an inhomogeneous Poisson process with intensity $\lambda(t)$.

5.2.1 Dynamics of the membrane potential density

First, we examine the dynamics of the membrane potential density when the firing threshold is ignored.

Single synaptic response

For simplicity, synapse index j is omitted in this paragraph. The probability density of the membrane response for a single synapse, $\boldsymbol{x}(t)$, is described as

$$g(x^t) \equiv \langle \delta(x^t - \boldsymbol{x}(t)) \rangle = \int_{-\infty}^{\infty} \frac{d\xi}{2\pi} \exp(\mathrm{i}\xi x^t) \Big\langle \exp\Big(-\mathrm{i}\xi \boldsymbol{x}(t)\Big) \Big\rangle, \tag{5.2}$$

where $\mathrm{i} = \sqrt{-1}$ and $\langle \cdot \rangle$ denotes an ensemble average over trials. Time $[0, t]$ is partitioned into intervals $[s_l, s_{l+1}]$ ($l = 0, \ldots, T-1$) whose period is Δs; namely, $s_l = l\Delta s$, $s_0 = 0$ and $s_T = T\Delta s = t$. If the time step Δs is small enough, the change of the membrane response at time t, which is caused by the spikes input within $[s_l, s_{l+1}]$, can be approximated as $\Delta \boldsymbol{x}^l(t) \approx u(t - s_l)\Delta \boldsymbol{n}^l$. Here, $\Delta \boldsymbol{n}^l$ denotes the number of spikes input within $[s_l, s_{l+1}]$. Then, the membrane response $\boldsymbol{x}(t)$ can be described by the summation of statistically independent random variables $\{\Delta \boldsymbol{x}^l(t) | l = 0, \ldots, T-1\}$, and the characteristic function of $\boldsymbol{x}(t)$ becomes

$$\begin{aligned} &\Big\langle \exp\Big(-\mathrm{i}\xi \boldsymbol{x}(t)\Big) \Big\rangle \approx \exp\Big(\sum_{l=0}^{T-1} \ln \Big\langle \exp\Big(-\mathrm{i}\xi u(t - s_l)\Delta \boldsymbol{n}^l\Big) \Big\rangle \Big) \\ = \;& \exp\Big(-\mathrm{i}\xi \sum_{l=0}^{T-1} u(t - s_l) \langle \Delta \boldsymbol{n}^l \rangle - \frac{\xi^2}{2} \sum_{l=0}^{T-1} u^2(t - s_l) (\langle (\Delta \boldsymbol{n}^l)^2 \rangle - \langle \Delta \boldsymbol{n}^l \rangle^2) + O(\xi^3) \Big). \end{aligned}$$

Using the Poisson intensity $\lambda(s)$, we obtain $\langle \Delta \boldsymbol{n}^l \rangle \approx \lambda(s_l)\Delta s$ and $\langle (\Delta \boldsymbol{n}^l)^2 \rangle - \langle \Delta \boldsymbol{n}^l \rangle^2 \approx \lambda(s_l)\Delta s$. Therefore, the mean and the variance of the membrane response $\boldsymbol{x}(t)$ are given by

$$\mu(t) = \int_0^t u(t - s)\lambda(s) ds, \quad \sigma^2(t) = \int_0^t u^2(t - s)\lambda(s) ds. \tag{5.3}$$

If the Poisson intensity $\lambda(t)$ is large enough in comparison to the decay of the membrane potential, α, the membrane response becomes the summation of large number of statistical independent random variables. Therefore, the membrane response density can be represented by a Gaussian distribution due to the central limit theorem.

Total density

When the input spikes are statistically independent with respect to synapse indices j, the density of the integrated membrane potential becomes

$$\begin{aligned} g(v^t) &= \frac{1}{\sqrt{2\pi\sigma_{\rm tot}^2(t)}}\exp\Big[-\frac{(v^t-\mu_{\rm tot}(t))^2}{2\sigma_{\rm tot}^2(t)}\Big], \\ \mu_{\rm tot}(t) &= \sum_{j=1}^{N} w_j\mu_j(t), \quad \sigma_{\rm tot}^2(t)=\sum_{j=1}^{N} w_j^2\sigma_j^2(t). \end{aligned} \tag{5.4}$$

5.2.2 Dynamics of the density mean and variance

If the Poisson intensity of inputs can be expanded into finite Fourier series:

$$\lambda(t)=\sum_{n=1}^{M}\left\{\lambda_n^c\cos(\omega_n t)+\lambda_n^s\sin(\omega_n t)\right\},$$

the mean and the variance of the density can be analytically obtained by calculating integral (5.3) with the response function (5.1).

Mean

Trigonometric functions are analytically integrated, and the mean is obtained as

$$\mu(t)=q\sum_{n=1}^{M}\Big\{A_1(\omega_n)e^{-\alpha t}\cos(\beta t-\theta_1(\omega_n))+A_2(\omega_n)\cos(\omega_n t-\theta_2(\omega_n))\Big\},$$

where

$$\begin{aligned} A_1(\omega_n) &= \sqrt{\frac{(\lambda_n^c\alpha-\lambda_n^s\omega_n)^2+(\lambda_n^c)^2\beta^2}{N_1(\omega_n)}}, \quad A_2(\omega_n)=\beta\sqrt{\frac{(\lambda_n^c)^2+(\lambda_n^s)^2}{N_1(\omega_n)}}, \\ \theta_1(\omega_n) &= \arctan\left(\frac{\alpha\lambda_n^c(\alpha^2+\beta^2+\omega_n^2)+\omega_n\lambda_n^s(\beta^2-\alpha^2-\omega_n^2)}{\beta\lambda_n^c(\alpha^2+\beta^2-\omega_n^2)-2\alpha\beta\omega_n\lambda_n^s}\right)+m\pi, \\ \theta_2(\omega_n) &= \arctan\left(\frac{2\alpha\omega_n\lambda_n^c+\lambda_n^s(\alpha^2+\beta^2-\omega_n^2)}{\lambda_n^c(\alpha^2+\beta^2-\omega_n^2)-2\alpha\omega_n\lambda_s}\right)+m\pi, \\ N_1(\omega) &= (\alpha^2+(\beta-\omega)^2)(\alpha^2+(\beta+\omega)^2). \end{aligned} \tag{5.5}$$

Here, m is an integer which is determined by the continuous conditions of $\theta_1(\omega)$ and $\theta_2(\omega)$ with respect to ω. Ignoring the decay term, we find

$$\mu(t)\approx\sum_{n=1}^{M}\beta\sqrt{\frac{(\lambda_n^c)^2+(\lambda_n^s)^2}{N_1(\omega_n)}}\cos(\omega_n t-\theta_2(\omega_n)).$$

Variance

The variance is also analytically obtained as

$$\begin{aligned}\sigma^2(t) &= q^2\sum_n\{e^{-2\alpha t}\{B_1(\omega_n)\cos(2\beta t-\phi_1(\omega_n))+B_3(\omega_n)\}\\ &\qquad +B_2(\omega_n)\cos(\omega_n t-\phi_2(\omega_n))\},\end{aligned}$$

where

$$\begin{aligned}B_1(\omega_n) &= \frac{1}{2}\sqrt{\frac{(2\lambda_n^c\alpha-\lambda_n^s\omega_n)^2+4(\lambda_n^c)^2\beta^2}{(4\alpha^2+(\omega_n+2\beta)^2)(4\alpha^2+(\omega_n-2\beta)^2)}},\\ B_2(\omega_n) &= 2\beta^2\sqrt{\frac{(\lambda_n^s)^2+(\lambda_n^c)^2}{N_2(\omega_n)}},\quad B_3(\omega_n)=-\frac{1}{2}\frac{(2\alpha\lambda_n^c-\lambda_n^s\omega_n)}{(4\alpha^2+\omega_n^2)},\\ \phi_1(\omega_n) &= \arctan\left(\frac{-2\beta\lambda_n^c(4\alpha^2+4\beta^2-\omega_n^2)+8\alpha\beta\omega_n\lambda_n^s)}{2\alpha\lambda_n^c(4\alpha^2+4\beta^2+\omega_n^2)-\lambda_n^s\omega(\omega^2+4\alpha^2-4\beta^2)}\right)+m\pi,\\ \phi_2(\omega_n) &= \arctan\left(\frac{\lambda_n^c\omega(12\alpha^2+4\beta^2-\omega_n^2)+\lambda_n^s\alpha(-6\omega_n^2+8\alpha^2+8\beta^2)}{\lambda_n^c\alpha(-6\omega_n^2+8\alpha^2+8\beta^2)+\lambda_n^s\omega_n(12\alpha^2+4\beta^2-\omega_n^2)}\right)+m\pi,\\ N_2(\omega) &= (4\alpha^2+\omega^2)(4\alpha^2+(\omega+2\beta)^2)(4\alpha^2+(\omega-2\beta)^2).\end{aligned}$$

Here, m is an integer which is determined by the continuous conditions of $\phi_1(\omega)$ and $\phi_2(\omega)$ with respect to ω. Ignoring the decay term, we find

$$\sigma^2(t)\approx\sum_{n=1}^{M}2\beta^2\sqrt{\frac{(\lambda_n^c)^2+(\lambda_n^s)^2}{N_2(\omega_n)}}\cos(\omega_n t-\phi_2(\omega_n)).$$

5.3 Resonance of the mean and firing probability

In this section, we assume that the Poisson intensity $\lambda(t)$ oscillates,

$$\lambda(t)=\lambda(1-\cos(\omega t)). \tag{5.6}$$

We examine how the dynamics of the membrane potential depend on frequency ω.

5.3.1 Resonance to oscillatory inputs

First, we examine how the statistics of the membrane potential density depends on ω. The mean and variance for the Poisson intensity (5.6) can be estimated as a special case of the solutions obtained in the previous section:

$$\begin{aligned}\mu_{\rm tot}(t) &\approx \frac{Nq\lambda\beta}{\alpha^2+\beta^2}-Nq\lambda A_2(\omega)\cos(\omega t-\theta_2(\omega)),\\ \sigma_{\rm tot}^2(t) &\approx \frac{Nq^2\lambda\beta^2}{4\alpha(\alpha^2+\beta^2)}-Nq^2\lambda B_2(\omega)\cos(\omega t-\phi_2(\omega)),\end{aligned} \tag{5.7}$$

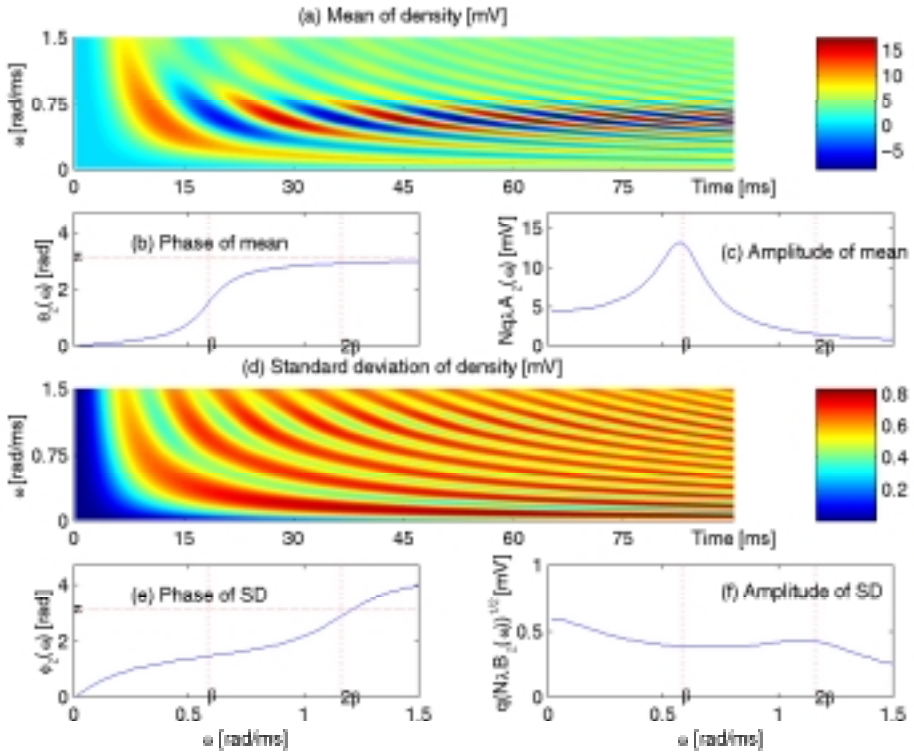

Figure 5.2: Mean and variance of the membrane potential density when the Poisson intensity is given by $\lambda(t) = \lambda(1 - \cos(\omega t))$. The number of inputs, N, is 8000, $\lambda = 6$ [Hz] and $w_j = 1$ for all j. (a) Variation of the density mean. (b,c) The phase and amplitude of the leading terms of equation (5.7), i.e., $\theta_2(\omega)$ in (b) and $Nq\lambda A_2(\omega)$ in (c). The amplitude is maximum around $\omega = \beta \sim 0.5818$ [rad/ms]. (d) Variation of the standard deviation of the density. (e,f) The phase and amplitude of the standard deviation, i.e., $\phi_2(\omega)$ in (e) and $Nq^2\lambda B_2(\omega)$ in (f). The amplitude has two peaks. One is around $\omega = 0$ and the other is around $\omega = 2\beta$.

where $w_j = 1$ for all j. From equation (5.5), the amplitude of the density mean, $A_2(\omega)$, has a peak at $\omega = \beta$ (see Fig. 2(c)). Around $\omega = \sqrt{\alpha^2 + \beta^2}$, the phase of the density mean, $\theta_2(\omega)$, drastically changes (see Fig. 2(b)). When ω is close to β, the spiking neuron hence resonates with the oscillatory inputs. This resonance can also be seen as a thick band in Fig. 2(a); namely, the amplitude of the mean is large around $\omega = \beta$. On the other hand, the variance has two peaks, around $\omega = 0$ and 2β. The standard deviation of the density does not significantly depend on ω (see Figs. 2(e) and 2(f)).

5.3.2 Estimation of the firing probability

Although the inducement of action potentials of the H-H model cannot be represented by a fixed firing threshold, rough estimation can be done by a threshold fire model (Kistler *et al.*, 1997). Here, we approximate the firing probability of our spiking neuron

model by using the error function of the density. It should be noted that we consider here firings from the sub-threshold potential. Namely, we consider a situation where the firing rate is small.

Firing probability

If the firing probability is small, it can be simply estimated by the complimentary error function:

$$\rho(t) = \frac{1}{2}\mathrm{erfc}\left(\frac{\vartheta - \eta - \mu_{\mathrm{tot}}(t)}{\sqrt{2\sigma^2_{\mathrm{tot}}(t)}}\right), \tag{5.8}$$

where $\eta = -1.8$ [mV], $\mathrm{erfc}(x) = 1 - \frac{2}{\sqrt{\pi}}\int_0^x e^{-y^2}dy$ and ϑ is the firing threshold. When the input intensity is given by $\lambda(t) = \bar{\lambda}(1 - \cos(\omega t))$, which is shown in Fig. 3(b), the firing probability estimated by (5.8) is shown in Fig. 3(a). White points in Fig. 3(a) signifies high firing probability. This figure shows that the firing probability is high when the input frequency is around $\omega = \beta$. The firing probability is mainly dependent on the variation of the mean rather than that of the variance. The variance is small because the sub-threshold potential means weak input stimuli.

Accordingly, the resonance of the density mean remarkably affects the firing probability. From this analysis using spiking neuron model that mimics the H-H model, we can see that the H-H neuron works as a bandpass filter around 92.6 ($\approx 1000\beta/(2\pi)$) [Hz]. This frequency corresponds to the natural frequency of the H-H model, which can be seen in Fig. 1(b). These resonance properties are observed at hair cells in the cochlea of amphibians, which prefer to respond to an acoustic stimulus of a particular frequency (Hudspeth, 1985; Hudspeth and Lewis, 1988). Our results imply that a neuron detects the input frequency rather than the input amplitude.

5.4 Gaussian process analysis of the oscillatory spiking neuron model

Based on the Gaussian process discussed in Chapter 3, the stochastic process of this type of neuron model can be analytically calculated. In this section, we carefully calculate the density dynamics where the spiking threshold is considered, and compare the results with the previous simplified method.

5.4.1 Formulation of the second order Markov process

From section 3.3.3, the exact dynamics for this stochastic process can also be obtained. Here, we define v^n as the membrane potential at time t_n, $\{v\}_n^m$ as a sequence $(v^n, \ldots, v^m)$, and $g_0(\{v\}_n^m)$ as the threshold free membrane potential density at time t_m which has not fired until time t_n.

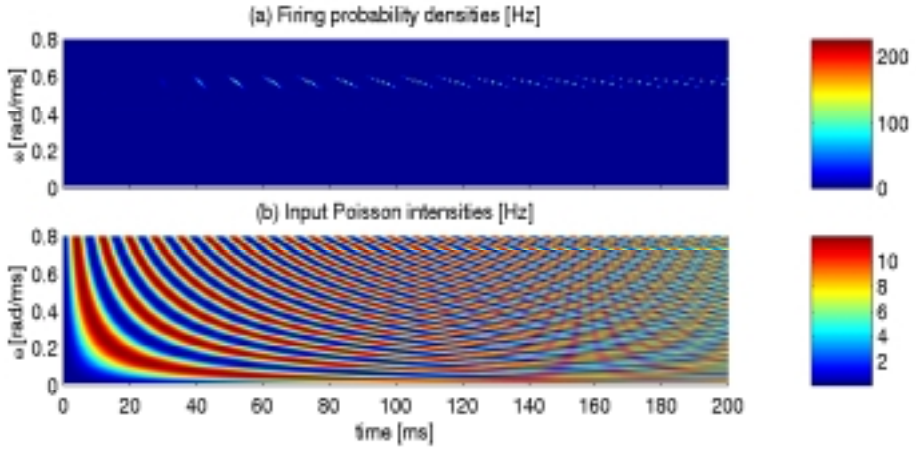

Figure 5.3: Estimated firing probability of the spiking neuron model. The number of inputs, N, is 8000. $\lambda = 6$ [Hz]. $\vartheta = 17$ [mV] and $w_j = 1$ for all j. (a) Estimated firing probability density. (b) Input Poisson intensity, $\lambda(t) = \lambda(1 - \cos(\omega t))$.

Here, we consider the dynamics for the response function $u(s) = qe^{-\alpha s}\sin(\beta s)\mathcal{H}(s)$, which is one of the solutions of second order ordinary differential equations. Because the stochastic process of this type consists of the second order Markov process, the density dynamics can be calculated by

$$\begin{aligned} g_0(v^1) = g(v^1), \quad g_0(v^2) = \int_{-\infty}^{\theta} g(v^2, v^1)dv^1, \quad g_0(v^2, v^1) = g(v^2, v^1); \\ g_0(v^m) = \int_{-\infty}^{\theta}\int_{-\infty}^{\theta} g(v^m|v^{m-1}, v^{m-2})g_0(v^{m-1}, v^{m-2})dv^{m-1}dv^{m-2}, \\ g_0(v^m, v^{m-1}) = \int_{-\infty}^{\theta} g(v^m|v^{m-1}, v^{m-2})g_0(v^{m-1}, v^{m-2})dv^{m-2}, \quad (m = 3, 4, \ldots). \end{aligned} \tag{5.9}$$

The transition probability, $g(v^m|v^{m-1}, v^{m-2})$, is

$$g(v^m|v^{m-1}, v^{m-2}) = \frac{1}{\sqrt{2\pi\gamma^m}}\exp\left(-\frac{(\omega^m - \kappa^m_{m-1}\omega^{m-1} - \kappa^m_{m-2}\omega^{m-2})^2}{2\gamma^m}\right) \tag{5.10}$$

where $\omega^m = v^m - \mu(t_m)$ and

$$\kappa^m_{m-1} = \frac{u_{m-1m}}{u_{m-1m-1}}, \quad \kappa^m_{m-2} = \frac{u_{m-2m}}{u_{m-2m-2}} - \frac{u_{m-2m-1}u_{m-1m}}{u_{m-2m-2}u_{m-1m-1}}, \quad \gamma^m = (u_{mm})^2. \tag{5.11}$$

In order to avoid the singularity of the inverse of the covariance matrix of the potential, here we define u_{ij} by

$$u_{ij} = \begin{cases} w \cdot u(t_{j+1} - t_i)\sqrt{\lambda(t_i)\Delta t}, & i \le j \\ 0, & i > j. \end{cases} \tag{5.12}$$

The mean $\mu(t)$ can be incrementally calculated as discussed in appendix section 5.A.2. Then, the correlation coefficient κ^m_{m-1} and conditional variance γ^m can be obtained using (5.11) as

$$\kappa^m_{m-1} = 2e^{-\alpha\Delta t}\cos(\beta\Delta t), \quad \kappa^m_{m-2} = -e^{-2\alpha\Delta t}, \quad \gamma^m = w^2q^2e^{-2\alpha\Delta t}\sin^2(\beta\Delta t)\lambda(t)\Delta t. \tag{5.13}$$

Because the double Markov-Gaussian process costs much computation time, we only estimate the firing probability density by (5.8) in this chapter. When we only consider the sub-threshold potential current, this estimation of the firing probability is not very erroneous.

5.5 Conclusion

This chapter theoretically examines the stochastic process of a spiking neuron model whose spike response imitates that of the H-H model. Our simplified model based on a linear differential equation can mimic the complex nonlinear H-H equation for the sub-threshold potential. The stochastic process of the linear model can be theoretically analyzed. The analysis reveals that the neuron resonates with Poisson input spikes whose intensity is oscillatory with a certain frequency. The firing of this neuron is significantly dependent on the input frequency, and the neuron works as a bandpass filter around its natural frequency.

5.A Appendix

5.A.1 Linearization of the Hodgkin-Huxley equation

The dynamics of the sub-threshold potential of the Hodgkin-Huxley equation stay around the fixed point. In this case, the linearization of the potential dynamics can approximate the real nonlinear dynamics. In this appendix section, the linearization procedure of the Hodgkin-Huxley equation is discussed.

Linearization of ionic currents

The linearization procedure is consisted of the variational method of the nonlinear path. Here, we adopt the first order variational approximation of the Hodgkin-Huxley equation. The potassium and sodium current which can be written as

$$I_{\mathrm{K}} = \bar{G}_{\mathrm{K}} n^4 (v(t) - E_{\mathrm{K}}), \quad I_{\mathrm{Na}} = \bar{G}_{\mathrm{Na}} m^3 h (v(t) - E_{\mathrm{Na}}) \tag{5.A1}$$

are linearized by the equation

$$\begin{aligned} \delta I_{\mathrm{K}} &= \left(\frac{\partial I_{\mathrm{K}}}{\partial v}\right)_{v_r} \delta v + \left(\frac{\partial I_{\mathrm{K}}}{\partial n}\right)_{v=v_r} \delta n, \\ \delta I_{\mathrm{Na}} &= \left(\frac{\partial I_{\mathrm{Na}}}{\partial v}\right)_{v_r} \delta v + \left(\frac{\partial I_{\mathrm{Na}}}{\partial m}\right)_{v=v_r} \delta m + \left(\frac{\partial I_{\mathrm{Na}}}{\partial h}\right)_{v=v_r} \delta h, \end{aligned} \tag{5.A2}$$

where v_r is the sub-threshold potential of the fixed point. n, m and h are functions of v and calculated by

$$\frac{dx}{dt} = \alpha_x(v)(1-x) - \beta_x(v)x, \tag{5.A3}$$

where x is n, m or h. The variation of n, δn, follows

$$\begin{aligned} \frac{d\delta n}{dt} &= \delta\alpha_n(1-n) - \alpha_n\delta n - \delta_n\beta n - \beta_n\delta n, \\ \frac{d\delta m}{dt} &= \delta\alpha_m(1-m) - \alpha_m m - m\delta\beta_m - \beta_m\delta m, \\ \frac{d\delta h}{dt} &= \delta\alpha_h(1-h) - \alpha_h h - h\delta\beta_h - \beta_h\delta h, \end{aligned} \tag{5.A4}$$

where

$$\delta\alpha_x(v) = \left(\frac{\partial\alpha_x}{\partial v}\right)_{v_r} \delta v, \quad \delta\beta_x(v) = \left(\frac{\partial\beta_x}{\partial v}\right)_{v_r} \delta v, \quad (x = n, m, h). \tag{5.A5}$$

Then, δn can be written by δv as

$$\left(\frac{d}{dt} + \alpha_n + \beta_n\right)\delta n = \left[\left(\frac{d\alpha_n}{dv}\right)_{v_r} - n\left(\frac{d(\alpha_n+\beta_n)}{dv}\right)_{v_r}\right]\delta v. \tag{5.A6}$$

The first order variation of the potassium current can be written as

$$\delta I_{\rm K} = \left[\bar{G}_{\rm K} + \frac{a}{d/dt + b}\right] \delta v, \tag{5.A7}$$

where the parameters

$$\begin{aligned} a &= 4\bar{G}_{\rm K} n^3 (v - E_{\rm K}) \left[\left(\frac{d\alpha_n}{dv}\right)_{v_r} - n\left(\frac{d(\alpha_n + \beta_n)}{dv}\right)_{v_r}\right], \\ b &= \alpha_{\rm n} + \beta_{\rm n}. \end{aligned} \tag{5.A8}$$

The electrical circuit for these equations is shown in Figure 5.4

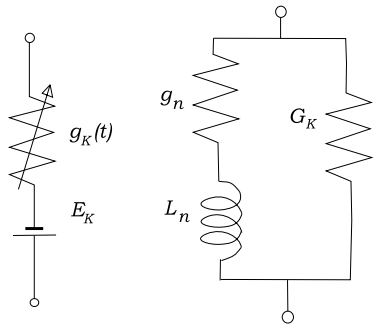

Figure 5.4: Linearization of the electrical circuit for potassium currents. Left figure denotes the real potassium current. The conductance $g_K(t)$ varies with time. Right figure denotes the linearized potassium currents described by equation (5.A7).

From (5.A2), the first order variational equation for the sodium currents becomes

$$\delta I_{\rm Na} = \left[G_{\rm Na} + \frac{g_m(\alpha_m + \beta_m)}{d/dt + \alpha_m + \beta_m} + \frac{g_h(\alpha_h + \beta_h)}{d/dt + \alpha_h + \beta_h}\right] \delta v. \tag{5.A9}$$

The coefficients are

$$G_{\rm Na} = \bar{g}_{\rm Na} m^3 h, \tag{5.A10}$$

$$g_x = \frac{\frac{d(m^3h)}{dx}(v - E_{\rm Na})[\left(\frac{d\alpha_x}{dv}\right)_r - x(\frac{d(\alpha_m+\beta_m)}{dv})_r]}{\alpha_m + \beta_m}, \tag{5.A11}$$

where x is m or h. The electrical circuit for this equation is shown in Figure 5.5.

Linearized equation for the H-H equation

With the input conductance changes

$$I_{\rm syn}(t) = \sum_{j=1}^{N} \sum_{f=1}^{n_j(t)} g_{\rm syn}(t - t_j^f)(v(t) - E_{\rm syn})\mathcal{H}(t - t_j^f), \quad g_{\rm syn}(s) = G_{\rm syn} e^{-\alpha_{\rm syn} s}, \tag{5.A12}$$

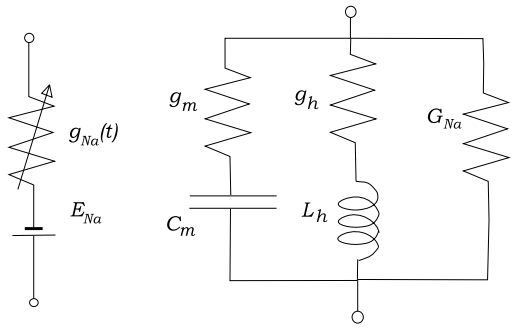

Figure 5.5: Linearization of the electrical circuit for sodium currents. Left figure denotes the real sodium current. The conductance $g_{\mathrm{Na}}(t)$ varies with time. Right figure denotes the linearized sodium currents described by equation (5.A9).

the linearized equation of the H-H model becomes

$$C\frac{d\delta v}{dt} = \sum_{j=1}^{N}\sum_{f=1}^{n_j(t)} g_{\mathrm{syn}}(t-t_j^f)\delta v\mathcal{H}(t-t_j^f) + G\delta v + \left(g_n + L_n\frac{d}{dt}\right)^{-1}\delta v + \left(g_h + L_h\frac{d}{dt}\right)^{-1}\delta v + \left(g_m + \frac{1}{C_m}\int dt\right)^{-1}\delta v. \tag{5.A13}$$

The electrical circuit for this equation is shown in Figure 5.6. The dynamics of equation (5.A13) can be numerically obtained, and forms decreasing oscillation which is similar to equation (5.1).

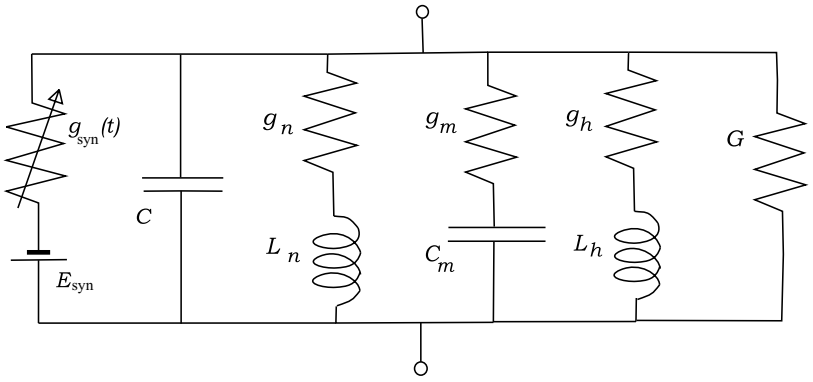

Figure 5.6: Linearized electrical circuit for the H-H equation which corresponds to the equation (5.A13).

5.A.2 Mean and variance for inhomogeneous Poisson inputs

In this appendix section, the incremental calculation method for the mean and variance is discussed.

Mean

For the response function $u(s) = qe^{-\alpha s}\sin(\beta s)$, the mean of the density can be decomposed into

$$\mu(t) = \int_0^t u(t-s)\lambda(s)ds = \sin(\beta t)A(t) - \cos(\beta t)B(t), \tag{5.A14}$$

where $w_0 = \sum_{j=1}^N w_j$ and

$$\begin{aligned} A(t) &= w_0 q \int_0^t e^{-\alpha(t-s)}\cos(\beta s)\lambda(s)ds, \\ B(t) &= w_0 q \int_0^t e^{-\alpha(t-s)}\sin(\beta s)\lambda(s)ds, \end{aligned} \tag{5.A15}$$

which are incrementally calculated as

$$\begin{aligned} A(t) &\approx e^{-\alpha\Delta t}A(t-\Delta t) + w_0 q\cos(\beta t)\lambda(t)\Delta t, \\ B(t) &\approx e^{-\alpha\Delta t}B(t-\Delta t) + w_0 q\sin(\beta t)\lambda(t)\Delta t. \end{aligned} \tag{5.A16}$$

Variance

The variance can be decomposed into

$$\begin{aligned} \sigma^2(t) &= \int_0^t w^2 u^2(t-s)\lambda(s)ds = w^2q^2\int_0^t e^{-2\alpha(t-s)}\sin^2(\beta(t-s))\lambda(s)ds \\ &= \frac{1}{2}\left\{C(t) - \cos(2\beta t)D(t) - \sin(2\beta t)E(t)\right\}, \end{aligned} \tag{5.A17}$$

where $w^2 = \sum_{j=1}^N w_j^2$ and

$$\begin{aligned} C(t) = w^2q^2\int_0^t e^{-2\alpha(t-s)}\lambda(s)ds, \quad D(t) &= w^2q^2\int_0^t e^{-2\alpha(t-s)}\cos(2\beta s)\lambda(s)ds, \\ E(t) &= w^2q^2\int_0^t e^{2\alpha(t-s)}\sin(2\beta s)\lambda(s)ds, \end{aligned} \tag{5.A18}$$

which can be incrementally calculated as

$$\begin{aligned} C(t) &\approx e^{-2\alpha\Delta t}C(t-\Delta t) + w^2q^2\lambda(t)\Delta t, \\ D(t) &\approx e^{-2\alpha\Delta t}D(t-\Delta t) + w^2q^2\cos(2\beta t)\lambda(t)\Delta t, \\ E(t) &\approx e^{-2\alpha\Delta t}E(t-\Delta t) + w^2q^2\sin(2\beta t)\lambda(t)\Delta t. \end{aligned} \tag{5.A19}$$

Chapter 6

Conclusion

Abstract. We will conclude this thesis with discussions about what the viewpoint of the stochastic spiking neuron clarifies about the neural coding problems, and what the future of this model will be. First we will see the relationship between the conventional rate coding and the stochastic spiking neuron model which we have discussed. Our stochastic spiking neuron model has various application, and will bridge the gap between spikes and psychophysical phenomena through population coding scheme.

6.1 Analysing spiking neuron models

Throughout this thesis, we analysed the density dynamics and firing probability density of the spiking neuron models whose inputs obey inhomogeneous Poisson process. Chapter 2 and 3 were devoted to the stochastic process of spiking neurons whose response function corresponds to the integrate-and-fire neurons. In chapter 3, we also discussed the general framework for any response function. In chapter 4, we discussed about the temporal aspects of the Hebbian learning and found that the deterministic spikes largely affect the learning of a periodical temporal sequence. In chapter 5, we discussed the resonance of the stochastic spiking neuron whose response function is similar to that of the Hodgkin-Huxley model. Throughout this thesis, we have found that the shapes of the response function highly affect the firing property of neurons, and in many cases temporal aspect of the neurodynamics cannot be neglected.

6.2 Rate coding reconsidered

One of the motivation of this thesis is to bridge the gap between neural coding problem and the neuron models. From the viewpoint of stochastic spikes, the neural coding problem, such as population coding scheme and the neural field dynamics, has been described by rate coding models, whose temporal dynamics can be written under the

mean field theory as

$$\tau \frac{d\mu_i(t)}{dt} = -\mu_i(t) + g\left(\sum_{j=1}^{N} w_j \mu_j(t)\right), \tag{6.1}$$

where τ is the temporal renewal parameter, and $g(v)$ is an activation function which we often define as an sigmoidal function such as

$$g(v) = \frac{1}{1 + e^{-\beta(v-\theta_0)}}. \tag{6.2}$$

As we have discussed in chapter 1, the parameters in this rate coding (connectionist) model cannot be physiologically interpreted. Here, we try to link our stochastic spiking neuron model to this rate coding model, and interpret these parameters in the rate coding model.

Interpretation of parameter τ

If we adopt the response function $u(s) = qe^{-\alpha s}\mathcal{H}(s)$, simple estimation of the firing probability density of the stochastic spiking neuron becomes

$$\psi_i(t) = \frac{1}{2}\mathrm{erfc}\left(\frac{\theta_1 - \mu(t)}{2\sigma(t)}\right), \tag{6.3}$$

where $\mu(t) = \sum_{j=1}^{N} w_j \mu_j(t)$ and $\sigma(t)$ is the standard deviation of the density. Each $\mu_j(t)$ can be described by the ordinary differential equation

$$\tau \frac{d\mu_j(t)}{dt} = -\mu_j(t) + \sum_{j=1}^{N} w_j \psi_j(t), \tag{6.4}$$

where $\tau = 1/\alpha$. Equations (6.1) and (6.4) are not exactly the same, but have similar dynamics. Then the parameter τ can be interpreted by the membrane time constant of the response function, namely, the EPSP (excitatory post-synaptic potential). θ_0 corresponds to the spiking threshold θ_1.

Interpretation of parameter β

The parameter β in equation (6.2) controls the sharpness of the activation. Because the complimentary error function $\mathrm{erfc}(-x)$ has the similar shape with the equation (6.2), one can correspond β with the standard deviation of the density, $\sigma(t)$. When we assume $\beta \approx 1/(1.4\sigma(t))$, the shapes of equation (6.2) and equation $y = \mathrm{erfc}((\theta_1 - v)/(2\sigma(t)))/2$ become similar. The maximum difference between them is within 0.05. These functions are shown in Figure 6.1. Then, we can hypothesize that the parameter β in the rate coding model denotes the inverse of the standard deviation of the density.

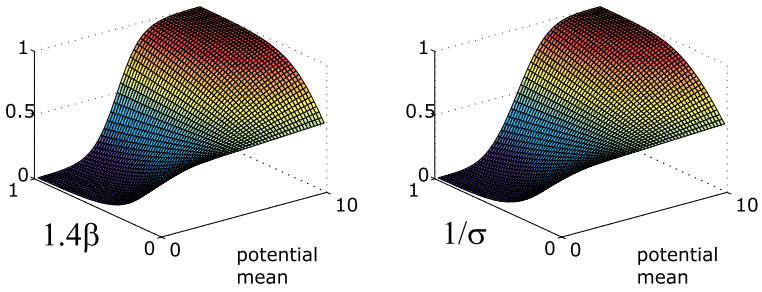

Figure 6.1: Comparison between the activation function (6.2) and the simple estimation of the firing probability of stochastic spiking neurons. Left figure denotes $g = 1/(1 + \exp(-1.4\beta(v - \theta)))$, and right figure denotes $y = \mathrm{erfc}((\theta - v)/(2\sigma))/2$, where $\theta = 5$.

It has been insisted that improving the performance of human subject with some drug, which increases the density of noradrenaline in the brain, may correspond to the increasing of the parameter β of the connectionist neuron model (Servan-Schreiber et al., 1990). Then, we may consider that the noradrenergic effect concerns narrowing the density of the stochastic membrane current. In stochastic spiking neurons, narrowing of the density significantly decreases the firing probability of the sub-threshold potential current, and causes de-noising. Namely, weak inputs are omitted. On the other hand, narrowing the density enhances the temporally synchronous firing for the super-threshold current. The total effect of the noradrenaline may be increasing the signal to noise ratio in the brain.

Comparison of two models

The rate coding model can then be described by the simple estimation of the stochastic spiking neuron model. The simple estimation of the firing probability is valid if the density current of the membrane potential is lower than the spiking threshold θ_1, namely sub-threshold. However, if the potential is larger than the spiking threshold, namely, super-threshold, the exact dynamics of the firing probability cannot be obtained by equation (6.3). The estimation becomes far from the real value. Similar error occurs in the rate coding equation (6.1), and the connectionist neuron model cannot correctly describe the super-threshold effect including spike synchronization.

6.3 Future of stochastic spiking neurons

6.3.1 Improvement of the model

Three important issues have not been considered enough in this thesis. First is the extension of the model itself. Based on the assumption of the spiking neuron model

(Gerstner 1998), we have considered the neuron model employing the response function which corresponds to the integrate-and-fire neuron model. However, our spike response model may not be sufficient for modeling the neurons in the brain. Detail explanation of the relationship between the H-H model and spiking neuron model will be an important issue. Chapter 5 is devoted to the analysis of the stochastic process of this problem. However, the property of the dynamics of the H-H equation has wide variety, and is very complex. More discussion will be needed for explanation the relation between spiking neuron and detail conductance based neuron models.

6.3.2 Development to population coding

Second future issue is about the relationship between the stochastic spiking neurons and population coding scheme. Based on the population coding scheme with statistical inference idea, the information expression among neurons corresponds to the posterior probability of Bayes rule. We have not yet discussed in detail the relationship between neurodynamics including spike synchrony and neural coding problem such as population coding. However, how the spike information is treated among the population of neurons is an interesting problem.

The network dynamics of the stochastic spiking neurons can be written as follows. We use the Poisson spike intensity $\lambda_i(t)$ for the spike input from a pre-synaptic neuron i. This can be represented by the firing rate of neuron i, $\psi_i(t) \equiv \rho(t)/\Delta t$. In the network, $\psi_i(t)$ may vary with time; namely, the firing rate is inhomogeneous. Then, in order to observe temporal behaviors of the network, the assumption that the element neurons may fire many times is important. Therefore, we consider that our approach is suitable for analyzing the interesting behaviors of network dynamics, including stability of the balanced state (Amit and Brunel, 1997a), synaptic plasticity (Kempter *et al.*, 1999, Tsodyks and Markram, 1997), syn-fire chain (Diesmann *et al.*, 1999), and so on. How these stochastic dynamics used for information processing such as statistical inference? This problem is very interesting from the viewpoint of neural coding.

6.3.3 Development to correlation coding

Throughout this thesis, the spikes are assumed to be statistically independent. Only the effect of the deterministic inputs is discussed. However, temporal correlations among spikes are experimentally observed especially at the stimulus onset or under the effect of attentional modulation. Although how these correlated spikes are treated is an important problem, this problem is hard for our framework to deal with. The only thing that we can do is to treat the spike correlation between synapses, namely "spatial" correlation. In chapter 2, section 3.3.1 and 3.3.2, we only assume the statistical independence among spikes input through one synapse. There we obtained the statistics and dynamics for each synapse. Then, the spatial (synaptic) correlation may be tractable within our scheme.

6.4 Conclusion

How the neurons in the brain process their spikes is an unsolved problem. Many complex dynamics which have not discussed in this thesis participate in the information processing. Even a complex Hodgkin-Huxley model may not be enough for the modeling neurons in the brain. In order to consider within theoretically tractable description, we need many assumptions. As we have seen in chapter 1, the spiking neuron model is not a perfect neuron model. However, more simplified rate coding model cannot treat “spikes”, and the more complicated Hodgkin-Huxley model is hard to analyse by stochastic process methods. Spiking neuron is one of the model which can deal with spikes, and is theoretically tractable. Throughout this thesis, we have analysed spiking neurons under the assumption that the spikes obeys an inhomogeneous Poisson process.

Acknowledgment

物理学しか知らなかった学部卒の当時、ニューラルネットという言葉の意味すらあまり良く分かっていなかった僕が、脳の研究を志して４年あまりになるでしょうか? その間で、一つの論文を作り上げることができたということは、望外の喜びです。それほど能力があるとは思えない自分がここまでやれたことは、多くの方々のご助力があってのことです。ここに記して、感謝の意にかえたいと思います。

スーパーバイザーである 石井 信 先生は、修士課程、博士課程の長きにわたり、研究の初期の段階から多くの指導をしていただきました。僕の論文のほとんどすべてに関係している共著者でもあり、分かりにくて曖昧な初稿を書き上げてくる学生に、懇切丁寧にご指導いただきました。また、論文発表に際しても、下手な研究発表を改めていただくなど、研究生活の上で、多くのサポートをしていただきました。伊藤 実 先生は、ニューロンの理論的研究という、一見良く分からないテーマを追求している僕を、暖かく見守ってくださいました。昨年から本研究室に赴任された 作村 勇一 先生には、目指すテーマが比較的近いこともあり、多くの示唆をいただきました。とくに、Hodgkin-Huxley モデルの役割に関しては、目から鱗の落ちる思いでした。

多くのグループから、資金面での支援をいただきました。国際会議の発表に際しては、伊藤研究室のみならず、奈良先端科学技術大学院大学支援財団、科学技術振興事業団 CREST「メタ学習と情動」銅谷賢治 研究チーム 等のサポートを得ました。

本研究は、多くの方のサジェスチョンのもとに生まれました。生物学系から情報学系への転身を遂げられた伊藤研究室の 欅谷 大 君には、僕を上回る神経科学の知識で、多くのことを学ばせてもらいました。

修士課程 2 年のころに、奈良先端科学技術大学院大学バイオサイエンス研究科の博士課程で学んでおられた 駒井 章治 さんと知り合うことができました。その後、平田 昭夫 さん、松本 和政 先生らとともに、週に 1 度、ニューロサイエンスの本の輪読を行いました。生理学がまるで分からない僕にはかなり苦しいものでしたが、勉強になりました。

博士課程 1 年の夏ににひらかれた神経回路学会主催の夏の学校で、京都大学情報学研究科 久保 雅義 先生と知り合うことができました。その後、同研究科の妻藤 公啓 さんを加えて 3、4ヶ月の間行われた共同研究は、本研究の礎をなしています。お二人には、確率スパイクという僕のコンセプトに関して、多くのサジェスチョンをいただきました。

伊藤研究室 脳と力学系研究グループの面々、新妻 弘崇 さん、長行 康男くん、吉岡 琢くん、綴木 潤くん、吉田 和子さん、吉本 潤一郎くん、玉越 大輝くん、大羽 成征くん、岡 充くん、中村 泰くん、久田 正樹くん、松野 陽一郎くん、矢野 真吾くん、窪島 智子さん、光武 眞意くん、森岡 涼子さん、そのほか多くのみなさんには、研究面でのサポートやサジェスチョンはもとより、長いようで短い学生生活を楽しいものにしてもらいました。たいへん感謝しています。我がグループには優れた人材が多く、常に刺激を受ける日々でした。

最後になってしまいましたが、不肖の息子に長い間にわたり、学問をするこ

とを許し、今まで育ててくださった両親に、深く感謝をしたいと思います。

Bibliography

Abott, L. F. & Dayan, P. (1998) The effect of correlated variability on the accuracy of a population code. *Neural Computation*, Vol.11, pp.91–101.

Abbott, L. F., & van Vreeswijk, C. (1993) Asynchronous states in networks of pulse-coupled oscillators. *Physical Review E*, Vol.48, pp.1483–1490.

Adrian, E. D. (1926) The impulses produced by sensory nerve endings: Part I. *Journal of Physiology*, Vol.61, pp.49–72.

Amari, S. (1977) Dynamics of pattern formation in lateral-inhibition type neural fields. *Biological Cybernetics*, Vol.27, pp.77–87.

Amemori, K. & Ishii, S. (1998) Unsupervised learning of sub-millisecond temporal coded sequence by a betwork of "coincidence detector" neurons. *ATR Technical report*, TR-H-249.

Amemori, K., & S. Ishii, S. (2000) Ensemble average and variance of a stochastic spiking neuron model. *IEICE Transaction Fundamentals*, Vol.E83-A, pp.575–578.

Amemori, K., & Ishii, S. (2000). Effect of the synaptic time constant on stochastic spiking neurons. *ICONIP-2000 Proceedings, 1*, 6-11.

Amit, D., & Brunel, N. (1997a) Model of global spontaneous activity and local structured activity during delay periods in the cerebral cortex. *Cerebral Cortex*, Vol. 7, pp.237–252.

Amit, D. J., & N. Brunel, N. (1997b) Dynamics of a recurrent network of spiking neurons before and following learning. *Network*, Vol.8, pp.373.

Anderson, C. H. (1994) Basic elements of biological computational systems. *International Journal of Modern Physics C*, Vol.5, No.2, pp.135–137.

Anderson, C. H. & Van Essen, D. C. (1994) Neurobiological Computational Systems. In *Computational Intelligence Imitating Life*, New York: IEEE Press, pp.213–222.

Artola, A. & Singer, W. (1993) Long-term depression of excitatory synaptic transmission and its relationship to long-term potentiation; *Trends in Neuroscience*, Vol. 16, pp.480–487.

Arieli, A., Sterkin, A., Grinvald, A., & Aertsen, A. (1996) Dynamics of ongoing activity: explanation of the large variability in evoked cortical responses. *Science*, Vol.273, pp.1868–1871.

Bair, W., & Koch, C. (1996) Temporal precision of spike trains in extrastriate cortex of the behaving macaque monkey. *Neural Computation*, Vol.8, pp.1185–1202.

Ben-Yahsai, R., Lev Bar-Or, R., & Sompolinsky, H. (1995) Theory of orientation tuning in visual cortex. *Proc. Natl. Acad. Sci. U. S. A.*, Vol.92, pp.3844–3843.

Brunel, N., & Hakim, V. (1999) Fast global oscillations in networks of integrate-and-fire neurons with low firing rates. *Neural Computation*, Vol.11, pp.1621–1671.

Brunel, N. (2000) Dynamics of sparsely connected networks of excitatory and inhibitory spiking neurons. *Journal of Computational Neuroscience*, Vol.8, pp.183–208.

Burkitt, A. N. & Clark, G. M. (1998) New method for analyzing the synchronization of synaptic input and spike output in neural systems. In T. Downs, M. Frean, and M. Gallagher, Eds., *Proceedings of the Ninthe Australian Conference on Neural Networks.*

Burkitt, A. N., & Clark, G. M. (1999) Analysis of the synchronization of synaptic input and spike output in neural systems. *Neural Computation*, Vol.11, pp.871–901.

Burkitt, A. N., & Clark, G. M. (2000) Calculation of interspike intervals for integrate and fire neurons with Poisson distribution of synaptic inputs. preprint.

Cepeda, C., Radisavljevic, Z., Peacock, W., Levine, M. S., & Buchwald, N. A. (1992) Differential modulation by dopamine of responses evoked by excitatory amino acids in human cortex. inputs. *Synapses*, Vol.11, pp.330–341.

Compte, A., Brunel, N., Goldman-Rakic, P. S. & Wang, X.-J. (2000) Synaptic mechanisms and network dynamics underlying spatial working memory in a cortical network model. *Cerebral Cortex*, Vol.10, pp.910–923.

Cooper, L. A., & Shephard, R. N. (1973) Chronometric studies of the rotation of mental images. In *Visual Information Processing*, New York: Academic Press, pp.75–176.

Chapeau-Blondeau, F., Godivier, X., & Chambet, N. (1996) Stochastic resonance in a neuron model that transmits spike trains. *Physical Review E*, Vol.53, pp.1273–1275.

deCharms, R. C. & Merzenich, M. M. (1996) Primary cortical representation of sounds by the coordination of action-potential timing; *Nature*, Vol. 381, pp.610–613

deCharms, R. C., Blake, D. T. & Merzenich, M. M. (1998) Optimizing sound features for cortical neurons. *Science*, Vol.280, pp.1439–1443.

deCharms, R. C. (1998) Information coding in the cortex by independent or coordinated populations. *Proc. Natl. Acad. Sci. USA*, Vol.95, pp.15166–15168.

Derrida, B., Gardner, E., & Zippelius, A. (1987) An exactly soluble asymmetric neural network model. *Europhys. Lett.*, Vol. 4, pp.167–173.

de Ruyter van Steveninck, R. & Bialek, W. (1988) Real-time performance of a movement sensitive neuron in the blowfly visual system: Coding and information transfer in short spike sequences, *Proc. R. Soc. Lond. Ser. B*, Vol.234, pp.379–414.

Diesmann, M., Gewaltig, M.-O., & Aertsen, A. (1999) Stable propagation of synchronous spiking in cortical neural networks. *Nature*, Vol.402, pp.529–532.

Durstewiz, D., Seamans, J. K., & Sejnowski, T. J. (2000) Dopamine-mediated stabilization of delay-period activity in a network of prefrontal cortex. *Journal of Neurophysiology*, Vol.83, pp.1733–1750.

Fujii, H., Ito, H., Aihara, K., Ichinose, N. & Tsukada, M. (1996) Dynamical cell assembly hypothesis - theoretical possibility of spatio-temporal coding in the cortex. *Neural Networks*, Vol. 9, pp.1303–1350.

Funahashi, S., Bruce, C. J., & Goldman-Rakic, P. S. (1989) Mnemonic coding of visual space in the monkey's dorsolateral prefrontal cortex. *J. Neurophysiol.*, Vol.61, pp.331–349.

Gergopoulos, A. P., Schwartz, A. B., & Ketter R. E. (1986) Neuronal population coding of movement direction. *Science*, Vol.233, pp.1416–1419.

Geogopoulos, A. P., Ketter. R. E., & Schwartz, A. B. (1988) Primate motor cortex and free arm movements to visual targets in three dimensional space. II. Coding of the direction of movement by a neuronal population. *J. Neurosci.*, Vol.8, No.8, pp.2928–2937.

Gergopoulos, A. P., Lurito, J. T., Petrides, M., Schwartz, A. B., & Massey J. T. (1989) Metal rotation of the neuronal population vector. *Science*, Vol.243, pp.234–236.

Gerstein, G. L., & Mandelbrot, B. (1964) Random walk models for the spike activity of a single neuron. *Biophysics Journal*, Vol.4, pp.41–68.

Gerstner, W., & van Hemmen, J. L. (1993) Why spikes? Hebbian learning and retrieval of time-resolved excitation patterns. *Biological Cybernetics*, Vol. 69, pp.503–515.

Gerstner, W., Kempter, R., van Hemmen, J. L., & Wagner, H. (1996) A neuronal learning rule for sub-millisecond temporal coding. *Nature*, Vol. 384, pp.76–78.

Gerstner, W. (1998) Spiking neurons. In *Pulsed Neural Networks*, (W. Maass & C.M. Bishop,eds.), MIT Press, pp.3–49.

Gerstner, W., Kempter, R., van Hemmen, J. L., & Wagner, H. (1998) Hebbian learning of pulse timing in the barn owl auditory system. In *Pulsed Neural Networks* (W. Maass & C.M. Bishop,eds.), MIT press, pp.353–377.

Gerstner, W. (2000) Population dynamics of spiking neurons: fast transients, asynchronous states, and locking. *Neural Computation*, Vol. 12, pp.43–89.

Gardiner, C. W. (1985) *Handbook of stochastic methods for physics, chemistry and the natural sciences*, Berlin: Springer.

Ginzburg, I., & Sompolinsky, H. (1994) Theory of correlations in stochastic neural networks. *Phys. Rev. E*, Vol.50, pp.3171–3190.

Gomi, H., Shidara, M. Takemura, A., Inoue, Y., Kawano, K., & Kawato, M. (1998) Temporal firing patterns of purkinje cells in the cerebellar ventral paraflocculus during ocular following responses in monkeys I: simple spikes. *Journal of Neurophysiology*, Vol.80, pp.818–831.

Hatsopoulos, N. G., Ojakangas, C. L., Paninski, L., & Donoghue, J. P. (1998) Information about movement direction obtained from synchronous activity of motor cortical neurons. *Proc. Natl. Acad. Sci. USA*, Vol.95, pp.15706-15711.

Hansel, D. & Sompolinsky, H. (1996) Chaos and synchrony in a model of a hypercolumn in visual cortex. *Journal of Computational Neuroscience*, Vol.3, pp.7-34.

Hansel, D. & Sompolinsky, H. (1998) Modeling feature selectivity in local cortical circuits. In *Methods in Neuronal Modeling: From Ions to Networks*, second edition, pp.499–567.

Hebb, D. O. (1949) *The Organization of behavior*. New York: John Wiley & Sons.

Hodgkin, A., L., & Huxley, A. F. (1952) A quantitative description of ion currents and its application to conduction and excitation in nerve membranes. *J. Physiol. (London)*, Vol.117, pp.500–544.

Hopfield, J. J. (1995) Pattern recognition computation using action potential timing for stimulus representation. *Nature*, Vol. 376, pp.33–36

Hida, T. (1980) *Brownian motion*. Springer-Verlag.

Hubel, D. H., & Wiesel, T. N. (1959) Receptive fields of single neurons in the cat's visual cortex. *J. Physiol.*, Vol.148, pp.574-591.

Hudspeth, A. J. (1985). The cellular basis of hearing: The biophysics of hair cells. *Science*, *230*, 745–752.

Hudspeth, A. J., & Lewis, R. S. (1988). A model for electrical resonance and frequqncy tuning in saccular hair cells of the bullfrog *Rana catesbeiana*. *J. Physiol., 400*, 275–297.

Iijima, T., Witter, M. P., Ichikawa, M., Tominaga, T. Kajiwara, R., & Matsumoto, G. (1996) Entorhinal-hippocampus interactions revealed by real-time imaging. *Science*, Vol. 272, pp.1176–1179.

Jung, P. (1993) Periodically driven stochastic systems. *Physics Reports*, Vol.234, pp.175-295.

Kempter, R., Gerstner, W., & van Hemmen, J. L. (1999) Hebbian Learning and Spiking Neurons. *Physical Review E*, Vol. 59, pp.4498–4514.

Kistler, W., Gerstner, W., & van Hemmen, J. L. (1997) Reduction of Hodgkin-Huxley equations to a single-variable threshold model. *Neural Computation*, Vol. 9, pp.1015–1045.

Kita, H., Oda, K., & Murase, K. (1999) Effects of dopamine agonists and antagonists on optical responses evoked in rat frontal cortex slices after stimulation of the subcortical white matter. *Exp. Brain Res.*, Vol. 125, pp.383–388.

Koch, C. (1984). Cable theory in neurons with active, linearized membranes. *Biol. Cybern., 50*, 15–33.

Koch, C. (1999) *Biophysics of computation: information processing in single neurons*. New York: Oxford University Press.

Koechlin, E., Anton, J. L., & Burnod Y. (1999) Bayesian inference in population of cortical neurons: a model of motion integration and segmentation in area MT. *Biol. Cybern.*, Vol.80, pp.25–44.

Kohonen, T. (1982) Self-organized formation of topologically correct feature maps. *Biological Cybernetics*, Vol. 43, pp.59–69.

Konishi, M. (1986) Centrally synthesized maps of sensory space. *Trends in Neuroscience*, Vol. 9, pp.163–168.

Kubo, M., Saito, K., & Amemori, K. (2000) High variance of ISIs in balanced dynamics of cortical network models. personal communication.

Law-Tho, D., Hirsch J. C., & Crepel F. (1994) Dopamine modulation of synaptic transmission in rat prefrontal cortex: an in vitro electrophysiological study. *Neurosci. Res.*, Vol.21, pp.151–160.

Mainen, Z. F. & Sejnowski, T. J. (1995) Reliability of spike timing in neocortical neurons. *Science*, Vol.268, pp.1503–1506

Markram, H., Lübke, J., Frotscher, M., & Sakmann, B. (1997) Regulation of synaptic efficacy by coincidence of postsynaptic APs and EPSPs. *Science*, Vol. 275, pp.213–215

Meister, M., Wong, R., Baylor, D., & Shatz, C. (1991) Synchronous bursts of action potentials in ganglion cells of the developing mammalian retina. *Science*, Vol. 252, pp.939–943

Mauro, A., Conti, F., Dodge, F., & Schor, R. (1970). Subthreshold behavior and phenomenological impedance of the squid giant axon. *J. Gen. Physiol.*, *55*, 497–523.

Papoulis, A. (1984) *Probability, Random Variables, and Stochastic Processes*. McGraw-Hill.

Pelaez, J. R. (1997) Plato's Theory of Ideas Revisited. *Neural Networks*, Vol.10, pp.1269–1288.

Plesser, H. E., & Tanaka, S. (1997) Stochastic resonance in a model neuron with reset. *Physics Letters A*, Vol.225, pp.228–234.

Plesser, H. E., & Geisel, T. (1998) Markov analysis of stochastic resonance in a periodically driven integrate-fire neuron. *Physical Review E*, (to appear).

Plesser, H. E., & Gerstner, W. (2000) Noise in integrate-and-fire neurons: from stochastic input to escape rates. *Neural Computation*, (to appear).

Press, W. H., Teukolsky, S. A., Vetterling, W. T., & Flannery, B. P. (1988) *Numerical Recipes in C*, 2nd Edition. Cambridge, UK: Cambridge University Press.

Rao, R. P. N., & Sejnowski, T. J. (2000) Predictive learning in recurrent neocortical circuits. *Advances in Neural Information Processing Systems 12*, pp.164–170.

Reyes, A. D., Rubel, E. W., & Spain W. J. (1994) Membrane properties underlying the firing of neurons in the avian cochlear nucleus. *Journal of Neuroscience*, Vol. 14, pp.5352–5354

Reyes, A. D., Rubel, E. W., & Spain W. J. (1996) In vitro analysis of optimal stimuli for phase-locking and time-delayed modulation of firing in avian nucleus laminaris neurons. *Journal of Neuroscience*, Vol. 16, pp.993–1007

Ricciardi, L. M., & Sato, S. (1988) First-passage-time density and moments of the Orstein-Uhlenbeck process. *Journal of Appl. Prob.*, Vol.25, pp.43–57.

Rice, S. O. (1944) Mathematical analysis of random noise. *Bell System Technical Journal*, Vol.23, pp.282.

Riehle, A., Grün, S., Diesmann, M., & Aertsen, A. (1997) Spike synchronization and rate modulation differentially involved in motor cortical function. *Science*, Vol.278, pp.1950–1953.

Rieke, F., Warland, D., de Ruyter van Steveninck, R., & Bialek, W. (1997) *Spikes: Exploring the Neural Code*, Cambridge, Massachusetts: The MIT Press.

Sakai, Y., Yoshizawa, S., & Shinomoto, S. (2000). Double stochastic Poisson process can reproduce spiking statistics of cortical neurons. *ICONIP-2000 Proceedings*, Vol. 2, pp.958–963.

Sanger, T. D. (1994) Theoretical consideration for the analysis of population coding in motor cortex. *Neural Computation*, Vol.6, pp.29–37.

Sanger, T. D. (1996) Probability density estimation for the interpretation of neural population codes. *Journal of Neurophysiology*, Vol.76, pp.2790–2793.

Schwartz, A. B., Ketter, R. E., & Geogopoulos, A. P. (1988) Primate motor cortex and free arm movements to visual targets in three dimensional space. I. Relation between single cell discharge and direction of movement. *J. Neurosci.*, Vol.8, No.8, pp.2913-2927.

Senn, W., Segev, I., & Tsodyks, M. (1998) Reading neuronal synchrony with depressing synapses. *Neural Computation*, Vol.10, pp.815–819.

Servan-Schreiber, D., Printz, H., & Cohen, J. D. (1990) A network model of catecholamine effects: gain, signal-to-noise ratio, and behavior. *Science*, Vol.249, pp.892–895.

Seung, H. S., & Sompolinsky, H. (1993) Simple models for reading neuronal population codes. *Proc. Natl. Acad. Sci. USA*, Vol.90, pp.10749–10753.

Shadlen, M. N., & Newsome, W. T. (1994) Noise, neural codes and cortical organization. *Current Opinion in Neurobiology*, Vol.4, pp.569–579.

Shadlen, M. N., & Newsome, W. T. (1998) The variable discharge of cortical neurons: implications for connectivity, computation, and information coding. *Journal of Neuroscience*, Vol.18, pp.3870–3896.

Shidara, M., Kawano, K., Gomi, H. & Kawato, M. (1993) Inverse-dynamics encoding of eye movement by Purkinje cells in the cerebellum. *Nature*, Vol. 365, pp.50-52.

Siegert, A. J. F. (1951) On the first passage time probability problem. *Phys. Rev.*, Vol.81, pp.617–623.

Softky, W. R., & Koch, C. (1993) The highly irregular firing of cortical cells is inconsistent with temporal integration of random EPSPs. *Journal of Neuroscience*, Vol.13, pp.334–350.

Softky, W. R. (1995) Simple codes versus efficient codes. *Current Opinion in Neurobiology*, Vol. 5, pp.239–247

Stanton, P. K., & Sejnowski, T. J. (1989) Associative long-term depression in the hippocampus induces by hebbian covariance. *Nature*, Vol. 339, pp.215–218

Stevens, C. F & Zador, A. (1996a) Information through a Spiking Neuron In. *Advances in Neural Information Processing Systems 8, D.S. Touretzky, M.C. Mozer and M.E. Hasselmo, eds.* MIT Press.

Stevens, C. F & Zador, A. (1996b) When is an Integrate-and-fire Neuron like a Poisson Neuron? In. *Advances in Neural Information Processing Systems 8, D.S. Touretzky, M.C. Mozer and M.E. Hasselmo, eds.* MIT Press.

Stevens, C. F & Zador, A. (1995) Neural coding: the engima of the brain, *Current Biology*, Vol. 12, pp.1370-1371.

Stein, R. (1965) A theoretical analysisof neuronal variability. *Biophysical journal*, Vol. 5, pp.173–194.

Stein, R. B. (1967) Some models of neuronal variability. *Biophysics Journal*, Vol.7, pp.37–68.

Teich, M. C., & Khanna, S. M. (1985) Pulse number distribution for the neural spike train in the cat's auditory nerve. *J. Acoust. Soc. Am.*, Vol. 77, pp.1110–1128.

Thorpe, S., Fize, D., & Marlot, C. (1996) Speed of processing in the human visual system. *Nature*, Vol.381, pp.520–522.

Toyama, K., Tanifuji, M., & Yamamoto, N. (1996) Pre- and postsynaptic structures in the rat cerebral cortical circuitry. In *Basic Neuroscience in Invertebrates* (Koike, H., Y. Kidokoro, K. Takahasi & T. Kanaseki eds.), Japan Scientific Societies Press. pp.333–339.

Tuckwell, H. C. (1977) On stochastic models of the activity of single neurons. *J. Theor. Biol.*, Vol. 65, pp.783–785.

Troyer, T. W., & Miller, K. D. (1997) Physiological gain leads to high ISI variability in a simple model of a cortical regular spiking cell. *Neural Computation*, Vol. 9, pp.971–983.

Tsodyks, M., & Markram, H. k(1997) The neural code between neocortical pyramidal neurons depends on neurotransmitter release probability. *Proc. Natl. Acad. Sci. USA*, Vol.94, pp.719–723.

Tsodyks, M., Pawelzik, K. & Markram, H. (1998) Neural network with dynamic synapses. *Neural Computation*, Vol. 10, pp.821–835.

Tsodyks, M., & Sejnowski, T. (1995) Rapid state switching in balanced cortical network models. *Network*, Vol.6, pp.111–124.

Tuckwell, H. C., & Cope, D. K. (1980) Accuracy of neuronal interspike times calculated from a diffusion approximation. *J. Theoret. Biol.*, Vol.83, pp.377–387.

Tuckwell, H. C. (1988) *Introduction to Theoretical Neurobiology: Volume 2, Nonlinear and Stochastic Theories*. Cambridge, UK: Cambridge University Press.

Tuckwell, H. C. (1989) *Stochastic Processes in the Neurosciences*. Philadelphia: Society for Industrial and Applied Mathematics.

van Kampen, N. G. (1992) *Stochastic Processes in Physics and Chemistry, 2nd Edition*. Amsterdam: North-Holland.

Vaadia, E., Haalman, I., Abeles, M., Bergman, H., Prut, Y., Solvin, H., & Aertsen, A. (1995) Dynamics of neuronal interactions in monkey cortex in relation to behavioural events. *Nature*, Vol. 373, pp.515–518.

von der Malsburg, Ch. (1973) Self-organization of orientation sensitive cells in the Striate cortex. *Kybernetik*, Vol. 14, pp.85–100.

van Vreeswijk, C., & Sompolinsky, H. (1996) Chaos in neuronal networks with balanced excitatory and inhibitory activity. *Science*, Vol. 274, pp.1724–1726.

van Vreeswijk, C., & Sompolinsky, H. (1998) Chaotic balanced state in a model of cortical circuits. *Neural Computation*, Vol.10, pp.1321–1371.

Wiesenfeld, K., Pierson, D., Pantazelou, E., Dames, C., & Moss, F. (1994) Stochastic resonance on a circle. *Physical Review Letters*, Vol.72, pp.2125–2129.

Wiesenfeld, K., & Jaramillo, F. (1998) Minireview of stochastic resonance. *CHAOS*, Vol.8, pp.539–548

Young, E. (1998) Cochlear nucleus. In *The Synaptic Organization of the Brain*, (eds, G. Shepherd), pp.121–157.

Zhang, K. (1996) Representation of spatial orientation by the intrinsic dynamics of the head-direction cell ensemble: A theory. *Journal of Neuroscience*, Vol.16, pp.2112–2126.

Zhang, L. I., Tao, H. W., Holt, C. E., Harris, W. A., & Poo, M. (1998) A critical window for cooperation and competition among developing retinotectal synapses. *Nature*, Vol. 395, pp.37–44.

Zemel, R. S., & Hinton, G. E. (1995) Learning population codes by mimimizing description length. *Neural Computation*, Vol.7, pp.549–564.

Zemel, R. S., Dayan, P., & Pouget, A. (1998) Probabilistic interpretation of population codes. *Neural Computation*, Vol.10, pp.403–430.

Zemel, R. S., & Dayan, P. (1999) Distributed population codes and multiple motion models. *Advances in Neural Information Processing Systems 11*, Cambridge: MIT Press.

Zemel, R. S. (2000) Cortical belief networks. In *Theories of Cortical Processing*, R. Hacht-Neilsen (Ed.), (to appear).

Publication list

Journal Papers

1. Ken-ichi Amemori & Shin Ishii (2001) Gaussian process approach to spiking neurons for inhomogeneous Poisson inputs. *Neural Computation*, (to appear).

2. Ken-ichi Amemori & Shin Ishii (2001) Spike-based competitive learning for spatio-temporal pattern. *Neural Networks*, (revised).

3. Kenichi Amemori & Shin Ishii (2000) Self-organization and association for fine spatio-temporal spike sequences. *Transactions of the Institute of Systems, Control and Information Engineers*, Vol.13, No.7, pp.308–317. (in Japanese)

4. Kenichi Amemori & Shin Ishii (2000) Ensemble average and variance of a stochastic spiking Neuron Model. *IEICE Transactions on Fundamentals of Electronics, Communications and Computer Sciences*, Vol.E83-A, No.3, pp.575–578.

International Conferences (reviewed)

1. Ken-ichi Amemori & Shin Ishii (2001) Gaussian process appraoch to stochastic spiking neurons with reset. International Conference on Artificial Neural Networks, (Vienna, Austria, Aug. 2001, **ICANN2001**). (to appear).

2. Ken-ichi Amemori & Shin Ishii (2001) Resonance of a stochastic spiking neuron mimicking the Hodgkin-Huxley model. International Conference on Artificial Neural Networks, (Vienna, Austria, Aug. 2001, **ICANN2001**). (to appear).

3. Ken-ichi Amemori & Shin Ishii (2000) Effect of the Synaptic Time Constant on Stochastic Spiking Neurons. In ICONIP-2000 Proceedings, Vol.1, pp.6–11. (Taejon, Korea, Nov., 2000, **ICONIP2000**).

4. Kenichi Amemori & Shin Ishii (2000) Self-organization and association for temporal coding. In ICANN99: Artificial Neural Networks, Vol.1, pp.162–167. (Univ. of Edinburgh, Scotland, Sept., 1999, **ICANN99**).

5. Kenichi Amemori & Shin Ishii (2000) Unsupervised learning for sub-millisecond temporal coded sequence. In JCIS'98 Proceedings, Vol.2, pp.80–83. (Research Triangle Park, U.S.A., Oct., 1998, **JCIS98**).

6. Kenichi Amemori & Shin Ishii (2000) Self-organizing network learning of sub-millisecond temporal coded information. In Proceedings of the Fifth International Conference on Neural Information Processing, Vol.3, pp.1285–1288. (Kitakyusyu, Japan, Oct., 1998, **ICONIP98**)

Workshops

1. Ken-ichi Amemori & Shin Ishii (2000) Analysis of spiking neurons by stochastic process methods. In the proceedings of *JNNS'2000 (The 10th Annual Meeting of Japan Neural Network Society)*, pp.200. (abstract only, in Japanese).

2. Ken-ichi Amemori & Shin Ishii (2000) Variation of the response functions in stochastic spiking neuron model. *Technical report of IEICE*, NLP2000-30, NC 2000-24, pp.1–8.

3. Kenichi Amemori, Masayoshi Kubo, & Shin Ishii (2000) Response of spiking neurons to Poisson spikes. *Technical report of IEICE*, NC99-142, pp.193–200. (in Japanese).

4. Kenichi Amemori & Shin Ishii (1999) Association of fine spatio-temporal sequence by a Hebbian spike-based learning rule, *Technical report of IEICE*, NC98-111, pp.99–106. (in Japanese).

5. Kenichi Amemori & Shin Ishii (1998) Unsupervised learning of temporal sequence coded by small interval differences. *Technical report of IEICE*, NC98-42, pp.93–100. (in Japanese).

Other Workshops and Publications

1. Ken-ichi Amemori & Shin Ishii (2001) A link between behavioral and physiological models about noradrenergic modulation. *CREST Workshop on Metalearning and Neuromodulation*, Kyoto.

2. Ken-ichi Amemori & Shin Ishii (2001) Gaussian process and Fokker-Planck equation approach to stochastic spiking neurons. *Mechanisms of Brain and Mind Workshop*, Hokkaido.

3. Masayoshi Kubo, Kimihiro Saito & Kenichi Amemori (2000) High variance of ISIs in balanced dynamics of cortical network models. submitted to *IEEE-INNS-ENNS International Joint Conference on Neural Networks*.

4. Dai Keyakidani, Kenichi Amemori & Shin Ishii (2000) Spike-based Hebbian Delay Adaptation. *IEICE Technical Report*, NLP99-172, pp.83–90, (in Japanese).

5. Kenichi Amemori & Shin Ishii (1998) Unsupervised learning of sub-millisecond temporal coded sequence by a network of "coincidence detector" neurons. *ATR Technical Report*, TR-H-249. Kyoto: ATR

6. Kenichi Amemori & Shin Ishii (1998) Self-organizing network learning of sub-millisecond temporal coded information. *NAIST Technical Report*, 98006. Nara: NAIST.